THEORETICAL AND EXPERIMENTAL INVESTIGATIONS OF SATURATION EFFECTS IN A GAS LASER

Thesis by

Hisatoshi Maeda

In Partial Fulfillment of the Requirements

For the Degree of

Doctor of Philosophy

California Institute of Technology

Pasadena, California

1973

(Submitted March 27, 1973)

ACKNOWLEDGMENT

The author wishes to express his sincere appreciation to Professor Amnon Yariv for his guidance and encouragement during the course of this research.

I thank Mr. Desmond Armstrong for his skilled advice in the laboratory.

I wish to express my gratitude to Dr. David W. Vahey and Mrs. Ruth Stratton for their patient and unselfish assistance in writing the manuscript.

I have also enjoyed many stimulating discussions with the other people associated with the Quantum Electronics Laboratory.

I am pleased to acknowledge financial support during the course of this work from the California Institute of Technology

ABSTRACT

Theoretical studies of standing and traveling wave lasers are presented. The spectral behavior of the amplified spontaneous emission (superradiance) in a pencil-shaped column is investigated theoretically and experimentally. Spectral narrowing followed by rebroadening has been observed as predicted by the theory.

A geometrical representation of an interacting two-level atomic system has been developed and applied to an optical laser. A semiclassical model for a standing wave laser has been examined using the rotating wave approximation, and compared to the exact solution. Depth and width of the Lamb dip are determined theoretically and experimentally. The effect of radial profile of the laser field has been studied using the self-consistent-field approach, and the radius of the beam was measured at various positions from the window.

TABLE OF CONTENTS

INTRODUCTION

Existing laser theories may be placed in one of three different categories, depending on their level of sophistication. Specifically, we have the rate equation formalism, the semiclassical formalism, and the complete quantum mechanical formalism.

The first chapter contains a rate-equation analysis of laser phenomena, and the second chapter deals with the semiclassical approach.

In Section 1.1 we derive rate equations for a four-level laser. Our model is such that each atom, interacting with two electromagnetic waves traveling in the cavity, has a Lorentzian line profile, and that the velocity distribution of the atoms has a Maxwellian profile.

In Section 1.2 we apply the rate equations to a standing-wave laser with a uniformly distributed loss. We include this section to facilitate later comparison of the rate equation approach to the semiclassical approach given in Chapter II, and also because resonators with highly reflective mirrors can be approximated by a distributed loss model.

As the localized losses at the end mirrors increase, the standing wave approximation is less valid. Section 1.3 presents a discussion of a monochromatic traveling wave laser in which the field amplitude is a function of position. The rate equations are solved using a computer. An experiment measuring the output power for various mirror reflectances was conducted, but the agreement of experimental results with theory was poor.

Section 1.4 consists of an investigation of the spectral behavior of the superradiance. The rate equation theory predicts spectral narrowing in the unsaturated region, and rebroadening after the onset of saturation. We have observed these features experimentally. Our experimental results were in close agreement with those predicted by theory.

In Chapter II we use a quantum mechanical approach to treat the case of an ensemble of atoms interacting with a quasi-stationary classical field.

Section 2.1 presents a simple geometrical representation for the density matrix of an atom with two discrete levels. A generalized transformation is developed which takes a non-Hermitian Schrödinger wave equation into a real three-dimensional vector equation and one scalar equation.

In Section 2.2 we use the geometrical representation to obtain the threshold condition and dispersion relation for an unsaturated optical laser. We solve a vector equation and a scalar equation to the lowest order in the field.

Section 2.3 describes a formal solution of the equation for geometrical representation to infinite order approximation in the field. The solution enables us to use this representation for high intensity fields.

In Section 2.4 we obtain an exact solution to the geometrical representation for the single mode laser field. We also evaluate the solution described in Section 2.3 with the rotating wave approximation (RWA). A physical interpretation of these two solutions is provided.

The rate equation approximation (REA) is shown to be equivalent to RWA.

Section 2.5 presents a discussion of a multimode laser. The evolution of the field is treated probabilistically. It is shown that the REA is valid under the following conditions:

(i) Each mode of the laser oscillation can be regarded as a random function.

(ii) There is no correlation between two different modes

(iii) The mode spacing is much greater than the decay rates of atoms from upper or lower levels of the lasing transition.

In Section 2.6 we consider the output power and dispersion in a standing wave laser vs. detuning and pumping. We use a plane wave, one-dimensional model. The relation between the frequency shift of the laser field and the change in the length of the resonator is described. An experiment was performed to measure the output power vs. the scanning distance of one mirror, but the agreement with theory was not satisfactory.

As a consequence of the poor agreement discussed in the previous section, we consider in the last section a three-dimensional laser model, where the beam radius and the radius of the curvature of the phase front satisfying self-consistency requirements, are obtained. A qualitative explanation of the discrepancies between theory and experiment in Section 2.6 is given. It is shown that a three-dimensional treatment is a good candidate for explaining the asymmetry of the two power maxima observed on the Lamb dip curve.

I. RATE EQUATION MODEL OF A LASER

A rate equation formalism is capable of accounting for many phenomena in a gas laser. In particular it enables us to keep track, in a bookkeeping fashion, of the exchange of energy between each "slice" of the intensity spectral distribution and each atomic velocity class. Thus the integro-differential equations are derived for both field and atoms. We first formulate the rate equations and apply them to a standing wave laser, to a traveling wave laser and finally to a superradiant laser. We discuss mainly the dependence of spectral behavior on the excitation density.

In the first section the rate equations for a four level maser are formulated. In the next section we obtain an integral equation for the field intensity in the standing wave laser for the purpose of comparing this to the results given by the rotating wave approximation in Chapter 2. Next, a traveling wave laser is treated where the rate equations are solved self-consistently with proper boundary conditions. In the last section the superradiant laser is described. The narrowing and rebroadening of the spectrum are predicted theoretically and observed experimentally.

1.1 Rate Equation for a Four-Level Laser

The rate equations for a four-level laser have been used by many authors[1-4]. For a group of atoms with velocity v, they are given by

$$\dot{n}_3(v,z) = S_3(v) - n_3(v,z)[A_3 + \int_0^\infty B_{32}^+(v,\nu')\ I^+(\nu',z)d\nu' + \int_0^\infty B_{32}^-(v,\nu')\ I^-(\nu',z)d\nu'] + n_2(v,z)\ [\int_0^\infty B_{23}^+(v,\nu')I^+(\nu',z)d\nu' + \int_0^\infty B_{23}^-(v,\nu')\ I^-(\nu',z)d\nu'] \quad (1.1.1)$$

$$\dot{n}_2(v,z) = S_2(v) + n_3(v,z)[A_{32} + \int_0^\infty B_{32}^+(v,\nu')\ I^+(\nu',z)d\nu' + \int_0^\infty B_{32}^-(v,\nu')\ I^-(\nu',z)d\nu'] - n_2(v,z)[A_2 + \int_0^\infty B_{23}^+(v,\nu')I^+(\nu',z)d\nu' + B_{23}^-(v,\nu')\ I^-(\nu',z)d\nu'] \quad (1.1.2)$$

where z is the position and ν' is frequency of the field. $n_3(v,z)$ and $n_2(v,z)$ are the density spectrum of atoms (atoms $\cdot m^{-4} \cdot$ sec) in the upper state 3 and lower state 2 at position z respectively. $I^+(\nu,z)$ and $I^-(\nu,z)$ are the spectral intensities (watt $\cdot m^{-2} \cdot$ sec) of right-going and left-going waves. The pumping densities (atoms$\cdot m^{-4}$) to level 3 and 2 via level 4 are given by $S_3(v)$ and $S_2(v)$ per unit velocity. A_3 and A_2 denote the total spontaneous decay rates (sec^{-1}) per atom from the upper and lower levels respectively. A_{32} is the rate of spontaneous decay (sec^{-1}) with photoemission. $B_{32}^+(v,\nu)$ and $B_{32}^-(v,\nu)$ are the stimulated transition coefficients ($m^2 \cdot watt^{-1} \cdot sec^{-1}$) from level 3 to level 2 of atoms moving with velocity v, and $B_{23}^+(v,\nu)$ and $B_{23}^-(v,\nu)$ denote absorption between level 2 and level 3. An energy diagram is shown in Fig. 1.1.

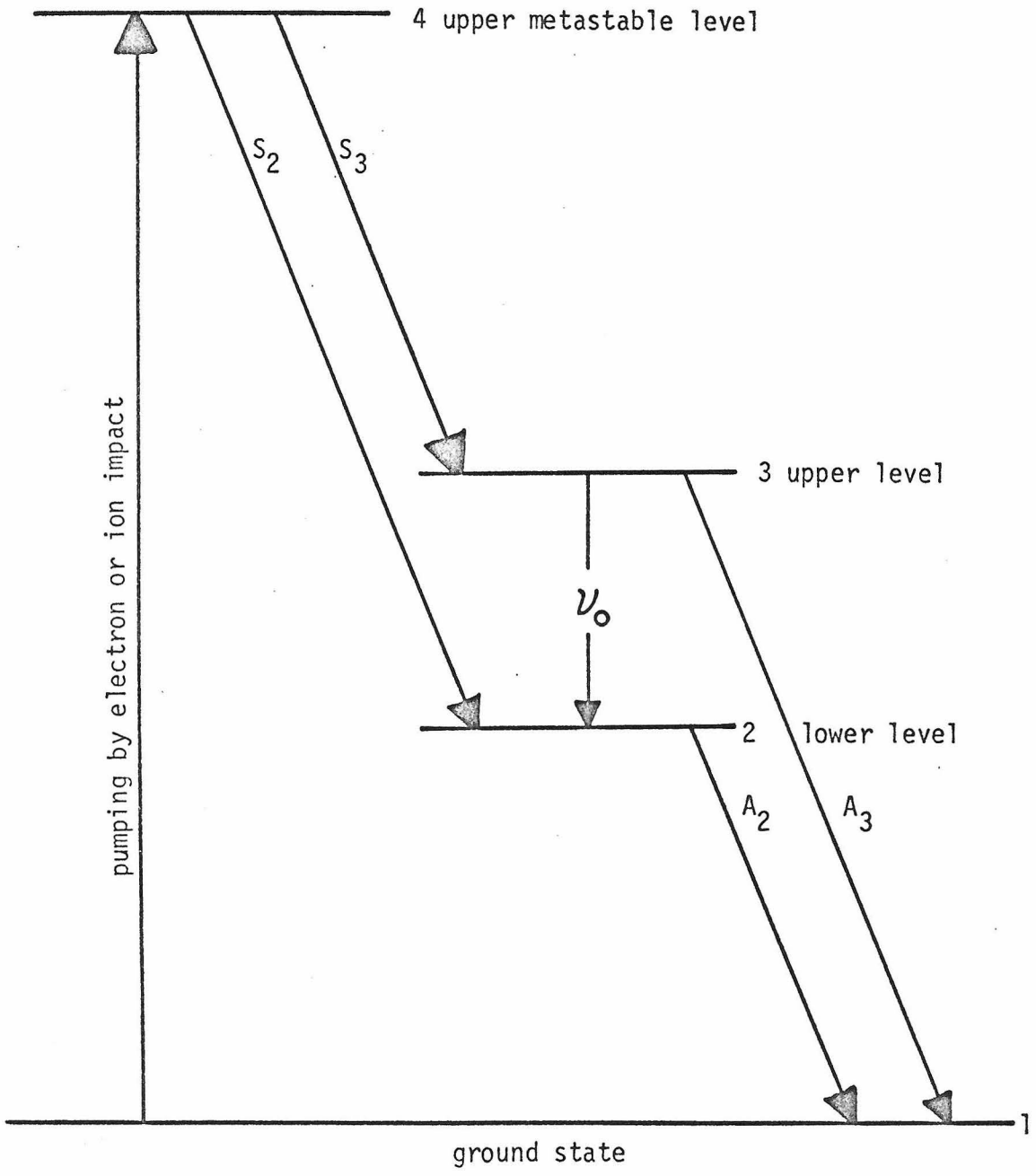

Fig. 1.1 Energy level diagram

We assume that the pumping density has a Doppler profile given by

$$S_i(v) = \frac{S_{io}}{u\sqrt{\pi}} e^{-v^2/u^2} \quad , \qquad (i=2,3) \qquad (1.1.3)$$

$S_{io}(m^{-3} \cdot sec^{-1})$ is the total pumping rate per unit volume and unit time to the ith level. u^2 is the mean squared velocity of the thermal distribution of atoms[5]. u is related to the Doppler width by

$$u = \frac{c_o}{2\nu} \frac{\Delta\nu_D}{\sqrt{\ell n\ 2}}$$

or

$$= \sqrt{\frac{2k_B T}{m}} \qquad (1.1.4)$$

where c_o = speed of light in the vacuum, ν = frequency of the electromagnetic field, $\Delta\nu_D$ = Doppler width of the gaseous medium, k_B = Boltzmann's constant, T = average atomic temperature, and m = atomic mass.

Under the stimulating frequency ν, the induced transition rate per atom between levels 2 and 3 due to a unit intensity is known to be a Lorentzian[6]

$$B_{32}(\nu) = \frac{g_2}{g_3} B_{23}(\nu)$$

$$= B_{32} \frac{2/\pi\Delta\nu_N}{1 + [2(\nu-\nu_o)/\Delta\nu_N]^2} \qquad (1.1.5)$$

$\Delta\nu_N$ is the natural line width of the concerned transition, ν_o is the resonant frequency, B_{32} is the Einstein B coefficient ($m^2 \cdot watt^{-1} \cdot sec^{-2}$), and g_2 and g_3 represent the degeneracies, or statistical

weights. Without loss of generality we may put $g_2 = g_3 = 1$ *, from now on. Atoms traveling with velocity v see a field which is different from that seen by stationary atoms. If an atom moves with speed v in the +z direction the Doppler shifted frequency of the field it sees is

$$\nu_{shifted} = \nu \pm kv/2\pi \tag{1.1.6}$$

The plus sign indicates light propagating in the minus z direction and vice-versa. k is the wave number of the field given by

$$k = 2\pi\nu/c_o \tag{1.1.7}$$

Combining (1.1.5) and (1.1.6), the induced transition rate of the atom with velocity v is written as

$$B_{32}^{\pm}(v,\nu) = B_{32} \frac{2/\pi\Delta\nu_N}{1 + [2(\nu-\nu_o \mp kv/2\pi)/\Delta\nu_N]^2} \tag{1.1.8}$$

Superscripts + and - denote the transition coefficients due to the positive and negative going waves, respectively.

If $I^+(\nu,z)$ and $I^-(\nu,z)$ are slowly varying functions of time, the growth rate of the intensities are

---

*In a steady state the following substitution is equivalent to the assumption $g_2 = g_3 = 1$:

$$A_3' = A_3 g_3 \quad , \quad A_2' = A_2 g_2 \quad ,$$

$$n_3' = n_3/g_3 \quad , \quad n_2' = n_2/g_2 \quad .$$

$$\frac{1}{c_o}\dot{I}^{\pm}(\nu,z) = h\nu\, I^{\pm}(\nu,z) \int_{-\infty}^{\infty} [B_{32}^{\pm}(v,\nu)\, n_3(v,z) -$$

$$B_{23}^{\pm}(v,\nu)\, n_2(v,z)]dv + h\nu \int_{-\infty}^{\infty} A_{32}'^{\pm}(v,\nu)\, n_3(v,z)dv$$

$$- \alpha I^{\pm}(\nu,z) \mp \frac{\partial}{\partial z} I^{\pm}(\nu,z) \qquad (1.1.9)$$

h is the Planck's constant (watt $\cdot$ sec^2) and $\alpha(m^{-1})$ is the loss per unit length. $A_{32}'^{\pm}(v,\nu)d\nu$ are the probabilities for emitting a photon with frequency between ν and $\nu+d\nu$ per unit time per atom with velocity v. These can also be written as

$$A_{32}'^{\pm}(v,\nu) = \eta A_{32} \frac{2/\pi\Delta\nu_N}{1 + [2(\nu-\nu_o \pm kv/2\pi)/\Delta\nu_N]^2} \qquad (1.1.10)$$

where η is the probability that a spontaneously decayed photon takes part in either $I^{\pm}(\nu,z)$, i.e., for a simple case η is a geometrical factor smaller than unity, equal to the fraction of the total spontaneous photons emitted into the observation solid angle. A_{32} is Einstein's A coefficient which is related to B_{32} through[7]

$$B_{32} = \frac{A_{32}\, c_o^2}{8\pi h\nu^3} \qquad (1.1.11)$$

Expressions (1.1.1), (1.1.2) and (1.1.9) are the basic equations of this chapter.

1.2 A Standing Wave Laser

We treat the standing wave laser as a simple, most intelligible example for the application of the rate equations. We discuss this

kind of laser to compare the results with that obtained in the next chapter. The agreement of rate equation approximation (REA) with the semiclassical model suggests the validity of REA.

Our model considers a laser with the following characteristics:

1. The loss is uniformly distributed along the cavity.
2. The feedback mirrors reflect all of the optical energy back into the cavity.

Such a laser has no gradient in the amplitude of the field, and is called a standing wave laser.

In expressions (1.1.1), (1.1.2) and (1.1.9) we have four integro-differential equations for the unknowns $n_3(\nu,z)$, $n_2(\nu,z)$, $I^+(\nu,z)$ and $I^-(\nu,z)$. In addition to the assumptions mentioned above, we make the following simplifications:

(i) The laser is in a steady-state, that is

$$\dot{n}_3(\nu,z) = \dot{n}_2(\nu,z) = \dot{I}^{\pm}(\nu,z) = 0 \tag{1.2.1}$$

Although the field itself oscillates with frequency ν, the corresponding intensity has no time-dependence. When one is concerned with relaxation oscillations, these time derivatives must not be neglected.

(ii) The spatial derivatives are also zero

$$\frac{\partial}{\partial z} I^{\pm}(\nu,z) = 0 \tag{1.2.2}$$

$\mp \frac{\partial}{\partial z} I^{\pm}(\nu,z)$ correspond to the net energy flow due to $I^{\pm}(\nu,z)$ per unit volume.

(iii) The spontaneous emission is negligible, that is

$$B_{32}^{\pm}(\nu,\nu)\ I^{\pm}(\nu,z) >> A_{32}'^{\pm}(\nu,\nu) \tag{1.2.3}$$

Self-induced decay plays an important role in the build-up of a field. After the intensity reaches some level, however, the spontaneous term can be ignored.

From these postulations, we may assume the electromagnetic field to be written in the form[8],

$$E(z,t) = \sum_n E_n \cos(2\pi\nu_n t)\ \sin k_n z \tag{1.2.4}$$

E_n is the time-independent amplitude, and ν_n is the frequency of the nth mode. k_n is given by

$$k_n = n\pi/L \tag{1.2.5}$$

L is the cavity length and n is a large integer. Then, we may write the intensity as

$$I^{\pm}(\nu',z) = \sum I_{\nu_n}\ \delta(\nu' - \nu_n) \tag{1.2.6}$$

We do not attempt to discuss the many modes case. We restrict the problem only to the single mode case, where

$$I^{\pm}(\nu',z) = I_{\nu}\delta(\nu' - \nu) \tag{1.2.7}$$

Solving Eqs. (1.1.1) and (1.1.2) for n_3 and n_2, we find

$$n_3(v,z) = \frac{[A_2S_3(v) + I_\nu\{S_3(v) + S_2(v)\}\ \{B^+_{23}(v,\nu) + B^-_{23}(v,\nu)\}\ ]}{[A_3A_2 + I_\nu(A_3 + A_2)\ \{B^+_{23}(v,\nu) + B^-_{23}(v,\nu)\}\ ]} \quad (1.2.8)$$

$$n_2(v,z) = \frac{[A_3S_2(v) + I_\nu\{S_3(v) + S_2(v)\}\ \{B^+_{23}(v,\nu) + B^-_{23}(v,\nu)\}\ ]}{[A_3A_2 + I_\nu(A_3 + A_2)\ \{B^+_{23}(v,\nu) + B^-_{23}(v,\nu)\}\ ]} \quad (1.2.9)$$

Substituting the above two equations into Eq. (1.1.9), we have the following integral equation for I_ν :

$$h\nu \int_{-\infty}^{\infty} \frac{[A_2S_3(v')\ B^\pm_{32}(v',\nu) - A_3S_2(v')\ B^\pm_{23}(v',\nu)]}{[A_3A_2 + I_\nu(A_3 + A_2)\ \{B^+_{23}(v',\nu) + B^-_{23}(v',\nu)\}\ ]}\, dv' - \alpha = 0 \quad (1.2.10)$$

Since $S_3(v)$, $S_2(v)$ and $B^+_{32}(v',\nu) + B^-_{32}(v',\nu)$ are even functions of v' , plus and minus signs in the numerator of the expression (1.2.10) give the same results. Equation (1.2.10) can be written more explicitly,

$$\frac{h\nu\ \bar{N}\ B_{32}}{u\sqrt{\pi}} \int_{-\infty}^{\infty} L(\nu,v')\ [1 + \frac{A_3 + A_2}{A_3\ A_2} B(\nu,v')]^{-1}\ e^{-v'^2/u^2}\, dv' - \alpha = 0 \quad (1.2.11)$$

$\bar{N}$ is the excitation density given by

$$\bar{N} = \frac{S_{30}}{A_3} - \frac{S_{20}}{A_2} \quad (1.2.12)$$

and

$$L(\nu,v) = \frac{2/\pi\Delta\nu_N}{1 + [2(\nu - \nu_o - kv/2\pi)/\Delta\nu_N]^2} \quad (1.2.13)$$

$$B(\nu,v') = I_\nu B_{32}\{L(\nu,v') + L(\nu,-v')\} \tag{1.2.14}$$

Equation (1.2.11) is the principal result of this section. The solution I_ν of this integral equation specifies the intensity of the laser field for a given detuning, the deviation of the frequency from line center, and a given pumping parameter $\overline{N}$. Expression (1.2.11) turns out to be equivalent to the equation derived from semiclassical theory. Numerical calculations and comparison with experiments will be given in Chapter 2.

1.3 A Traveling Wave Laser

To optimize the output power by choosing the reflectivity and the transmittance of the mirrors is an important problem in designing a laser. An actual laser has a mirror with finite transmittance (otherwise there is no output power). When the mirror has very high reflectivity, the standing wave approximation is valid. However, in a laser with low reflectance mirrors the amplitude of the field has a gradient along the axis of the resonator. The degree of saturation is different from place to place and the gain varies along the cavity. Moreover, there are two waves traveling in opposite directions. Consequently the problem is very difficult. A rigorous treatment of the traveling wave laser requires solving Eqs. (1.1.1), (1.1.2) and (1.1.9) simultaneously.

(A) Theory

If there is a strong energy absorption or loss at an end mirror, the laser field has a gradient along the cavity length. When there is

a net energy flow inside, we speak of a traveling wave laser. In this case the spatial derivative of the intensity across the cavity length no longer vanishes. Under the same assumptions made in the previous section excluding (ii), we find the following relation from Eq. (1.1.9):

$$h\nu\, I^{\pm}(\nu,z) \int_{-\infty}^{\infty} [B_{32}^{\pm}(\nu',\nu)\, n_3(\nu',z) - B_{23}^{\pm}(\nu',\nu) n_2(\nu',z)]\, d\nu' - \alpha I^{\pm}(\nu,z) \mp \frac{\partial}{\partial z} I^{\pm}(\nu,z) = 0 \tag{1.3.1}$$

The formal solution for this differential equation is found to be

$$I^{\pm}(\nu,z) = \text{const} \times \exp\Big[\mp \alpha z \pm h\nu \int_0^z \int_{-\infty}^{\infty} \{ B_{32}^{\pm}(\nu',\nu)\, n_3(\nu',\xi) - B_{23}^{\pm}(\nu',\nu)\, n_2(\nu',\xi)\}\, d\nu'\, d\xi\Big] \tag{1.3.2}$$

If we assume that the field is monochromatic and single-mode we have

$$I^{\pm}(\nu',z) = I_{\nu}^{\pm}(z)\, \delta(\nu' - \nu) \tag{1.3.3}$$

Then, Eqs. (1.1.1) and (1.1.2) give the populations

$$n_3(\nu,z) = \frac{[(S_3(\nu) + S_2(\nu))\, B(\nu,z) + A_2 S_3(\nu)]}{[A_3 A_2 + (A_3 + A_2)\, B(\nu,z)]} \tag{1.3.4}$$

$$n_2(\nu,z) = \frac{[(S_3(\nu) + S_2(\nu))\, B(\nu,z) + A_3\, S_2(\nu)]}{[A_3 A_2 + (A_3 + A_2)\, B(\nu,z)]} \tag{1.3.5}$$

where

$$B(\nu,z) = B_{23}^{+}(\nu,\nu)\ I_{\nu}^{+}(z) + B_{23}^{-}(\nu,\nu)\ I_{\nu}^{-}(z) \tag{1.3.6}$$

The solution is then written as

$$I_{\nu}^{\pm}(z) = \text{const} \times \exp\left[\mp \alpha z \pm h\nu \int_{0}^{z}\int_{-\infty}^{\infty} \frac{B_{32}^{\pm}(\nu',\nu)\{A_2S_3(\nu') - A_3S_2(\nu')\}}{A_3A_2 + (A_3 + A_2)B(\nu',\xi)}\, d\nu' d\xi\right] \tag{1.3.7}$$

When a laser is operating at line center, it can easily be shown from the above that the product of the two intensities is a constant. That is,

$$I_{\nu_o}^{+}(z)\ I_{\nu_o}^{-}(z) = \text{constant} \tag{1.3.8}$$

This equation does not hold for $\nu \neq \nu_o$.

A typical cavity configuration is shown in Fig. 1.2. One end mirror has transmission T and reflectance R , while the other has one hundred percent reflectance. We have to solve Eqs. (1.3.4) through (1.3.7) subject to the boundary conditions

$$I_{\nu}^{+}(0) = I_{\nu}^{-}(0) \tag{1.3.9}$$

$$I_{\nu}^{-}(L)/I_{\nu}^{+}(L) = R \tag{1.3.10}$$

Even in the Doppler limit, we cannot solve the equations. When $B_{32}^{\pm}(\nu,\nu)$ has a finite line width, it is almost impossible to obtain a general solution for arbitrary ν , $\overline{N}$ and $\Delta\nu_D$ analytically. We resort thus to a numerical solution of these equations.

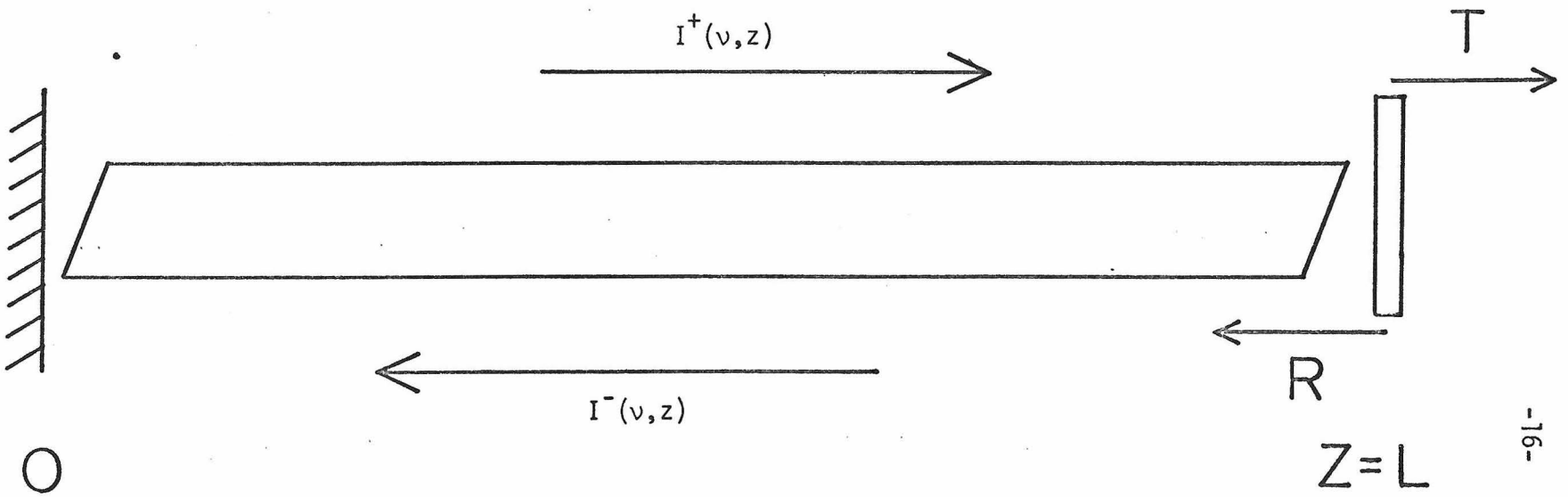

Fig. 1.2 A traveling wave laser

Before proceeding to the numerical calculations, we pause to discuss the threshold condition. By letting $I_\nu^+(z)$ and $I_\nu^-(z)$ go to zero simultaneously in Eq. (1.3.7), we find the following threshold pumping density:

$$\bar{N}_T = \frac{2\alpha L - \ell n\, R}{h\nu \dfrac{2LB_{32}}{u\sqrt{\pi}} \displaystyle\int_{-\infty}^{\infty} L(\nu_0, v') e^{-v'^2/u^2} dv'} \tag{1.3.11}$$

Using the parameters appropriate to the Xe 3.51 micron transition[9], i.e., $\Delta\nu_N = 3.73$ MHz and $\Delta\nu_D = 115$ MHz, $\bar{N}_T$ is approximated by

$$\bar{N}_T \sim 1.2 \times 10^8 (\alpha - \frac{\ell n\, R}{2L})\ \text{cm}^{-3}\ \text{sec}$$

We have solved Eqs. (1.3.6) and (1.3.7) simultaneously with the boundary conditions (1.3.9) and (1.3.10) using a numerical iteration method. We used the IBM 370 computer at the California Institute of Technology. A detailed description is given in Appendix A. The computed output power vs detuning $\Delta\nu = \nu - \nu_0$ is shown in Fig. 1.3 for mirror of 30% reflectivity, and for one pass gain 2. The depth of the Lamb dip is 47% in the figure, but a much smaller value was observed experimentally. Figure 1.4 shows calculated output power vs mirror reflectance for the various losses with the arrangement of Fig. 1.2. These values were obtained at line center $\nu = \nu_0$, assuming $R+T = 1$.

(B) Experiment on measurement of the output power at line center

The experiment was conducted using the Xe 3.51μ line[10,11,12]. The length of cavity was 1.25m with the discharge section 1.10 m long

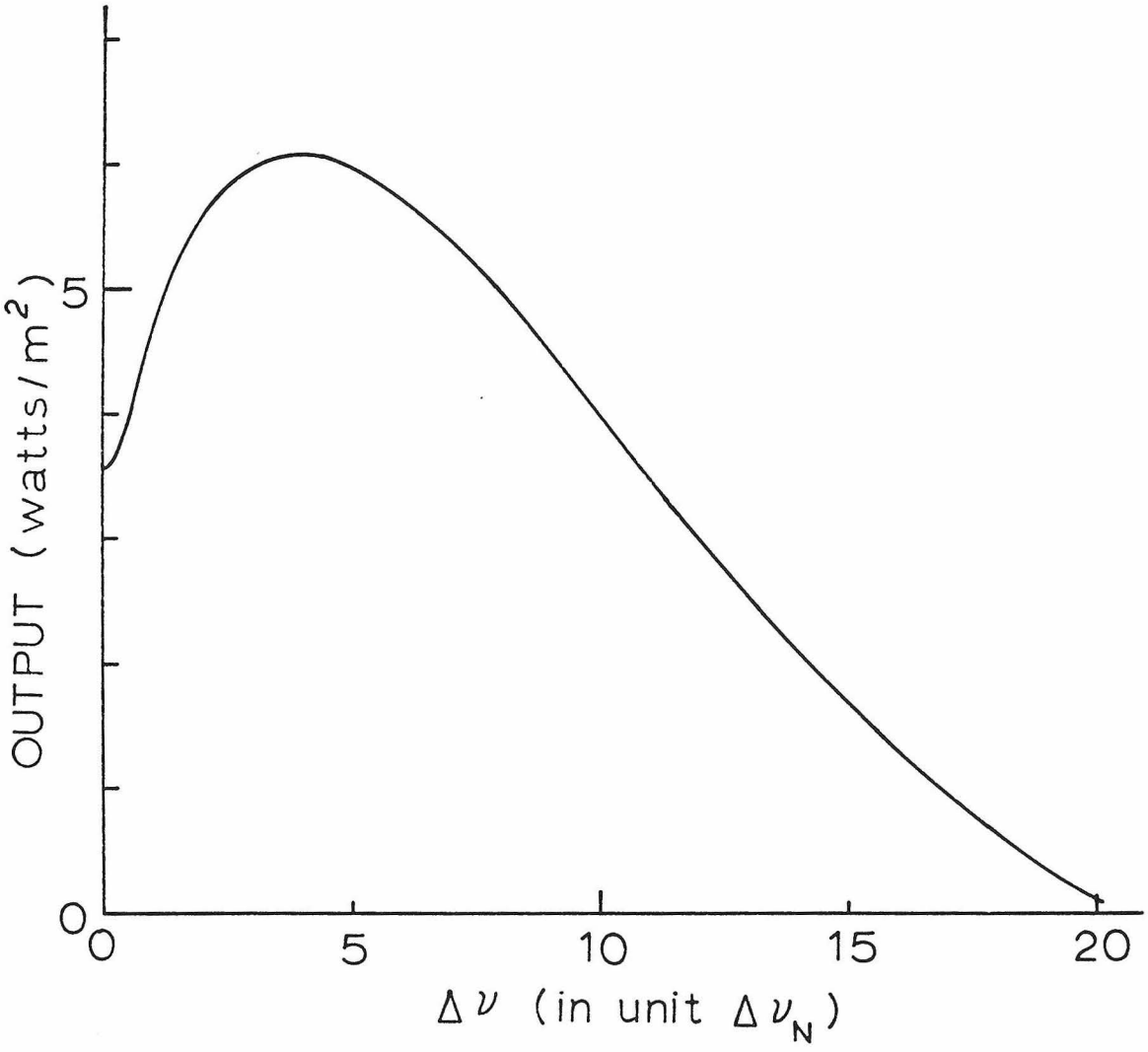

Fig. 1.3 Computed output power from traveling wave laser

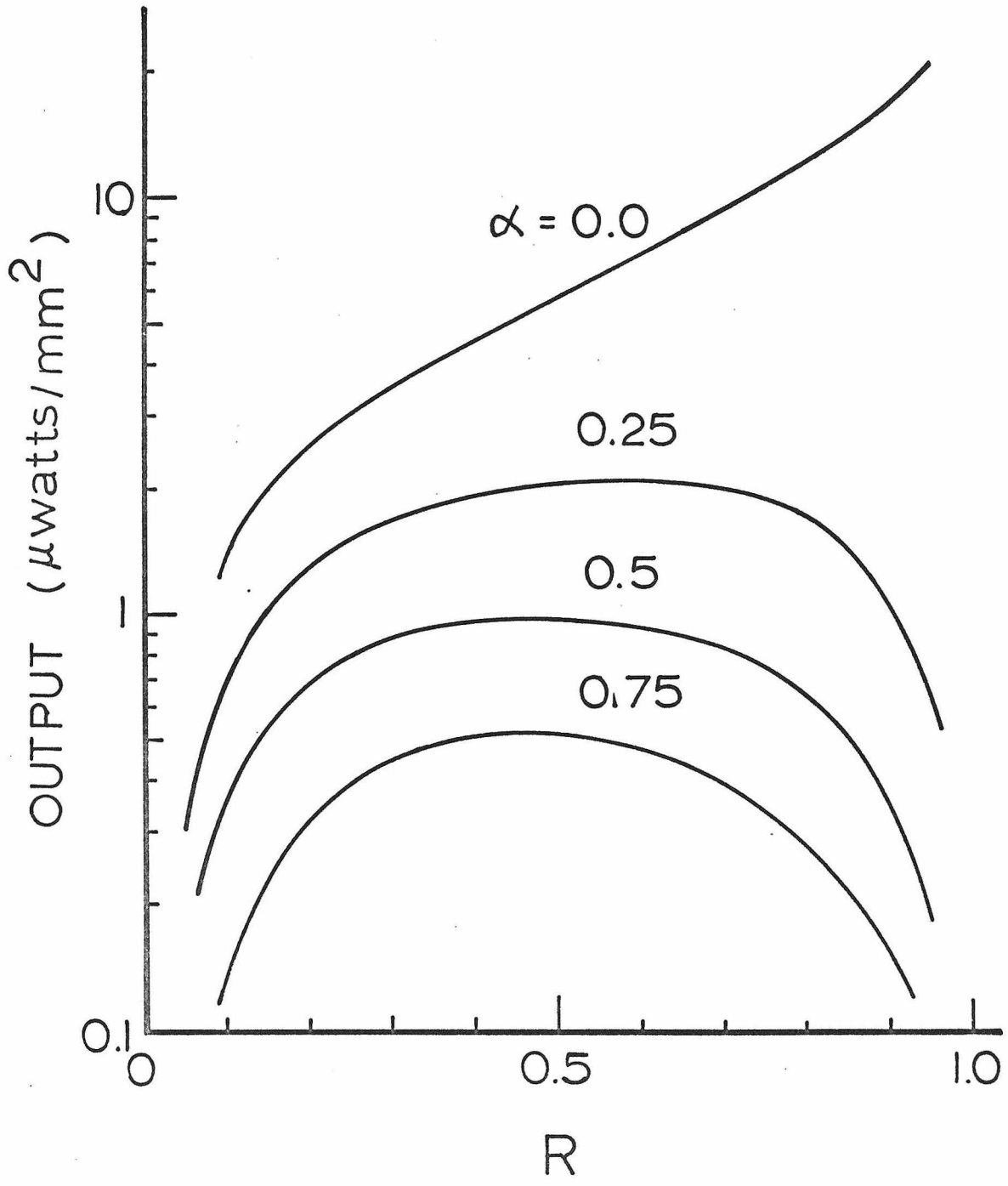

Fig. 1.4 Calculated output vs mirror reflectance. α is the loss per one pass.

and 5.5 mm in diameter. The excitation was done by d.c. discharge. The pressure of the Xe gas was kept approximately at 5×10^{-3}Torr by a liquid nitrogen trap[13]. The cavity was set up on a stable iron table supported on inner tubes. The experimental configuration is shown in Fig. 1.5.

We made mirrors by evaporating gold on microscope slides. Since we could not control the thickness of the thin films, we made many samples and chose those with appropriate reflectivities.

One of the mirrors of the cavity was scanned over a distance of about 5 μm, using a piezo-electric transducer driven by a saw-tooth voltage. The output was chopped at 200 Hz and focused on a PbS detector followed by a PAR lock-in amplifier, Model HR-8. The signal was recorded on paper and the power at Lamb dip was measured. We corrected the output using the following expression:

$$P_{corrected} = \frac{1 - R_{measured}}{T_{measured}} P_{measured}$$

where $R_{measured}$ is the measured reflectivity of the mirror and $T_{measured}$ is that of the transmittance.

The corrected data are shown in Fig. 1.6. The agreement with the theory of this section (see Fig. 1.4) is not satisfactory. Probably the discrepancies come from difficulty in aligning the laser, and also uncertainty in mirror reflection and transmission.

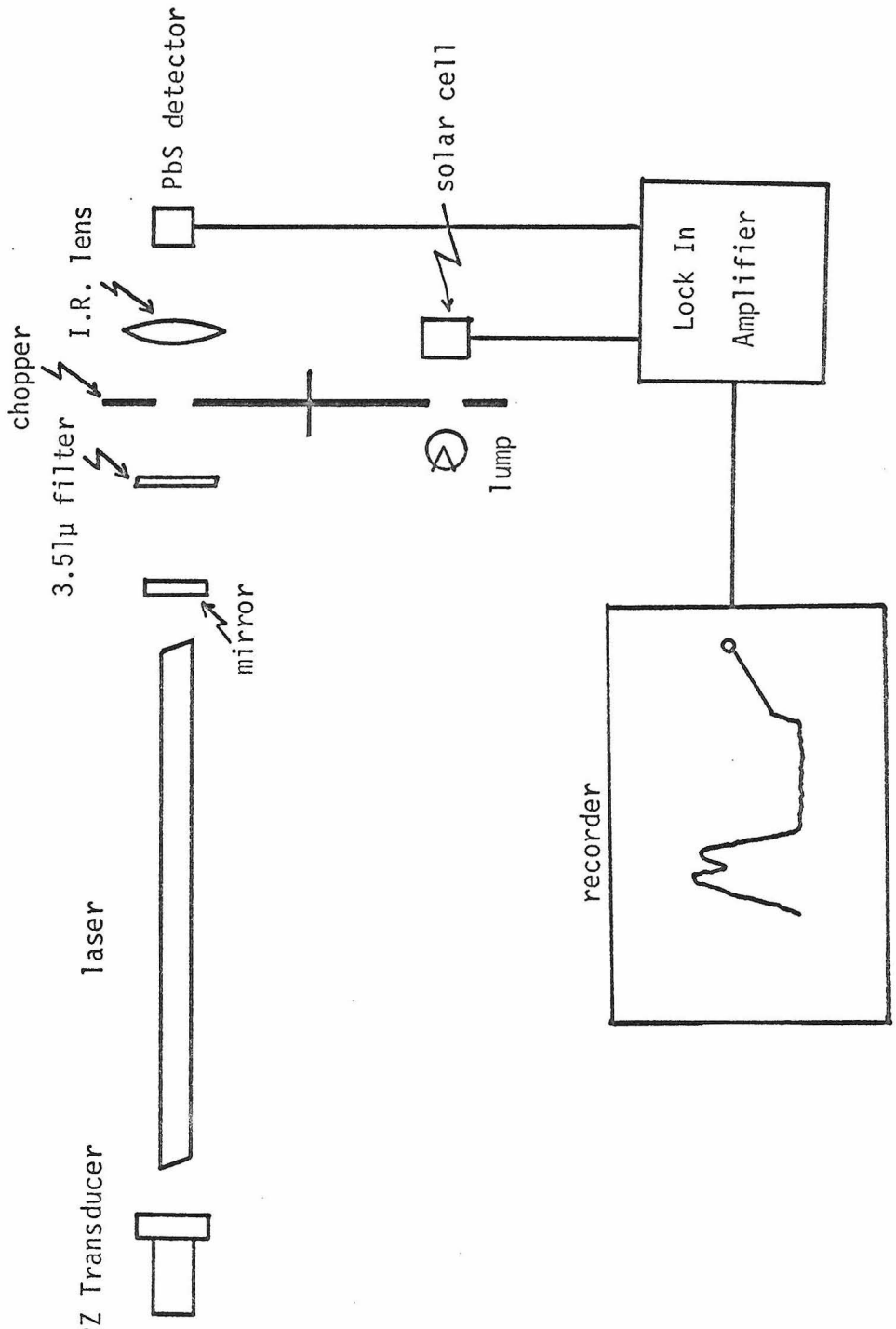

Fig. 1.5 Experimental set up for recording the output power of a traveling wave laser

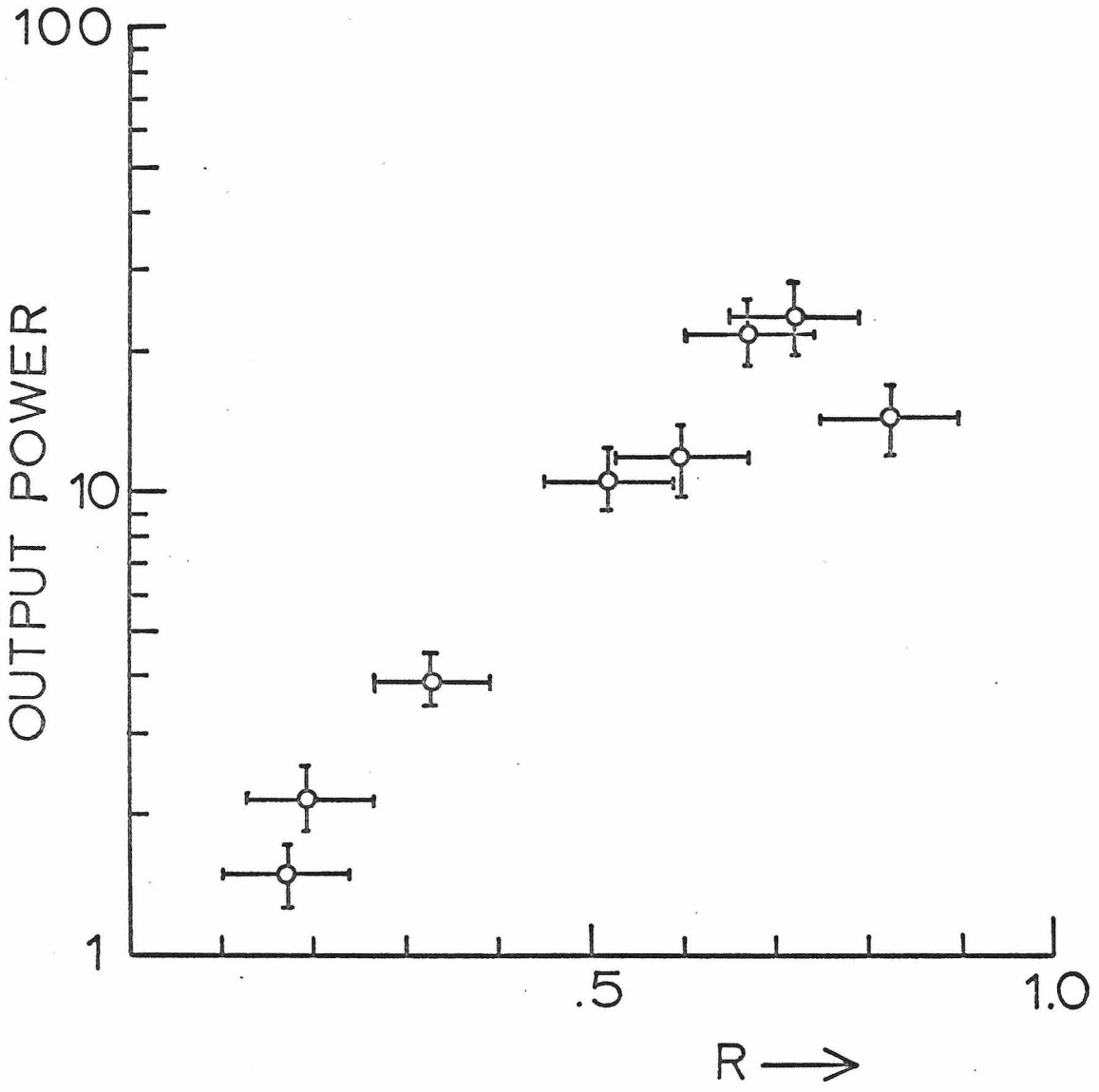

Fig. 1.6 Corrected output power (arbitrary units) from a traveling wave laser vs. reflectivity of a mirror

1.4 A Superradiant Laser

The problem of line narrowing and rebroadening in high gain masers is of great interest; in particular also with respect to astrophysical applications, where the optical path length can be considerable[14].

Superradiance is defined as a cooperative decay of atoms[15-18] under the influence of a common radiation field. Hence all the atoms cannot be treated as independent. However, we are considering here an active medium with dimensions much larger than the interatomic distance, which is in turn much greater than the wavelength of the field. A photon, which is produced by spontaneous emission, may travel many wavelengths before it interacts with another atom. The spatial phase coherence of the induced dipoles which is a prerequisite to cooperative phenomena is lacking also, due to the large transverse cross section. Each atom thus sees only the local field at its position which is assumed to be uncorrelated with that at other atomic positions[15]. We also assume that the spontaneous emission of each atom occurs independently of the other atoms. We will treat this problem using the rate equations.

(A) Theory

The spectral intensity of spontaneous emission in a gas is Doppler broadened. The resultant amplified spontaneous emission spectral intensities $I^{+}(\nu,z)$ and $I^{-}(\nu,z)$ have a finite spectral width. Therefore, it becomes far more difficult to solve the rate equations than in the previous examples. Assumptions (ii) and (iii) in Section 1.2 have to be eliminated. Assuming no external input, the boundary

conditions are

$$I^{+}(\nu,-L) = 0$$

$$I^{-}(\nu,L) = 0 \qquad (1.4.1)$$

where $2L$ is the length of superradiant laser, and the origin of coordinate z is taken at the center. The configuration of the laser is shown in Fig. 1.7. The second term in Eq. (1.1.9), $h\nu \int_{-\infty}^{\infty} A_{32}^{\prime\pm}(v,\nu) n_3(v,z)dv$, is the source of the field. $A_{32}^{\prime\pm}(v,\nu)$ is proportional to η which gives the probability that a spontaneously emitted photon joins either $I^{+}(\nu,z)$ or $I^{-}(\nu,z)$ as mentioned in Section 1.1. η may depend on z , but it is very difficult to analyze the case where there is reflection from the dielectric wall (Fig. 1.8), or where focusing effects[19] come in. Instead of using $\eta = \eta(z)$, we will use $\eta_{eff} = \text{const}$, the effective η for all z .

Taking into account the spontaneous emission term A_{32} , one finds the following from Eqs. (1.1.1) and (1.1.2):

$$n_3(v,z) = \frac{A_2 S_3(v) + (S_3(v) + S_2(v))\, B(v,z)}{A_3 A_2 + (A_3 + A_2 - A_{32})\, B(v,z)} \qquad (1.4.2)$$

$$n_2(v,z) = \frac{A_3 S_2(v) + A_{32} S_3(v) + (S_3(v) + S_2(v))\, B(v,z)}{A_3 A_2 + (A_3 + A_3 - A_{32})\, B(v,z)} \qquad (1.4.3)$$

where

$$B(v,z) = \int_{0}^{\infty} \{B_{23}^{+}(v,\nu') I^{+}(\nu',z) + B_{23}^{-}(v,\nu') I^{-}(\nu',z)\}\, d\nu' \qquad (1.4.4)$$

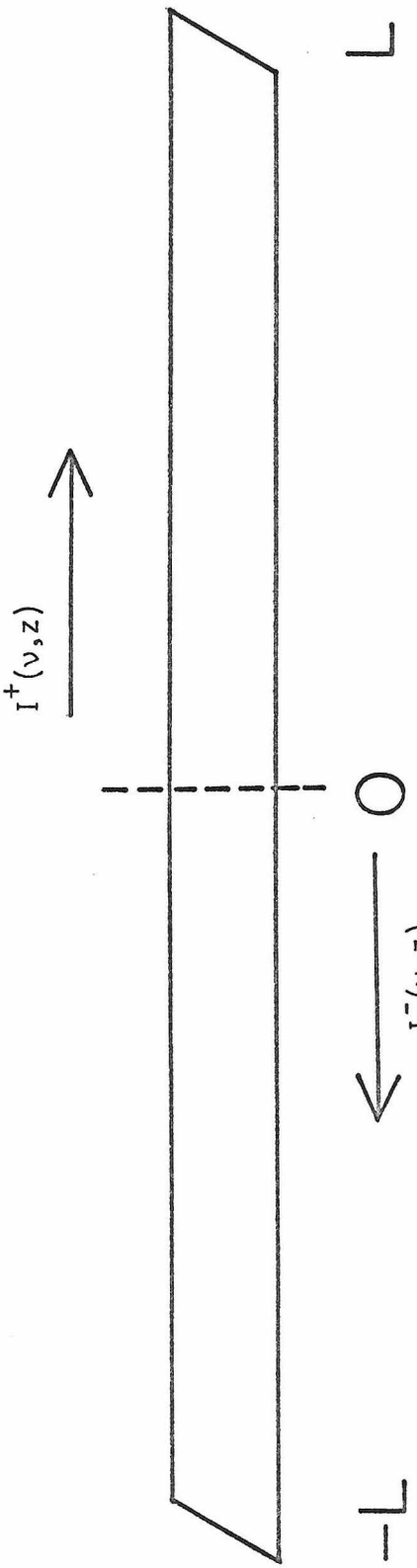

Fig. 1.7 One pass superradiance

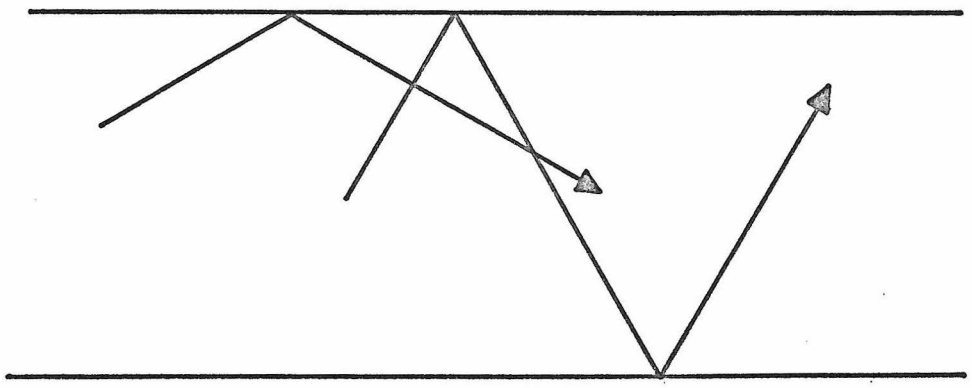

Fig. 1.8 Photons are reflected at the wall and propagate bouncing between the walls.

With the substitutions

$$g(\nu,z) = h\nu \int_{-\infty}^{\infty} \{B_{32}^{\pm}(\nu',\nu)n_3(\nu',z) - B_{23}^{\pm}(\nu',\nu)n_2(\nu',z)\}\, d\nu' \qquad (1.4.5)$$

$$h(\nu,z) = h\nu \int_{-\infty}^{\infty} A_{32}^{\pm}(\nu',\nu)n_3(\nu',z)\, d\nu' \qquad (1.4.6)$$

Eq. (1.1.9) becomes simplified to

$$h(\nu,z) + g(\nu,z)I^{\pm}(\nu,z) - \alpha I^{\pm}(\nu,z) \mp \frac{\partial}{\partial z} I^{\pm}(\nu,z) = 0 \qquad (1.4.7)$$

The plus and minus superscripts on $g(\nu,z)$ (m^{-1}) and $h(\nu,z)$(watt m^{-3} sec) are dropped because both signs give the same values on the right hand sides of Eqs. (1.4.5) and (1.4.6). Solutions satisfying the boundary conditions (1.4.1) are formally

$$I^{+}(\nu,z) = \int_{-L}^{z} h(\nu,\xi) \exp\{\int_{\xi}^{z} (g(\nu,\zeta) - \alpha)\, d\zeta\}\, d\xi \qquad (1.4.8)$$

$$I^{-}(\nu,z) = \int_{z}^{L} h(\nu,\xi) \exp\{\int_{z}^{\xi} (g(\nu,\zeta) - \alpha)\, d\zeta\}\, d\xi \qquad (1.4.9)$$

These results show that spontaneous emission originating at the position $\xi < z$ is amplified exponentially by a factor $\exp\{\int_{\xi}^{z} (g(\nu,\zeta) - \alpha)\, d\zeta\}$. The net intensity of the right going wave at z is given by the sum of all amplified spontaneous emissions initiated between $-L$ and z.

(B) Application of the formula

(i) Unsaturated region

It is well known[20,21,22,23] that the spectral profile of amplified spontaneous emission narrows as a function of distance towards the line center. In the unsaturated region, the intensity of the field is so weak that it does not affect the population inversion. As a result, even though the intensity of the superradiance may vary with position, we may take $n_3(v,z)$ and $n_2(v,z)$ as independent of z. Under this condition they are given by

$$n_3(v)_{unsat} = \frac{S_3(v)}{A_3} \tag{1.4.10}$$

$$n_2(v)_{unsat} = \frac{S_2(v)}{A_2} + \frac{A_{32}}{A_3 A_2} S_3(v) \tag{1.4.11}$$

where the subscript "unsat" means the quantity in the unsaturated region. With the help of the above relations, we get the unsaturated gain and spontaneous emission rate as

$$h(\nu)_{unsat} = h\nu \int_{-\infty}^{\infty} A^{\pm}(\nu',\nu) \frac{S_3(\nu')}{A_3} d\nu' \tag{1.4.12}$$

$$g(\nu)_{unsat} = h\nu \int_{-\infty}^{\infty} B_{32}^{\pm}(\nu',\nu) \frac{(A_2 - A_{32})S_3(\nu') - A_3 S_2(\nu')}{A_3 A_2} d\nu' \tag{1.4.13}$$

Equation (1.4.8) is integrated to give

$$I^{+}(\nu,L)_{unsat} = \frac{h(\nu)_{unsat}}{g(\nu)_{unsat} - \alpha} [\exp 2(g(\nu)_{unsat} - \alpha)L - 1] \tag{1.4.14}$$

If $g(\nu)_{unsat} >> \alpha$, we may neglect α on the right hand side. In the unsaturated region, $g(\nu)_{unsat}$ and $h(\nu)_{unsat}$ are proportional to

$$\int_{-\infty}^{\infty} \frac{e^{-v'^2/u^2}}{1 + [2(\nu - \nu_o + kv'/2\pi)/\Delta\nu_N]^2} dv'$$

Defining the frequency $\nu_{1/2}$ such that $I^+(\nu_{1/2},L)_{unsat}$ is one-half the intensity at line center, we find that $\nu_{1/2}$ satisfies the following:

$$\frac{1}{2} = \frac{I^+(\nu_{1/2},L)_{unsat}}{I^+(\nu_o,L)_{unsat}} = \frac{\exp\{2L\ g(\nu_{1/2})_{unsat}\} - 1}{\exp\{2L\ g(\nu_o)_{unsat}\} - 1}$$

$$\sim \exp 2L\ \{g(\nu_{1/2})_{unsat} - g(\nu_o)_{unsat}\} \quad (1.4.15)$$

We discuss two limiting cases. First, when the medium is inhomogeneously broadened, $g(\nu)_{unsat}$ is given by

$$g(\nu)_{unsat} = k_o \exp\{-\frac{4\ \ell n\ 2}{\Delta\nu_D^2}\ (\nu - \nu_o)^2\} \quad (1.4.16)$$

k_o (m^{-1}) is the unsaturated gain at the resonance. From Eq. (1.4.15) we get

$$\exp\{-\frac{4\ \ell n\ 2}{\Delta\nu_D^2}\ (\nu_{1/2} - \nu_o)^2\} - 1 \simeq -\frac{\ell n\ 2}{2Lk_o} \quad (1.4.17)$$

Expanding the exponential and taking the first power on the left hand side of the above relation, we find the full width at half maximum (FWHM) $\Delta\nu_{inhom}$ to be

$$\Delta\nu_{inhom} \sim \frac{\Delta\nu_D}{\sqrt{x_o}} \tag{1.4.18}$$

x_o (dimensionless) is the exponential gain given by

$$x_o = 2Lk_o \tag{1.4.19}$$

and is thus equal to the single pass unsaturated gain at line center expressed in nepers.

Second, in the homogeneously broadened case, $g(\nu)_{unsat}$ is given by

$$g(\nu)_{unsat} = \frac{k_o}{1 + [2(\nu - \nu_o)/\Delta\nu_N]^2} \tag{1.4.20}$$

Similarly one finds the FWHM $\Delta\nu_{homo}$ for the homogeneous case[22] to be

$$\Delta\nu_{homo} \sim \sqrt{\frac{\ell n\ 2}{x_o}}\ \Delta\nu_N \tag{1.4.21}$$

(ii) Transition region

Many authors have discussed spectral narrowing in a high gain medium[20-23], but none have considered spectral narrowing in which the simultaneous presence of the oppositely traveling radiation fluxes.

The existing theories predict rebroadening of the spectrum after saturation sets in. So far, two reasons have been considered to be the cause of rebroadening. First, in a Doppler broadened medium, a spontaneous photon near line center is amplified more strongly than photons near the wings of the spectrum. This is the mechanism responsible for the narrowing of the amplified spontaneous emission spectrum.

Saturation, consequently, sets in at line center first, and gradually spreads toward the wings as the light propagates through the medium. After the onset of saturation, amplification at the wings is greater than at line center. This reverses the narrowing process and, finally, the spectral profile returns to the original spontaneous emission profile.

A second cause of rebroadening has to do with the fact that there actually exist two oppositely traveling waves in the pencil shaped medium. After sufficient amplification, each traveling wave burns a hole in the inversion profile which amplifies the wave propagating in the opposite direction. This causes broadening by the same mechanism as that described above. This hole burning effect accelerates the rebroadening.

Once saturation becomes important, we cannot take $n_3(v,z)$ and $n_2(v,z)$ to be independent of z, as in the unsaturated case. The term $B(v,z)$ in Eq. (1.4.4) has to be considered. In discussing this problem, it is useful to make the following substitutions:

$$y \equiv (\nu - \nu_o)/\Delta\nu_N \tag{1.4.22}$$

$$\beta \equiv \frac{kv}{2\pi\Delta\nu_N} = \frac{\nu}{\Delta\nu_N}\ \frac{v}{c} \tag{1.4.23}$$

$$x \equiv k_o(z + L) \tag{1.4.24}$$

$$\varepsilon \equiv 2\sqrt{\ell n\ 2}\ \Delta\nu_N/\Delta\nu_D \tag{1.4.25}$$

$$\alpha' \equiv \alpha/k_o \tag{1.4.26}$$

and also to define the dimensionless functions:

$$g(\nu,z) \equiv \frac{h\nu\, B_{32}}{\Delta\nu_N}\left\{\left(\frac{1}{A_3} - \frac{A_{32}}{A_3A_2}\right)S_{30} - \frac{S_{20}}{A_2}\right\}\tilde{g}(y,x) \tag{1.4.27}$$

$$h(\nu,z) \equiv \frac{\eta h\nu\, A_{32}}{\Delta\nu_N}\frac{S_{30}}{A_3}\,\tilde{h}(y,x) \tag{1.4.28}$$

$$I^{+}(\nu,z) \equiv \frac{\eta h\nu\, A_{32}S_{30}}{\Delta\nu_N A_3 k_o}\,\tilde{I}(y,x) \tag{1.4.29}$$

$$I^{-}(\nu,z) \equiv \frac{\eta h\nu\, A_{32}S_{30}}{\Delta\nu_N A_3 k_o}\,\tilde{I}(y,x_o-x) \tag{1.4.30}$$

Using the expressions (1.4.2) to (1.4.9), we have the following relations:

$$\tilde{g}(y,x) = \frac{2\varepsilon}{\pi^{3/2}}\int_{-\infty}^{\infty}\frac{e^{-\varepsilon^2\beta^2}}{1+4(y-\beta)^2}\,\frac{d\beta}{1+s\tilde{B}(\beta,x)/g_o} \tag{1.4.31}$$

$$\tilde{h}(y,x) = \frac{2\varepsilon}{\pi^{3/2}}\int_{-\infty}^{\infty}\frac{e^{-\varepsilon^2\beta^2}}{1+4(y-\beta)^2}\,\frac{1+t\tilde{B}(\beta,x)/g_o}{1+s\tilde{B}(\beta,x)/g_o}\,d\beta \tag{1.4.32}$$

$$\tilde{I}(y,x) = \int_0^x \tilde{h}(y,\xi)\,\exp\left[\int_\xi^x \{\tilde{g}(y,\zeta)/g_o - \alpha'\}\,d\zeta\right]\,d\xi \tag{1.4.33}$$

where

$$\tilde{B}(\beta,x) = \frac{2}{\pi}\int_{-\infty}^{\infty}\left\{\frac{\tilde{I}(y,x)}{1+4(y-\beta)^2} + \frac{\tilde{I}(y,x_o-x)}{1+4(y+\beta)^2}\right\}\,dy \tag{1.4.34}$$

$$g_o = \frac{2\varepsilon}{\pi^{3/2}}\int_{\infty}^{\infty}\frac{e^{-\varepsilon^2\beta^2}}{1+4\beta^2}\,d\beta \tag{1.4.35}$$

s and t are given by

$$s = \eta \frac{A_{32}}{A_3} \frac{A_2 + A_3 - A_{32}}{A_2} \frac{S_{30}}{A_3} \left\{ \left(\frac{1}{A_3} - \frac{A_{32}}{A_3 A_2} \right) S_{30} - \frac{S_{20}}{A_2} \right\}^{-1} \qquad (1.4.36)$$

$$t = \eta \frac{A_{32}}{A_3} \frac{S_{30} + S_{20}}{A_2} \left\{ \left(\frac{1}{A_3} - \frac{A_{32}}{A_3 A_2} \right) S_{30} - \frac{S_{20}}{A_2} \right\}^{-1} \qquad (1.4.37)$$

In a typical lasing medium, $A_3 << A_2$ and $S_{30}/A_3 >> S_{20}/A_2$. (This is a necessary condition for population inversion). With these approximations, Eqs. (1.4.36) and (1.4.37) simplify to

$$s \sim \eta\delta \qquad (1.4.38)$$

$$t \sim \frac{A_3}{A_2} s \qquad (1.4.39)$$

where

$$\delta = A_{32}/A_3 \qquad (1.4.40)$$

As may easily be seen from expressions (1.4.31) and (1.4.32), s and t determine the degree of saturation, once the dimensionless spectral density $\tilde{I}(y,x)$ is given. Since s is A_2/A_3 times larger than t, we may define s as a saturation parameter. We will call $s\tilde{B}(\beta,x)/g_0$ a saturation term. Saturation is determined by what fraction of the total spontaneous decays from the upper state contributes to the superradiance. For example if s is nearly equal to zero, most of the spontaneous photons escape and the intensity of amplified spontaneous emission is small. On the other hand, if s is close to unity, most of the spontaneous emission joins the superradiance and the saturation sets in at small x.

When the output power spectrum has a much wider spectral width than the natural line width $\Delta\nu_N$, we have

$$\tilde{B}(\beta,x_o)\Big|_{\beta=0} = \frac{2}{\pi}\int_{-\infty}^{\infty}\frac{\tilde{I}(y,x_o)}{1+4y^2}\,dy$$

$$\simeq \tilde{I}(0,x_o)$$

The saturation term for the group of atoms with velocity zero in Eqs. (1.4.31) and (1.4.32) is rewritten

$$s\tilde{B}(0,x_o)/g_o = \frac{A_3+A_2-A_{32}}{A_3A_2}B_{32}\,I^+(0,L)$$

$$= I^+(0,L)/I_s \qquad (1.4.41)$$

where

$$I_s = \frac{8\pi h\nu^3 A_3A_2}{c^2(A_3+A_2-A_{32})A_{32}}$$

$$= \frac{8\pi h\nu}{\lambda^2\phi}$$

$$\phi = \frac{A_{32}(A_3+A_2-A_{32})}{A_3A_2} \qquad (1.4.42)$$

I_s is the saturation parameter for a monochromatic field[24].

The solution for Eqs. (1.4.31) to (1.4.35) in the Doppler limit is described by a transcendental equation given in Appendix B. We do not consider it here because of analytical difficulties in solving the equation, and also because the Doppler approximation is highly

questionable. In the Xe 3.51 micron transition, the FWHM is only ten times larger than the natural line width when x_0 is approximately 10. For this reason we undertook numerical calculations with the computer at the California Institute of Technology. The iteration method is the most suitable for our Xe superradiance problem. A detailed description is given in Appendix C. Since we had no information about η, the parameters were varied from 10^{-4} to 10^{-16} in steps of 10^{-4}. Owing to the limited capacity of the computer, we did not calculate cases for which x_0 was greater than 50. The convergence was reached after almost six iterations.

We made use of the atomic parameters appropriate to the Xe 3.51 micron line, i.e., $\Delta\nu_N$ = 3.73 MHz and $\Delta\nu_D$ = 115 MHz. Calculated profiles at different positions are shown in Fig. 1.9 for x_0 = 15 and $s = 10^{-6}$. Hole burning of the intensity profile due to the oppositely traveling wave can be seen at distances from the mirror up to $x \tilde{=} 5$. The FWHM at different positions with various saturation parameters are plotted in Fig. 1.10. The hole burning effect slows down the narrowing as s gets larger. The rebroadening becomes more evident. Figure 1.11 shows the FWHM of the output spectrum vs the total gain x_0 of the tube, for various s. Figure 1.12 is the total output power vs x_0 for different s. Tick marks on the curves indicate turning points of the FWHM of the spectrum.

(iii) Saturation region

As already mentioned, the spectral profile becomes rebroadened after the onset of saturation. Thus, we may assume $I^+(\nu, z)$ has a

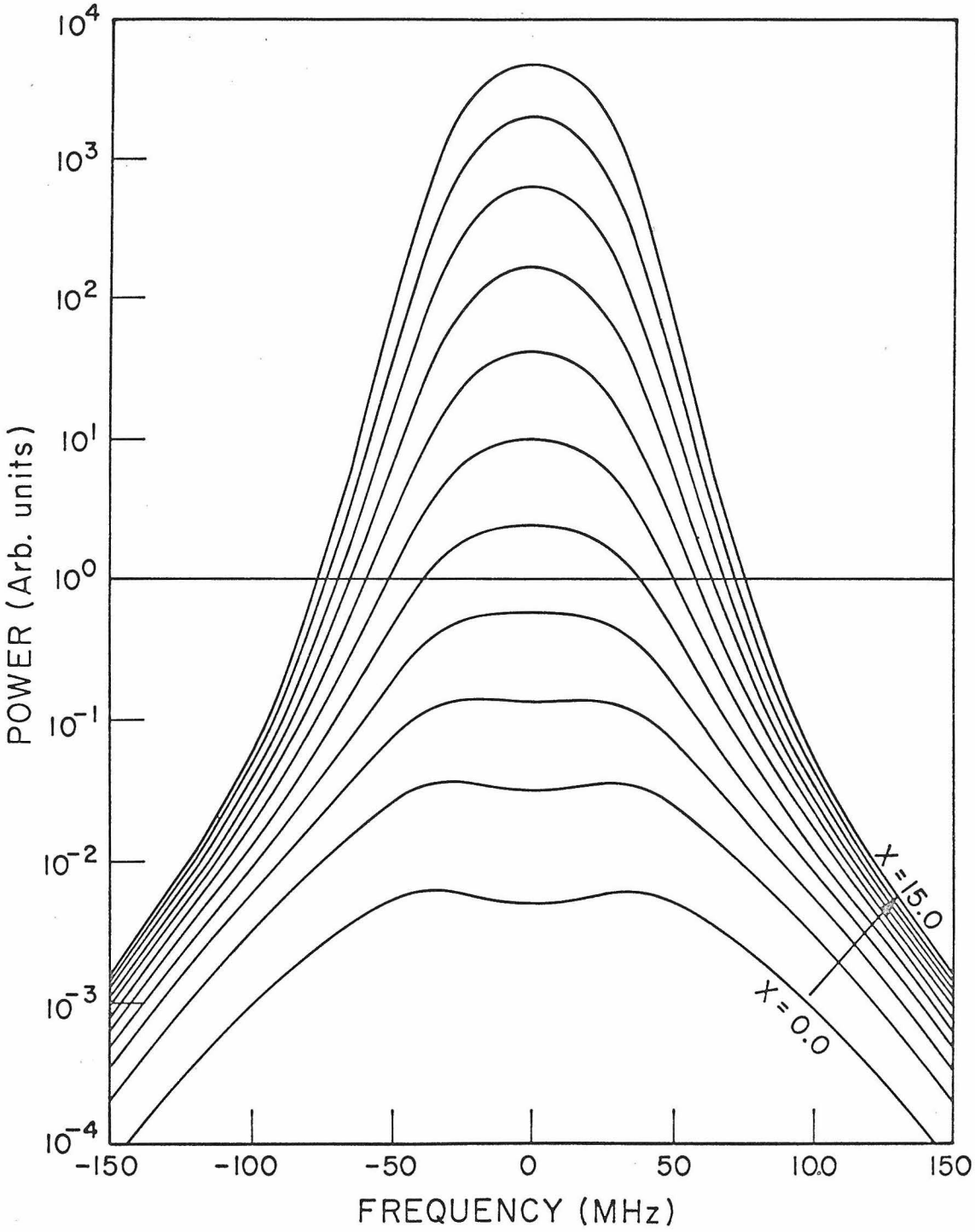

Fig. 1.9. Intensity profile at different positions x, for $x_0 = 15$ and $\delta\eta = 10^{-6}$

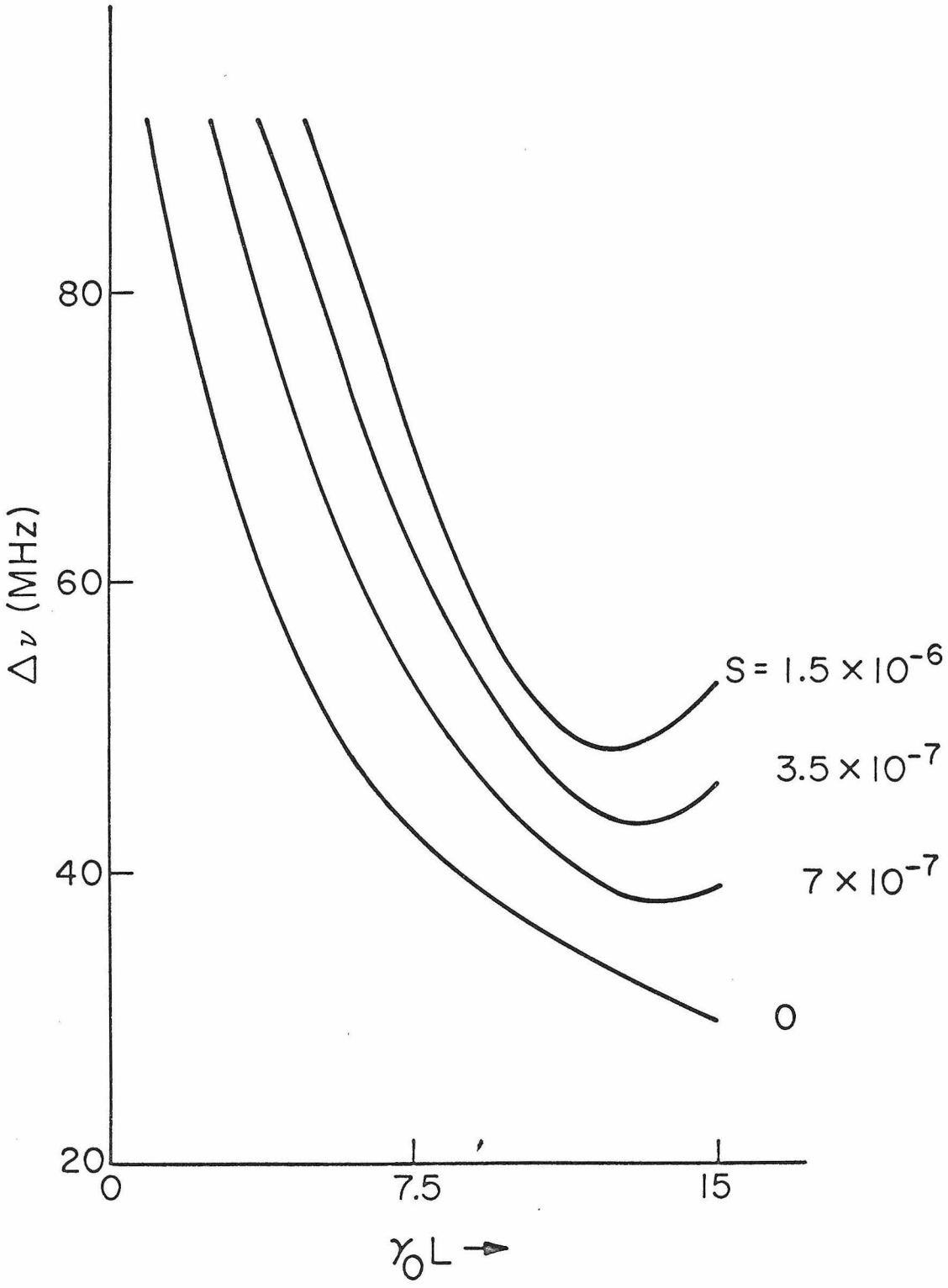

Fig. 1.10 The FWHM at different positions with different $s = \delta\eta$

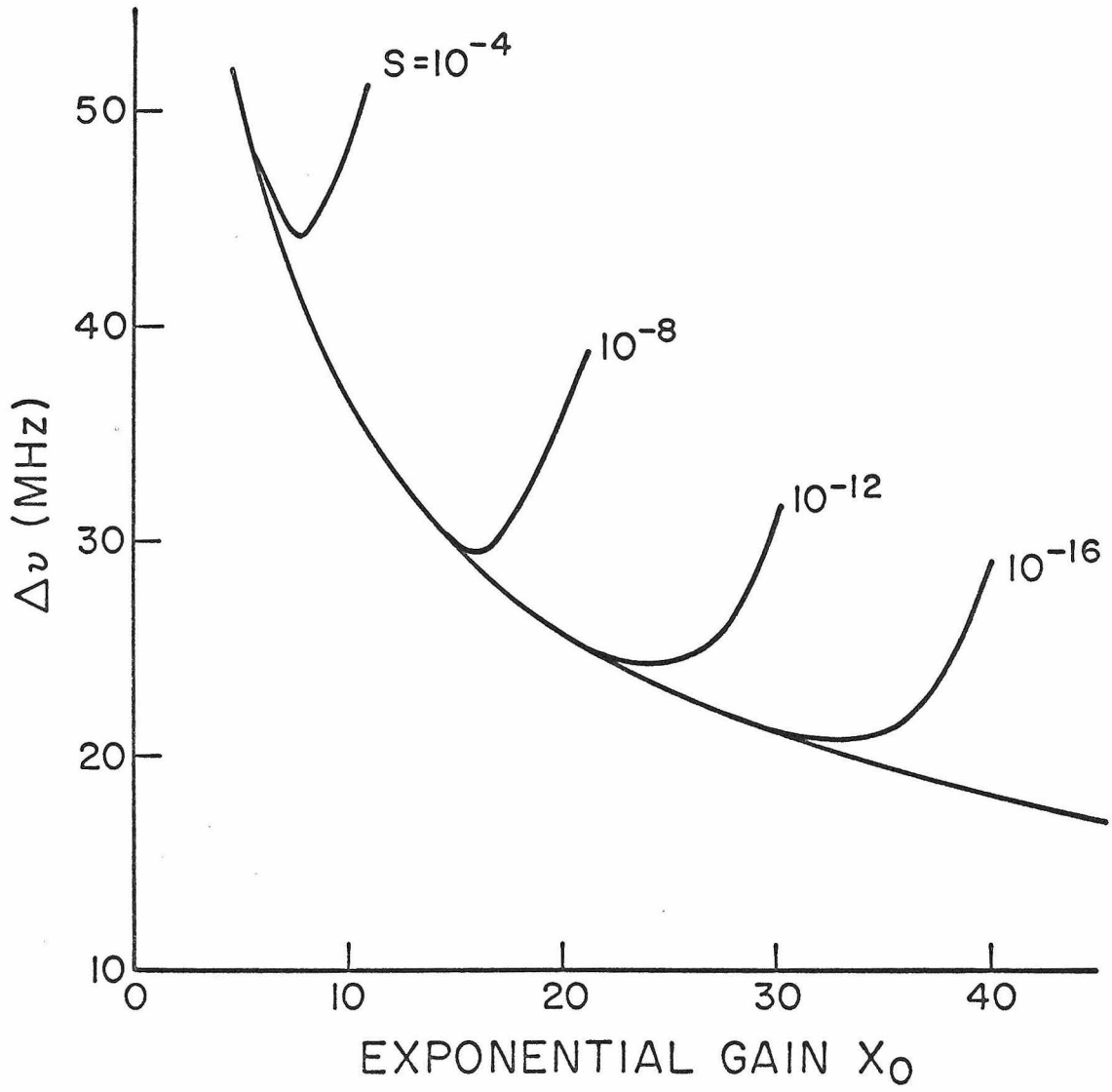

Fig. 1.11 The FWHM of the output spectrum for different saturation parameters $x_0 = 2k_0L$ where $2L$ is the length of the tube and k_0 is the unsaturated exponential gain constant

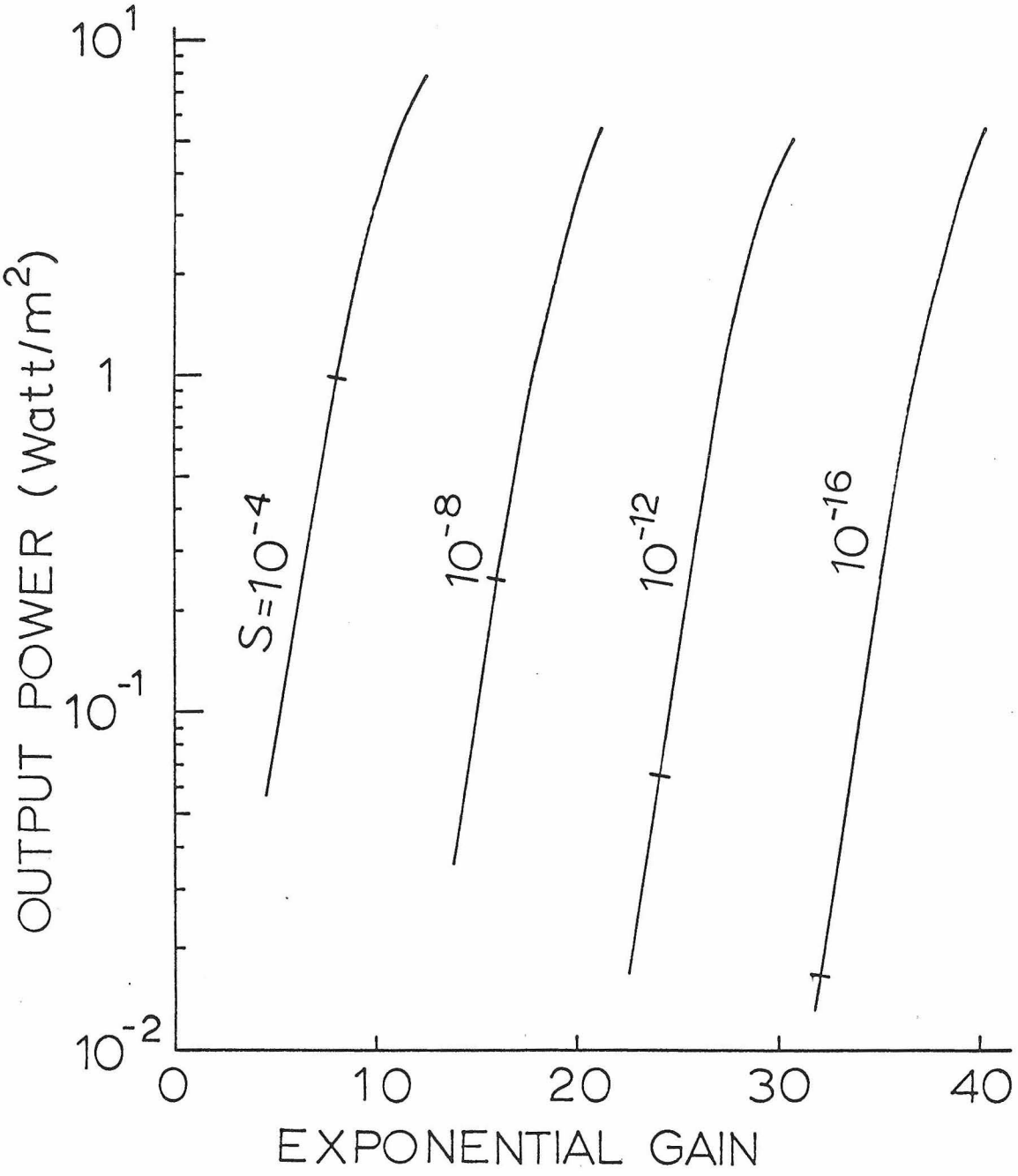

Fig. 1.12 The computed total output power vs x_o

much wider spectrum than the natural line width in the saturation regime. With this assumption we may determine from Eq. (1.4.34) that

$$\tilde{B}(\beta,x)_{sat} \cong \tilde{I}(\beta,x)_{sat} \tag{1.4.43}$$

where we assume near $x = x_o$,

$$I^+(\nu,x) >> I^-(\nu,x)$$

The subscript "sat" designates the quantities to be discussed in the saturation region. Also we have from Eq. (1.4.31) that

$$\tilde{g}(y,x)_{sat} \cong \frac{\varepsilon}{\sqrt{\pi}} \frac{e^{-\varepsilon^2 y^2}}{1 + s\tilde{I}(\beta,x)_{sat}/g_o} \tag{1.4.44}$$

Since in the fully saturated medium there is no net gain from stimulated emission, we may set the gain equal to the loss. Thus we have from Eq. (1.4.33)

$$\frac{e^{-\varepsilon^2 y^2}}{1 + s\tilde{I}(\beta,x)_{sat}/g_o} - \alpha' \cong 0 \tag{1.4.45}$$

After some algebraic manipulation, we find the FWHM $\Delta\nu_{sat}$ of the superradiance to be

$$\Delta\nu_{sat} \cong \frac{\ell n\ 2 - \ell n(1 + \alpha')}{\ell n\ 2} \Delta\nu_D \tag{1.4.46}$$

For the lossless case, the relation $\Delta\nu_{sat} \simeq \Delta\nu_D$ is well known[22]. When the loss is close to the line center gain, there is no amplification of spontaneous emission at the wings. Only photons near line

center are amplified. If it is possible to make $\alpha' \to 1$, we can have $\Delta\nu_{sat} \to 0$.

(C) A superradiant laser with a mirror at one end

A laser with only one mirror is frequently employed as a superradiant source. The mirror permits one to obtain a higher intensity from the device. Figure 1.13 shows the configuration of a superradiant laser, which we will briefly examine for the case where saturation is not important.

There is always some loss at the end mirror. Not all of the energy coming out of the laser is reflected back into the tube at $z = 0$. The boundary conditions for the laser are

$$I^-(\nu,L) = 0$$

$$I^+(\nu,0) = \Theta I^-(\nu,0) \tag{1.4.47}$$

Θ is the fraction of energy that is reflected back into the laser. By modifying Eqs. (1.4.8) and (1.4.9), we find the following:

$$I^-(\nu,z) = \int_z^L h(\nu,\xi)\, \exp\{\int_z^\xi (g(\nu,\zeta) - \alpha)\, d\zeta\}\, d\xi \tag{1.4.48}$$

$$I^+(\nu,z) = \int_0^z h(\nu,\xi)\, \exp\{\int_\xi^z (g(\nu,\zeta) - \alpha)\, d\zeta\}\, d\xi$$

$$+ \Theta I^-(\nu,0)\, \exp\{\int_0^z (g(\nu,\zeta) - \alpha)\, d\zeta\} \tag{1.4.49}$$

In the unsaturated region, the integrations can easily be carried out and we get

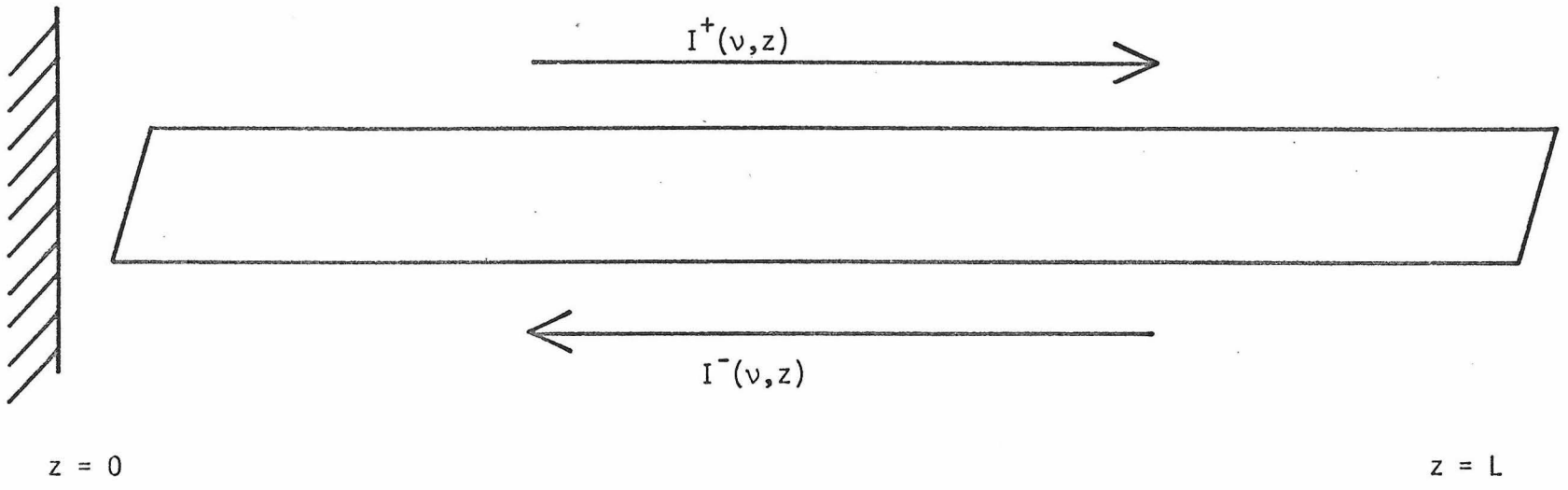

Fig. 1.13 Superradiant laser with one mirror on one end

$$I^{-}(\nu,z)_{unsat} = \frac{h(\nu)_{unsat}}{g(\nu)_{unsat} - \alpha} \left[e^{(g(\nu)_{unsat} - \alpha)(L-z)} - 1\right] \quad (1.4.50)$$

$$I^{+}(\nu,z)_{unsat} = \frac{h(\nu)_{unsat}}{g(\nu)_{unsat} - \alpha} \left[e^{(g(\nu)_{unsat} - \alpha)z} - 1 \right.$$

$$\left. + \theta\{e^{(g(\nu)_{unsat} - \alpha)L} - 1\} e^{\{g(\nu)_{unsat} - \alpha\}z}\right] \quad (1.4.51)$$

Then the output from the single-mirror superradiant laser is given by

$$I^{+}(\nu,L)_{unsat} = \frac{h(\nu)_{unsat}}{g(\nu)_{unsat} - \alpha} \left[e^{(g(\nu)_{unsat} - \alpha)L} - 1\right]$$

$$\left[1 + \theta\, e^{(g(\nu)_{unsat} - \alpha)L}\right] \quad (1.4.52)$$

If α is small compared to $g(\nu)_{unsat}$, we may neglect α in the above expression. Using the notation defined by Eq. (1.4.19), we have

$$I^{+}(\nu,L) = \frac{h(\nu)_{unsat}}{g(\nu)_{unsat}} \left[e^{x_o/2} - 1\right]\left[1 + \theta\, e^{x_o/2}\right] \quad (1.4.53)$$

For the inhomogeneously broadened case, the FWHM $\Delta\nu_{inhom}$ is written as

$$\Delta\nu_{inhom} \cong \begin{cases} \dfrac{\Delta\nu_D}{\sqrt{x_o/2}} & \text{for } \theta\, e^{x_o/2} \ll 1 \\ \dfrac{\Delta\nu_D}{\sqrt{x_o}} & \text{for } \theta\, e^{x_o/2} \gg 1 \end{cases} \quad (1.4.54)$$

(D) Experiment

It is difficult to measure amplified spontaneous emission from a high gain medium because of the presence of some nonresonant feedback[25] coming from the Brewster windows, the epoxy cement, and other components. The detector itself reflects undesirable light into the system. Even though elaborate care is taken to minimize this feedback, at some gain value the laser will start oscillating. We measured the spectral profile of the Xe 3.51 micron line, which has one of the highest gains known[10]. Because of this high gain, even a small amount of feedback causes the superradiant laser to oscillate.

We performed the experiment using three different discharge tubes. Tube 1 had a discharge length of 1.1 m and an inside diameter of 5.5 mm. There was a highly reflective silver mirror at one end. Tubes 2 and 3 had the same discharge length of 1.6 m, but with inner diameters 4.0 mm and 5.5 mm, respectively. We did not use any mirrors for these tubes. All three tubes were filled with the Xe 136 isotope. The liquid nitrogen trap kept the pressure at about 5×10^{-3} Torr. The excitation was done by d.c. discharge.

To measure the gain at line center, we fed a monochromatic signal derived from a reference xenon laser into the amplifier tube whose gain was measured. The intensity of output from the amplifier tube was compared with that of the input. To avoid frequency stability problems, we scanned one of the mirrors of the reference Xe laser, thus tuning the frequency of the source. The output power from the amplifier was measured at the Lamb dip. The setup is shown in Fig. 1.14. Figure 1.15 shows typical output power from the source laser

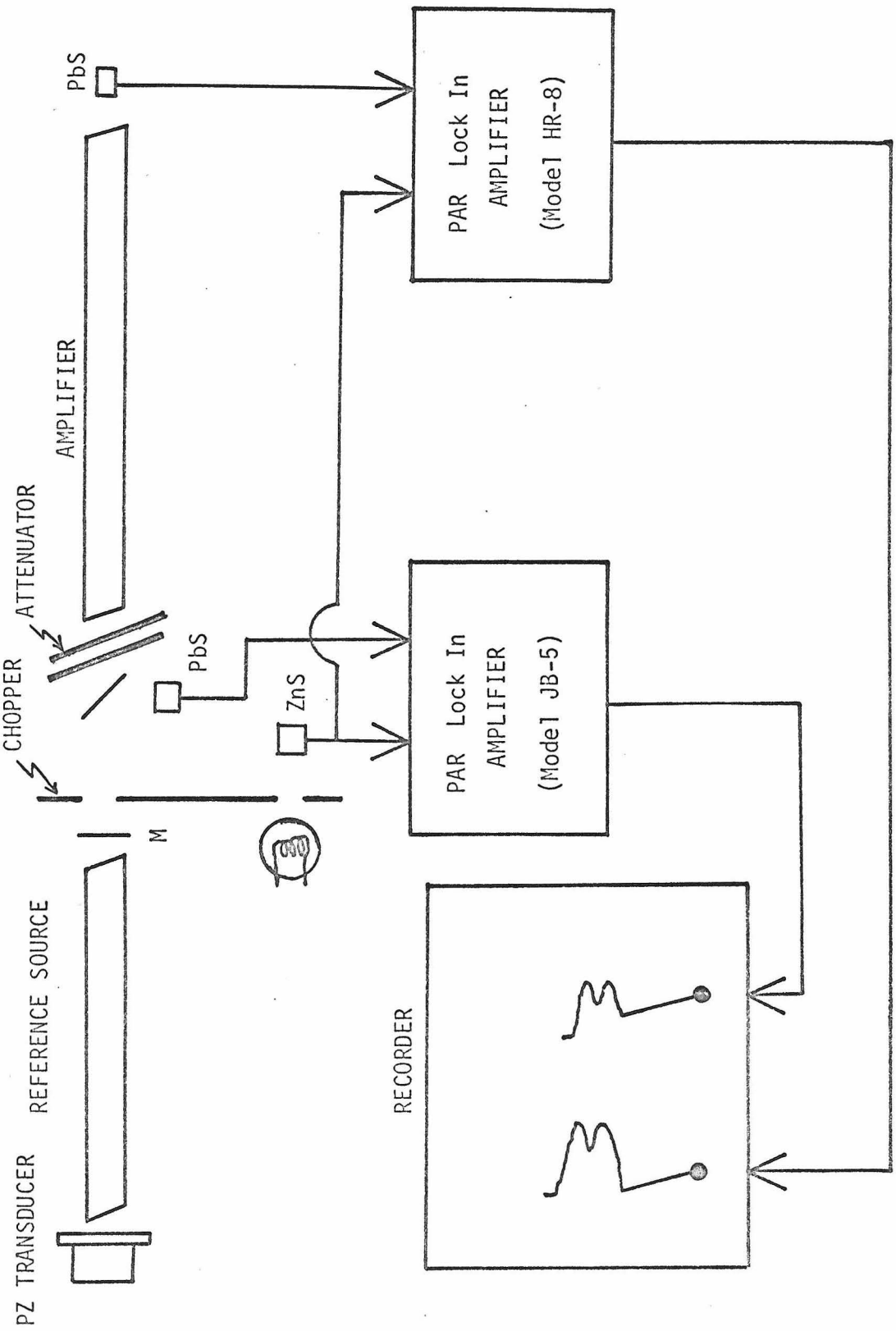

Fig. 1.14 Setup for the measurement of the gain

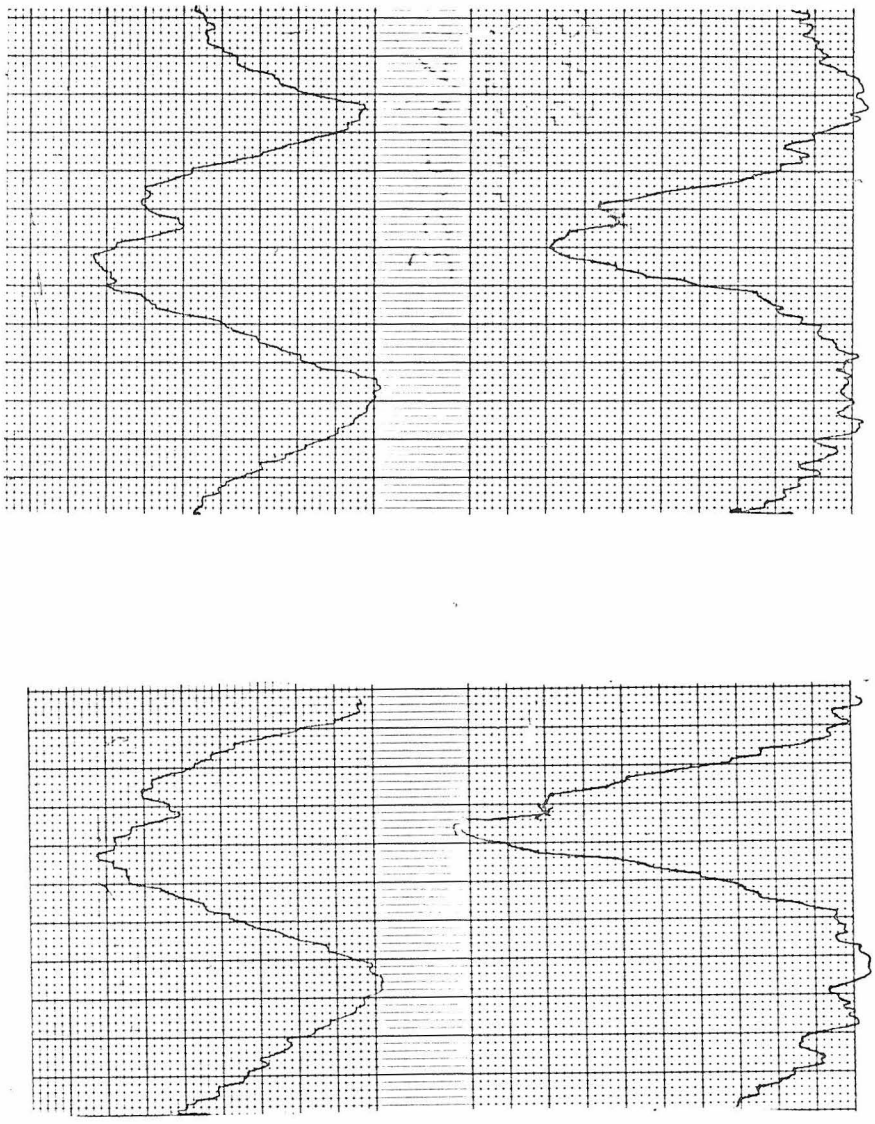

Fig. 1.15 Typical signals before (upper)and after (lower) the amplification

and the amplifier. The apparent gain narrowing[26] is seen in the figure. Caution must always be taken to keep the power level of the input as low as possible to avoid any saturation effects in the amplifier. Figure 1.16 shows the one-pass gain vs pumping current.

Figure 1.17 is a plot of output power vs X_0 for the superradiant laser. We used a PbS detector. The data were calibrated with an Eppley thermopile. The slopes of the output curves give good agreement with the theoretical values taken from Fig. 1.12. We do not observe any saturation of superradiance for tube 1, even when X_0 is as high as 15. We see saturation for longer tubes. Small diameter tube 2 begins saturating at about $X_0 \simeq 15$, while for tube 3 the effect begins at about $X_0 \simeq 10$.

It is difficult to measure the narrowed-output profile by conventional interferometry. As shown in Fig. 1.17 if we change X_0 by 10, the output power varies by a factor of about a thousand. Because of this variation, output profile must be measured by a heterodyne technique at small values of X_0, and a homodyne technique at larger values.

Heterodyning method

In the heterodyning detection, the signal to be detected is mixed with a second optical field by a square law detector[27]. The beating of signal radiation against a local oscillator, referred to as a reference signal, gives the frequency distribution as an RF beat spectrum.

The advantage of heterodyning[27-30] is that a very low level signal can be detected. It has the disadvantage that the heterodyning

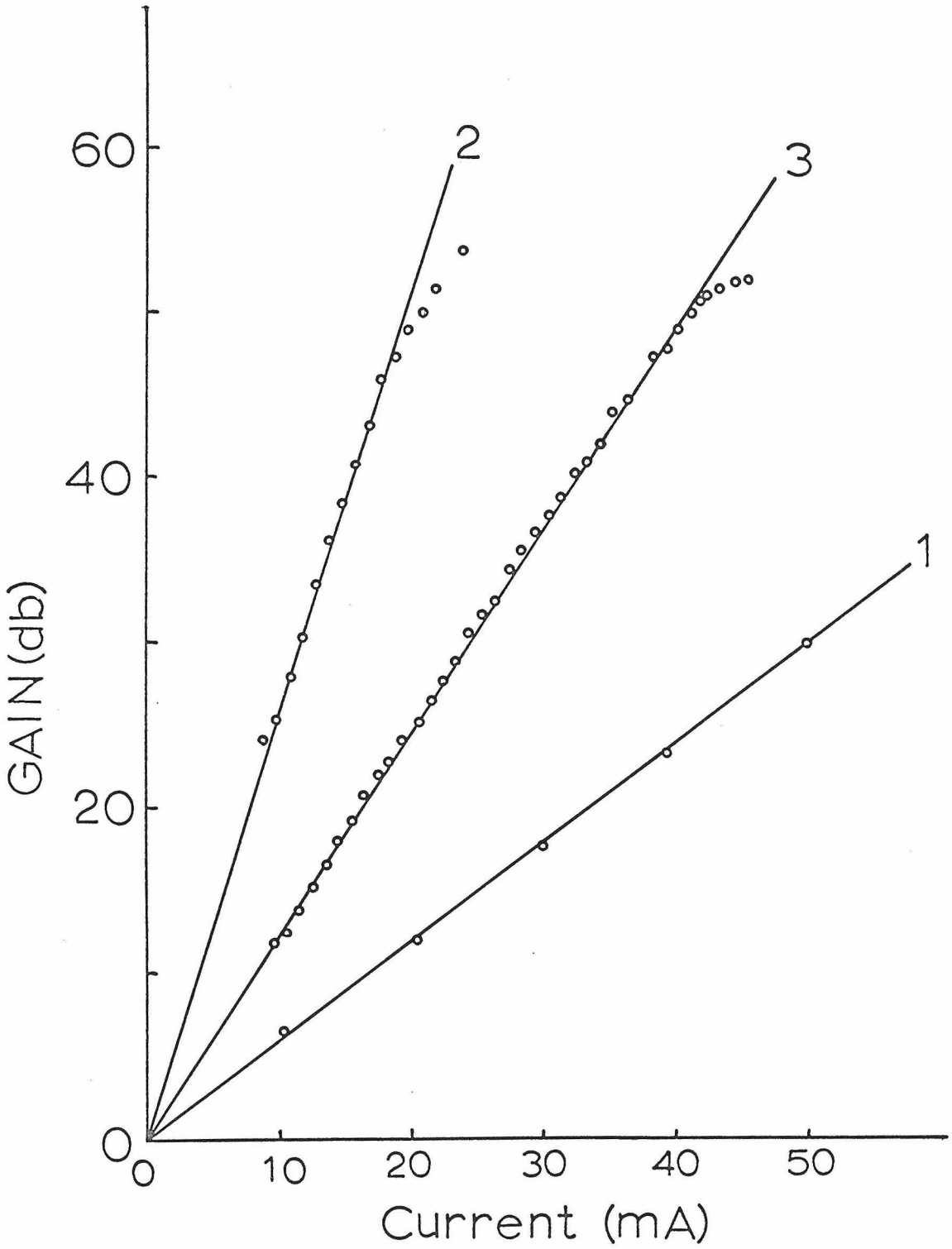

Fig. 1.16 One-pass gain for each tube

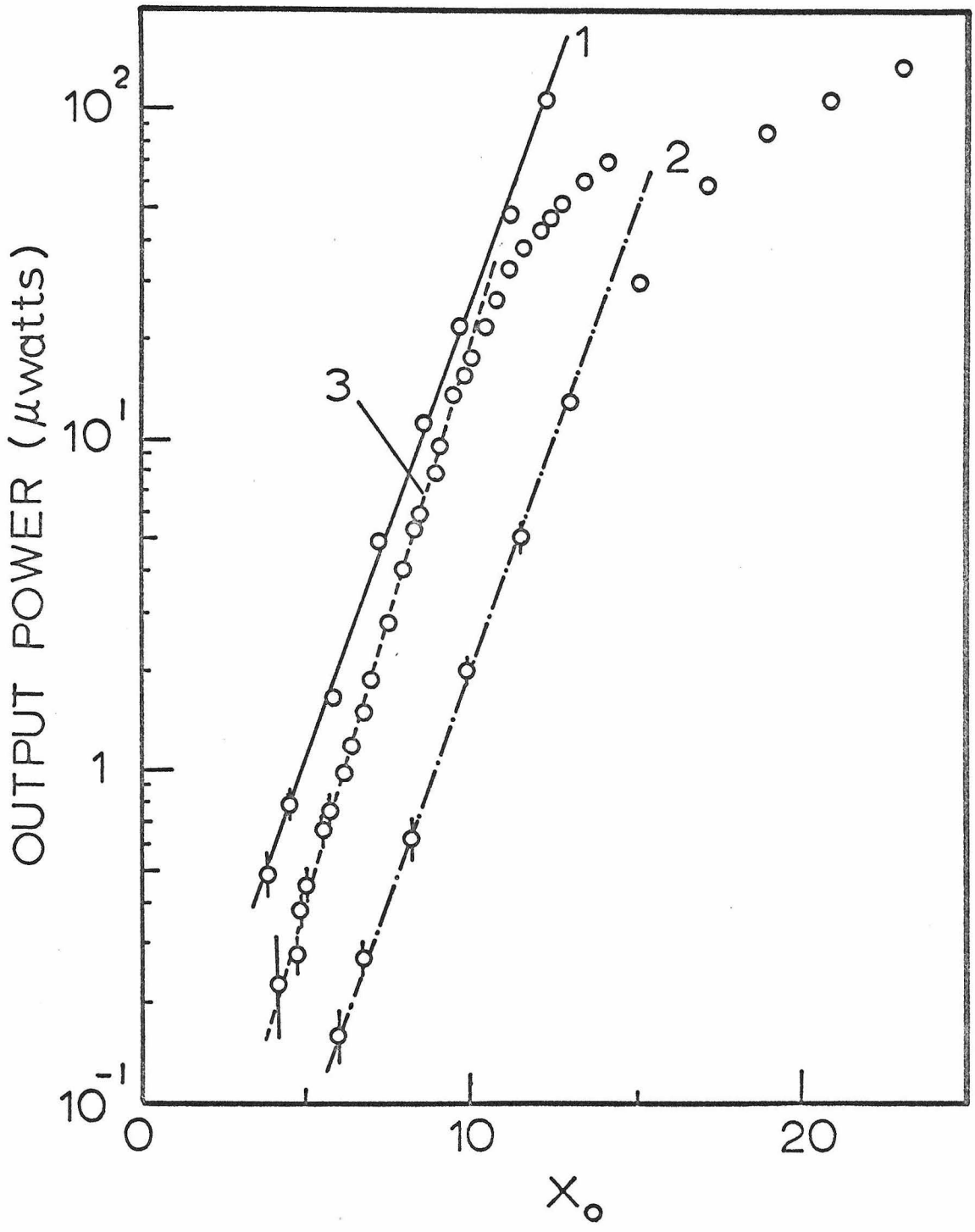

Fig. 1.17 Output power from the superradiant laser vs X_o. X_o is product of unsaturated gain and length.

reference source must be stabilized both in frequency and power level. Also, the source may interact with the superradiant laser and cause undesirable laser oscillation. We avoid the interference problem by shifting the Xe 3.51μ transition about 100 MHz by applying a magnetic field using its Zeeman splitting[31-33]. We placed the reference laser resonator on a very stable iron table which was isolated acoustically from the floor. The experiments were carried out mainly on Saturday and Sunday nights when street and building traffic was at its lowest. Shields were used so that the mirrors of the local oscillator were not disturbed by drafts.

The Zeeman split laser output has two circularly polarized components. Only one, however, is necessary for heterodyning. A quarter-wave plate made of mica and a CaF_2 polarizer were put in the optical path to eliminate one field component from the output. Mixing of the reference beam with the superradiant signal was done by using a Philco-Ford InAs detector. The local oscillator had a 75 cm cavity length with a 55 cm discharge section. The inner diameter of the tube was 2.5 mm. The pressure of the local oscillator was kept slightly above 5×10^{-3}Torr using a temperature adjustable liquid nitrogen trap[13]. Similarly, the pressure of the superradiant laser was adjusted to 5×10^{-3}Torr.

The setup is shown in Fig. 1.18. The signal from the InAs detector was fed into the Hewlett Packard 461A amplifier followed by the Tektronix type 1L20 spectrum analyzer. We did the experiment only for tube 1. Typical output signals are shown in Fig. 1.19. The peak on the left hand side of the picture is due to the noise from

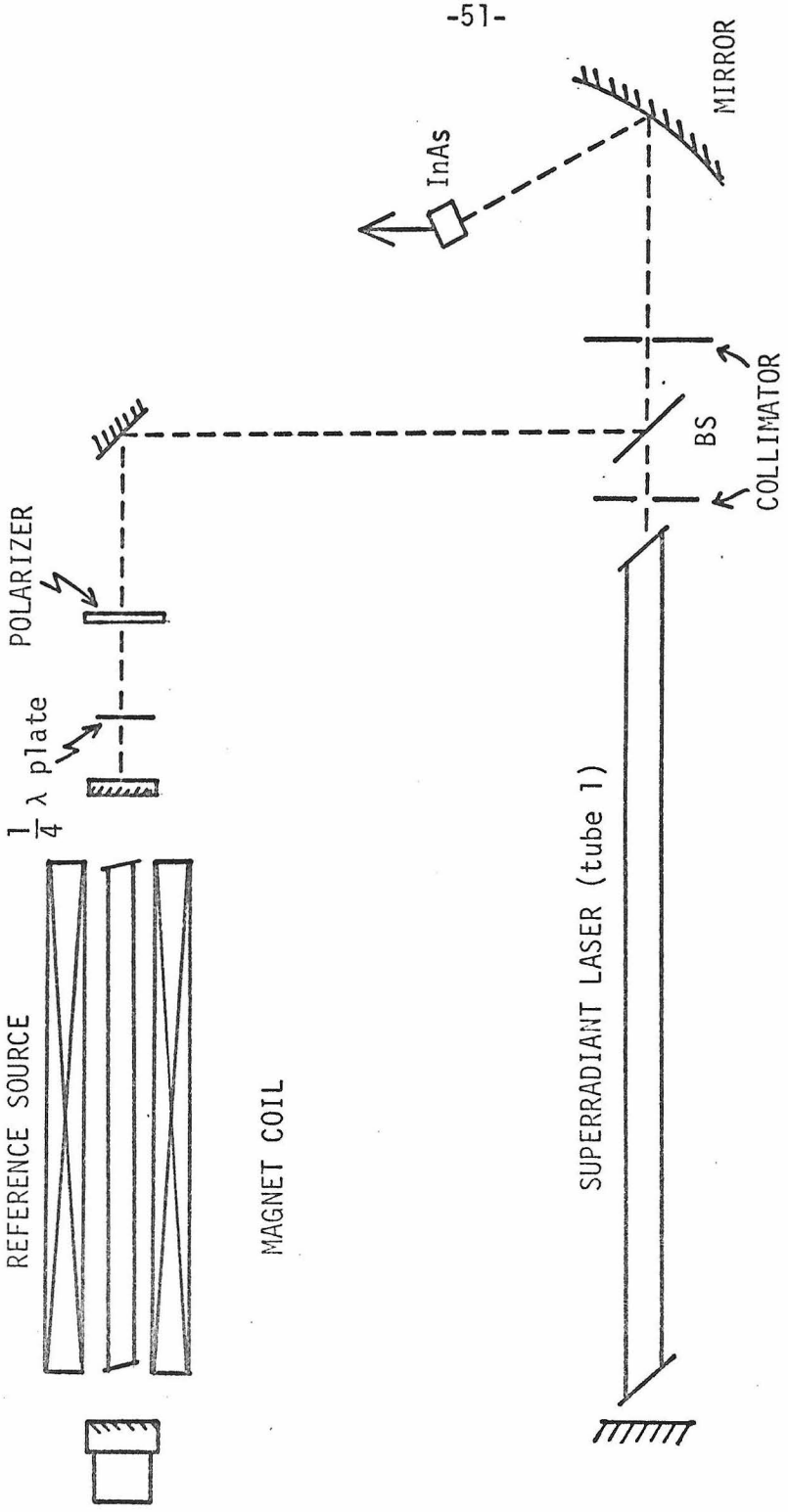

Fig. 1.18 Setup for heterodyning method

(a) $X_o = 15$

(b) $X_o = 11$

(c) $X_o = 7.6$

TYPICAL HETERODYNED SIGNALS

(5 MHz/div)

Fig. 1.19 Typical output signals of superradiant laser obtained by heterodyning method

the spectrum analyzer. The center frequency is approximately 100 MHz.

Homodyning method

When the superradiant power becomes large, we can employ the homodyning technique[28,29] to study the output spectrum. The arrangement is shown in Fig. 1.20. Typical frequency spectra are shown in Fig. 1.21. Picture (a) and (b) show the signal from tube 2. One can see that (a) has broader FWHM than (b), which has lower gain than that of (a). (c) is the signal from tube 3. There is a hump in the spectral profile near 30 MHz. We were not able to eliminate this hump, which possibly results from non-resonant feedback oscillation due to reflection from the Brewster windows. (We attached the windows somewhat differently than for tube 2). The experimental results of the spectral measurements are plotted in Figs. 1.22 and 1.23 for tubes 1 and 2, respectively. The solid line corresponds to the theoretical FWHM corresponding to Eq. (1.4.18).

(E) Conclusion

According to the results of the rate equation theory, the spectrum of amplified spontaneous emission in a high gain medium narrows toward line center, and then rebroadens after the onset of saturation. We observed spectral narrowing in two similar laser tubes, one with a feedback mirror, and the other without. The degree of narrowing agreed with theoretical predictions for a line having a Doppler width $\Delta\nu_D$ = 115 MHz. In the tube with no mirror we found spectral rebroadening to begin at ~ 3.0 watt/m^2 when the laser gain was 16. Numerical calculations predict that this onset intensity should be 0.25 watt/m^2

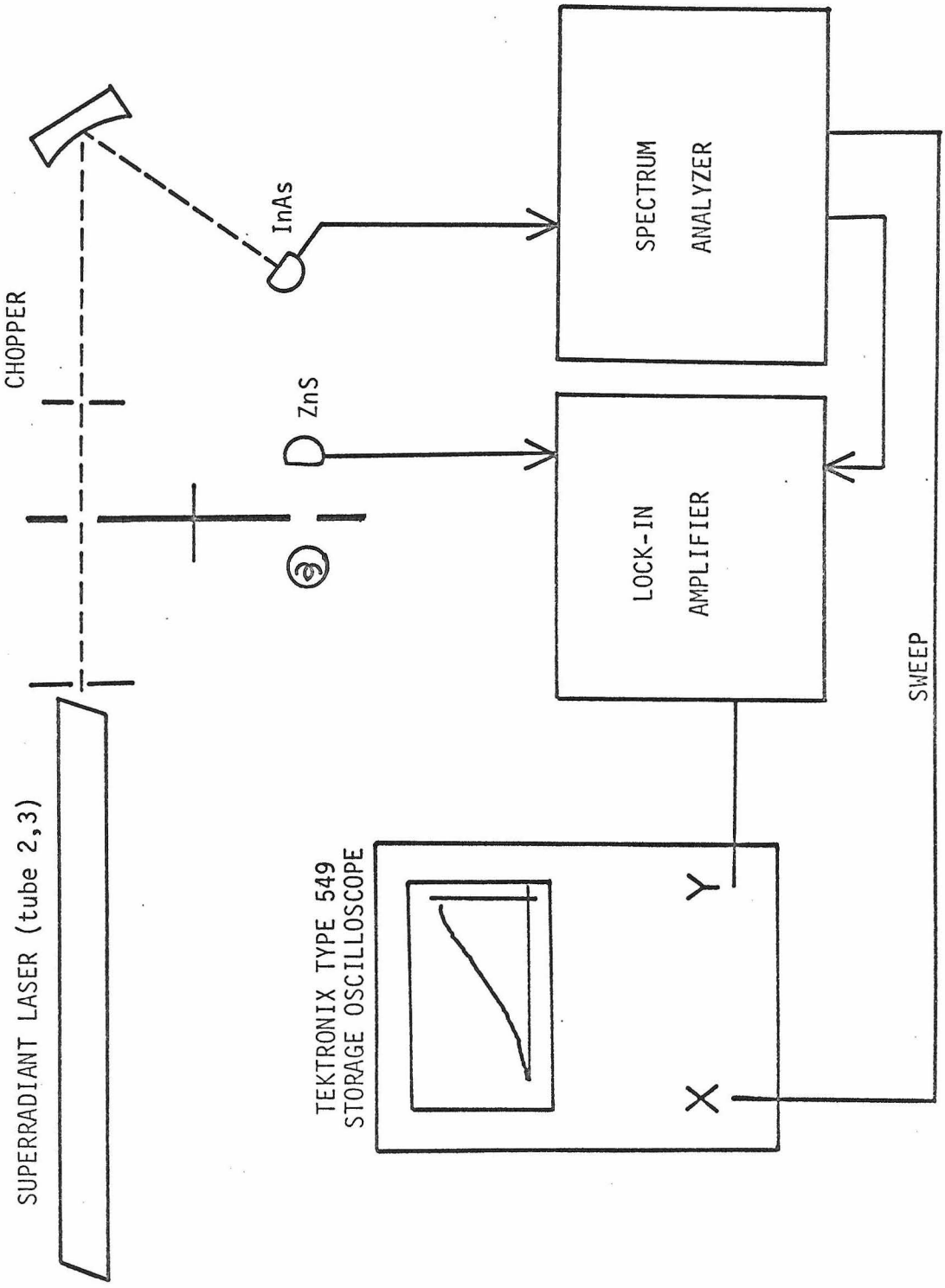

Fig. 1.20 Experimental set-up for homodyning measurement

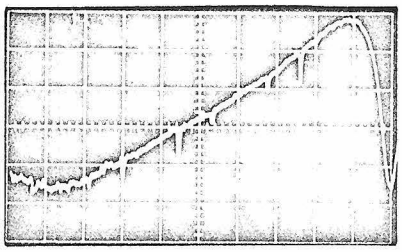

(a) $X_o = 20$

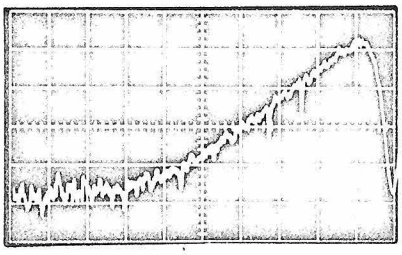

(b) $X_o = 15$

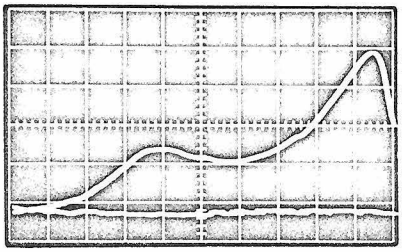

(c) $X_o = 14$

TYPICAL HOMODYNED SIGNALS

(5 MHz/div)

Fig.1.21 Typical homodyned signals

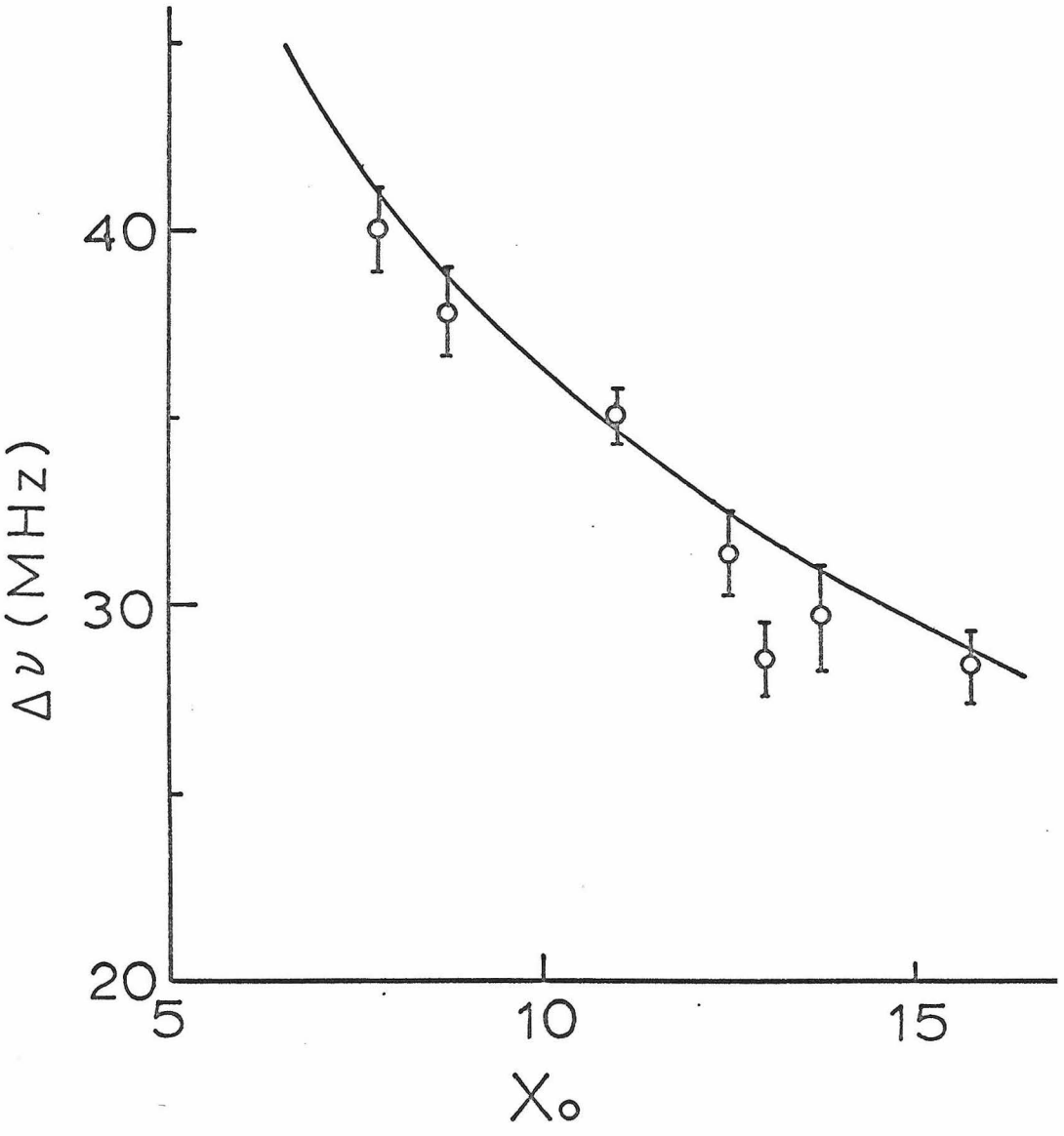

Fig. 1.22 FWHM of the superradiance laser (tube 1). Solid line corresponds to the theoretical value without any saturation.

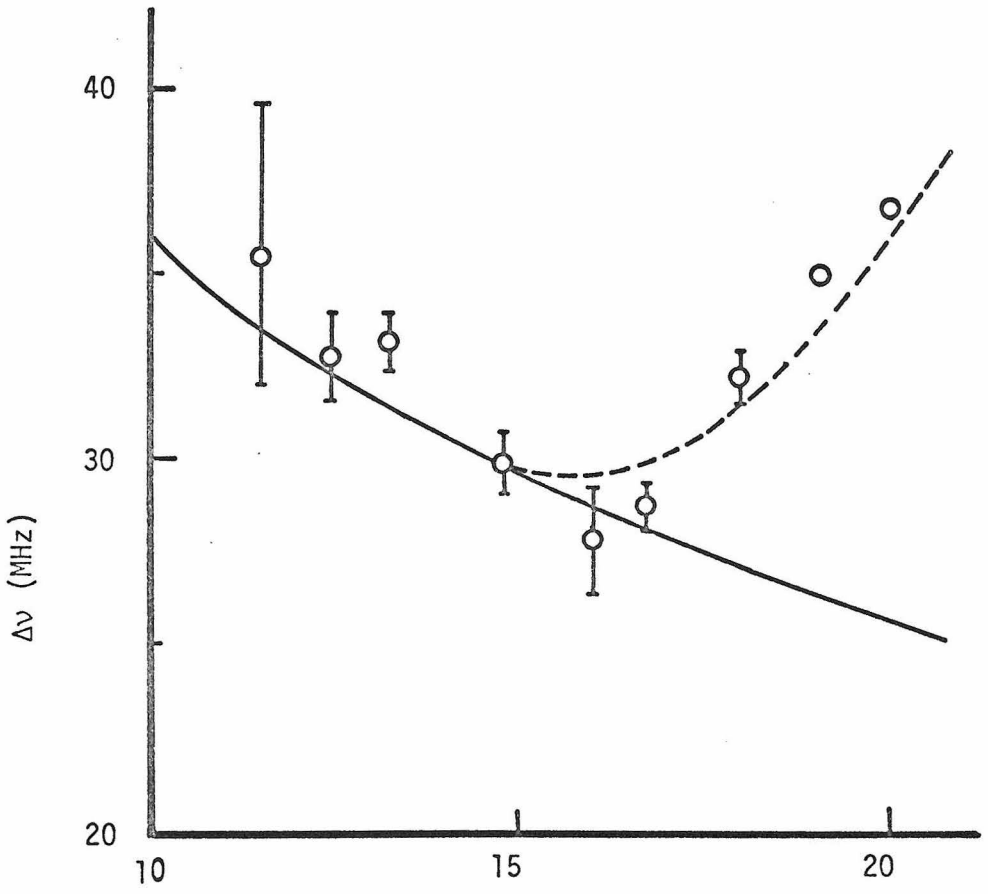

Fig. 1.23 FWHM from superradiant laser. Broken line is the theoretical value for $s = 10^{-8}$.

(see Fig. 1.12). This discrepancy by a factor of 12 might originate from our neglect of the degeneracy of the lasing atomic levels. An experiment by Klüver[24] indicates that the degeneracy is approximately 20. This is fairly consistent with what we have observed.

References for Chapter I

1. E. I. Gordon, A. D. White and J. D. Rigden, Symp. Optical Masers, Polytechnic Inst. of Brooklyn (1963), pp. 309.
2. P. W. Smith, IEEE J. Quant. Elect. QE-8, 704 (1972).
3. P. Goldreich and D. A. Keeley, Astro. Jour. 174, 517 (1972).
4. A. Szöke and A. Javan, Phys. Rev. 145, 137 (1966).
5. C.K.N. Patel, Phys. Rev. 131, 1582 (1963).
6. A. Messiah, Quantum Mechanics, John Wiley & Sons, Inc. (1966), p. 959.
7. A. Yariv, Quantum Electronics, John Wiley & Sons, Inc. (1967), p. 210.
8. A. Yariv, Introduction to Optical Electronics, Holt Rinehart & Winston (1971), Chap. 4.
9. L. Allen, D.G.C. Jones,and D. G. Schofield, J. Optics of America 59, 842 (1969).
10. P. O. Clark, IEEE J. Quant. Elect. QE-1, 109 (1965).
11. C.K.N. Patel, W. L. Faust and R. A. McFarlane, Appl. Phys. Lett. 1, 84 (1962).
12. W. L. Faust, R. A. McFarlane, C.K.N. Patel and C.G.B. Garret, Appl. Phys. Lett. 1, 85 (1962).
13. D. Armstrong, IEEE J. Quant. Electr. QE-4, 968 (1968).
14. P. Goldreich, D. A. Keeley and J. Kwan, Astrophys. Jour. 179, 111 (1973).
15. R. H. Dicke, Phys. Rev. 93, 99 (1954).
16. F. Haake and R. J. Glauber, Phys. Rev. A 5, 1457 (1972).
17. R. H. Lehmberg, Phys. Rev. A 2, 883 (1970).
18. R. K. Nesbet, IBM Research Report RJ810 (1971).

19. L. W. Casperson, Ph.D. Thesis, California Institute of Technology, p. 117.

20. A. Yariv and R.C.C. Leite, J. Appl. Phys. 34, 3410 (1963).

21. M. M. Litvak, Phys. Rev. 2, 2107 (1970).

22. L. W. Casperson and A. Yariv, IEEE J. Quant. Elect. QE-8, 80 (1972); L. W. Casperson, Ph.D. Thesis, p. 246.

23. L. Allen and G. I. Peters, J. Phys. A, General Phys. 5, 695 (1972)

24. J. W. Klüver, J. Appl. Phys. 37, 2987 (1966).

25. R. V. Ambartsumyan, N. G. Basov, P. G. Kryukov and V. S. Letokhov, Progress in Quantum Electronics, Vol. 1, Part 3, Pergamon Press (1970).

26. D. H. Hotz, Appl. Opt. 4, 527 (1965).

27. A. Yariv, Introduction to Optical Electronics, Holt, Rinehart & Winston (1971), p. 285.

28. M. Adam, A. H. Melin and P. Bergé, Optica Acta 16, 337 (1969).

29. A. T. Forrester, J. Opt. Soc. of America 51, 253 (1961).

30. J. B. Cole and J. H. Sanders, J. Phys. B, Atom. Molec. Phys. 5, 371 (1972).

31. V. S. Letokhov, JETP Lett. 6, 101 (1967).

32. K. Sakurai, J. Phys. Soc. Japan 21, 1214 (1966).

33. K. Shimoda, J. Phys. Soc. Japan 23, 103 (1967).

II. SEMICLASSICAL MODEL OF A LASER

In many cases of practical interest the rate equation approximation is an attractive tool for describing the behavior of a gas laser. However, a rigorous treatment requires a more formal use of quantum mechanics. In this chapter we treat the atoms quantum mechanically and describe a field classically.

In Section 2.1 we develop a geometrical representation of a two-level system in a generalized form so that phenomenological decay or pumping terms can be taken care of. This formalism is then applied to laser theory and solved to the lowest order in the laser field. In the following section the formal solution in the infinite order approximation is dealt with. In Section 2.4 the exact solution for the perturbed Hamiltonian is compared with the results obtained either by rate equation approximation or by rotating wave approximation. A physical meaning of these approximations is studied. In Section 2.5 the validity of the rate equation approach is considered for a multimode laser. In the following section, the Lamb dip in a single mode laser is examined closely by using the rotating wave approximation and the results are compared with experiments. Finally, a radial profile of a laser field is treated by using self-consistent field theory. The effect of the beam radius and the radius of curvature of the phase front are considered.

2.1 Geometrical Representation of Two-Level System

The application of a simple geometrical representation of the two-level Schrödinger equation to laser problems was first suggested

by Feynman et al[1]. In this section a generalized transformation is developed which can bring the non-Hermitian Schrödinger equation into the form of a real three-dimensional vector equation $d\vec{r}/dt = \vec{\omega} \times \vec{r} + f(\vec{r},\rho)$ and one scalar equation $d\rho/dt = g(\vec{r},\rho)$. The quantum mechanical behavior of the states is easily visualized by simply observing how $\vec{r}$ and ρ vary.

Formulation

We are concerned with a two-level system. The time-dependent wave function for any one individual atom may be described by the superposition of the time independent eigenfunctions ψ_a and ψ_b (where a and b denote the upper and lower level of the system, respectively). That is,

$$\psi(t) = a(t)\,\psi_a + b(t)\,\psi_b \tag{2.1.1}$$

where $a(t)$ and $b(t)$ are the time dependent amplitudes of state a and b respectively. We start from the time dependent perturbation theory. Schrödinger equation is written as[2]

$$i\hbar \frac{\partial \psi(t)}{\partial t} = (H_o + \lambda V)\,\psi(t) \tag{2.1.2}$$

where $\hbar$ is the Planck's constant divided by 2π, H_o is the unperturbed Hamiltonian, and λV is the perturbation. λ is a real parameter, which will be used for bookkeeping purposes[3]. Assuming the diagonal elements of the perturbation are zero, we get the following equations of motion for the amplitudes $a(t)$ and $b(t)$:

$$i\hbar\,\dot{a}(t) = w_a\, a(t) + \lambda V_{ab}\, b(t)$$

$$i\hbar\,\dot{b}(t) = w_b\, b(t) + \lambda V_{ba}\, a(b) \qquad (2.1.3)$$

It is advantageous to use the density matrix formalism for calculating the ensemble-averaged behavior of a system[4]. It obeys the equation of motion

$$\dot{\rho} = -\frac{i}{\hbar}[H,\rho]$$

where, with the abbreviation of notations $a(t)$ and $b(t)$ by a and b, respectively,

$$\rho = \begin{pmatrix} |a|^2 & ab^* \\ a^*b & |b|^2 \end{pmatrix}$$

$$= \begin{pmatrix} \rho_{aa} & \rho_{ab} \\ \rho_{ba} & \rho_{bb} \end{pmatrix} \qquad (2.1.4)$$

and

$$H = H_o + \lambda V \ .$$

One may introduce phenomenological terms F and G. The above equation becomes

$$\dot{\rho} = -\frac{i}{\hbar}[H,\rho] + \frac{1}{2}(F\rho + \rho F) + G \qquad (2.1.5)$$

where

$$H = \begin{pmatrix} w_a & \lambda V_{ab} \\ \lambda V_{ba} & w_b \end{pmatrix} \qquad (2.1.6)$$

$$F = \begin{pmatrix} F_{aa} & F_{ab} \\ F_{ba} & F_{bb} \end{pmatrix} \tag{2.1.7}$$

$$G = \begin{pmatrix} G_{aa} & G_{ab} \\ G_{ba} & G_{bb} \end{pmatrix} \tag{2.1.8}$$

F is usually used to describe phenomenologically decay from the upper and lower state. F makes the system non-Hermitian. G is a pumping term[5,6].

It is well known that there are four linearly independent bases necessary to specify a 2×2 matrix. For these linearly independent bases, we may choose the Pauli spin matrices σ_1, σ_2, σ_3 and also an identity matrix I. We can construct a scalar ρ_o and a vector (r_1,r_2,r_3) which are functions of a and b as follows:

$$\vec{r} = Tr[\rho\vec{\sigma}]$$

or

$$\rho_o = aa^* + bb^* \tag{2.1.9}$$

$$r_1 = ab^* + ba^* \tag{2.1.10}$$

$$r_2 = i(ab^* - ba^*) \tag{2.1.11}$$

$$r_3 = aa^* - bb^* \tag{2.1.12}$$

in which Tr designates the "trace" operation. With these expressions for ρ_o and $\vec{r}$, the matrix ρ is reconstructed as

$$\rho = \frac{1}{2}(\rho_o I + \vec{r}\cdot\vec{\sigma}) \tag{2.1.13}$$

Likewise, the other three matrices H, F, and G are given by

$$H = \frac{1}{2} H_o I + \frac{1}{2}(\vec{\omega}\cdot\vec{\sigma}) \tag{2.1.14}$$

$$F = F_o I + (\vec{F}\cdot\vec{\sigma}) \tag{2.1.15}$$

$$G = \frac{1}{2} G_o I + \frac{1}{2}(\vec{G}\cdot\vec{\sigma}) \tag{2.1.16}$$

where,

$$H_o = \mathrm{Tr}[H] \tag{2.1.17}$$

$$\vec{\omega} = \mathrm{Tr}[H\vec{\sigma}]/\hbar \tag{2.1.18}$$

$$F_o = \frac{1}{2}\mathrm{Tr}[F] \tag{2.1.19}$$

$$\vec{F} = \frac{1}{2}\mathrm{Tr}[F\cdot\vec{\sigma}] \tag{2.1.20}$$

$$G_o = \mathrm{Tr}[G] \tag{2.1.21}$$

$$\vec{G} = \mathrm{Tr}[G\vec{\sigma}] \tag{2.1.22}$$

It is shown in Appendix D that the following equation of motion can be derived from Eqs. (2.1.5) and (2.1.13) through (2.1.22):

$$d\rho_o/dt = \rho_o F_o + \vec{F}\cdot\vec{r} + G_o \tag{2.1.23}$$

$$d\vec{r}/dt = \vec{\omega}\times\vec{r} + (F_o\vec{r} + \rho_o\vec{F}) + \vec{G} \tag{2.1.24}$$

If we define a scalar function f and a vector function $\vec{S}$, according to

$$\rho_o = f\, e^{F_o t} \tag{2.1.25}$$

$$\vec{r} = \vec{S}\, e^{F_o t} \tag{2.1.26}$$

Eqs. (2.1.23) and (2.1.24) are simplified to

$$df/dt = \vec{F}\cdot\vec{S} + G_o e^{-F_o t} \tag{2.1.27}$$

$$d\vec{S}/dt = \vec{\omega}\times\vec{S} + f\vec{F} + \vec{G}e^{-F_o t} \tag{2.1.28}$$

The total Hamiltonian H consists of the unperturbed part H_o and the perturbation λV. Corresponding to this Hamiltonian, $\vec{\omega}$ can be broken into two parts, namely,

$$\vec{\omega} = \vec{\omega}_o + \lambda\vec{\omega}_p$$

where

$$\vec{\omega}_o = Tr[H_o\vec{\sigma}]/i\hbar$$

$$\vec{\omega}_p = Tr[V\vec{\sigma}]/i\hbar \tag{2.1.29}$$

As in the Rayleigh-Schrödinger perturbation method[3], we may assume that f and $\vec{S}$ can be expanded in powers of the perturbation parameter λ. Thus,

$$f = f^{(0)} + \lambda f^{(1)} + \lambda^2 f^{(2)} + \ldots \tag{2.1.30}$$

$$\vec{S} = \vec{S}^{(0)} + \lambda\vec{S}^{(1)} + \lambda^2\vec{S}^{(2)} + \ldots \tag{2.1.31}$$

From Eqs. (2.1.27) through (2.1.31) the zero order approximation in the perturbation is given by

$$df^{(0)}/dt = \vec{F}\cdot\vec{S}^{(0)} + G_o e^{-F_o t} \tag{2.1.32}$$

$$d\vec{S}^{(0)}/dt = \vec{\omega}_o \times \vec{S}^{(0)} + f^{(0)}\vec{F} + \vec{G}e^{-F_o t} \tag{2.1.33}$$

The nth recursion relation is

$$df^{(n)}/dt = \vec{F}_o \vec{S}^{(n)} \tag{2.1.34}$$

$$d\vec{S}^{(n)}/dt = \vec{\omega}_o \times \vec{S}^{(n)} + \vec{\omega}_p \times \vec{S}^{(n-1)} + f^{(n)}\vec{F} \tag{2.1.35}$$

Equations (2.1.34) and (2.1.35) are the main results of this section. Application of this formalism will be presented in the following sections.

2.2 An Application to an Optical Laser (Lowest Order Approximation)

An application of the geometrical representation formalism to the theory of an optical laser is given below. The equations determining the field have a differential form rather than the well-known integrated form[7].

We consider a high-Q multimode cavity in which an electromagnetic field acts on an atomic medium. We will assume that this medium consists of a collection of atoms of which only the atomic states, a and b, contribute to the laser action. The effect of the field inside the cavity is to produce a microscopic electric polarization of each atom. This microscopic polarization is derived for a group of atoms moving with velocity v. In this section the solution is obtained only to lowest order in the field. This microscopic

polarization of the moving atoms is used to find an average macroscopic polarization $\vec{P}(\vec{r},t)$ which acts as a source for the electromagnetic field in accordance with Maxwell's equations. The requirement for self-consistency (that the field produced by the polarization should be equal to the field assumed initially) determines the amplitudes and the frequencies of possible laser oscillations. In this section, the threshold conditions and also the dispersion relations (neglecting any saturation effects) are derived.

Equations of motion for f and $\vec{S}$

In the mks system of units, which we shall use throughout this chapter, Maxwell's equations are[8]

$$\text{div } \vec{D} = 0 \qquad \text{curl } \vec{E} = -\frac{\partial \vec{B}}{\partial t}$$

$$\text{div } \vec{B} = 0 \qquad \text{curl } \vec{H} = \vec{J} + \frac{\partial \vec{D}}{\partial t}$$

$$\vec{D} = \varepsilon_o \vec{E} + \vec{P}\,, \quad \vec{B} = \mu \vec{H}\,, \quad \vec{J} = \sigma \vec{E} \tag{2.2.1}$$

The electromagnetic field may be shown to satisfy

$$\text{curl curl } \vec{E} + \mu_o \sigma \frac{\partial \vec{E}}{\partial t} + \mu_o \varepsilon_o \frac{\partial^2 \vec{E}}{\partial t^2} = -\mu_o \frac{\partial^2 \vec{P}}{\partial t^2} \tag{2.2.2}$$

We assume that $\vec{E}$ has only a transverse component and that it depends only on the axial coordinate z. Under these conditions, the first term in Eq. (2.2.2) is replaced by $-\partial^2 E/\partial z^2$. The ohmic conductivity σ represents a loss inside the cavity. It gives an appropriate damping of the field.

For the nth normal mode of a cavity with length L, we have the eigenfunctions

$$U_n(z) = \sin k_n z \tag{2.2.3}$$

with wave number

$$k_n = n\pi/L \tag{2.2.4}$$

where n is a large integer.

In the presence of a given polarization $P(z,t)$ the forced oscillations of the electric field can be expanded in normal mode eigenfunctions

$$E(z,t) = \sum_n E_n(t)\, U_n(z) \tag{2.2.5}$$

and the polarization can be written as

$$P(z,t) = \sum_n P_n(t)\, U_n(z) \tag{2.2.6}$$

Since the lasing field is known to be very nearly monochromatic[9], we make the simplification that $E_n(t)$ varies sinusoidally with the amplitude and the phase fixed. That is,

$$E_n(t) = E_n \cos(\omega_n t + \phi_n) \tag{2.2.7}$$

The equation of motion for the density matrix might be given by[5] Eq. (2.1.5) as

$$\dot{\rho} = -\frac{i}{\hbar}[H,\rho] - \frac{1}{2}(\Gamma\rho + \rho\Gamma) + \Lambda \tag{2.2.8}$$

where

$$\Gamma = \begin{pmatrix} \gamma_a & 0 \\ 0 & \gamma_b \end{pmatrix} \tag{2.2.9}$$

$$\Lambda = \begin{pmatrix} \Lambda_a & 0 \\ 0 & \Lambda_b \end{pmatrix} \tag{2.2.10}$$

Γ is the phenomenological damping matrix, which has been shown to be diagonal[6]. Λ is the excitation matrix describing the pumping rates Λ_a and Λ_b to the upper level a and lower level b respectively. The off-diagonal elements of the excitation matrix may average to zero when one takes the excitation processes into account[5]. The diagram of this system is shown in Fig. 2.1. By substituting $F \to -\Gamma$, and $G \to \Lambda$ in Eqs. (2.1.23) and (2.1.24), we get the following equations:

$$\frac{\partial \rho_o}{\partial t} = -\rho_o \Gamma_o - \vec{\gamma}\cdot\vec{r} + \Lambda_o \tag{2.2.11}$$

$$\frac{\partial \vec{r}}{\partial t} = (\vec{\omega}\times\vec{r}) - (\Gamma_o \vec{r} + \rho_o \vec{\gamma}) + \vec{\Lambda} \tag{2.2.12}$$

where

$$\Lambda_o = Tr[\Lambda] = \Lambda_a + \Lambda_b$$

$$\vec{\Lambda} = Tr[\Lambda\vec{\sigma}] = (0,0,\Lambda_a-\Lambda_b) \tag{2.2.13}$$

$$\Gamma_o = \frac{1}{2} Tr[\Gamma] = \frac{1}{2}(\gamma_a+\gamma_b)$$

$$\vec{\gamma} = \frac{1}{2} Tr[\Gamma\vec{\sigma}] = (0,0,\frac{1}{2}(\gamma_a-\gamma_b)) \tag{2.2.14}$$

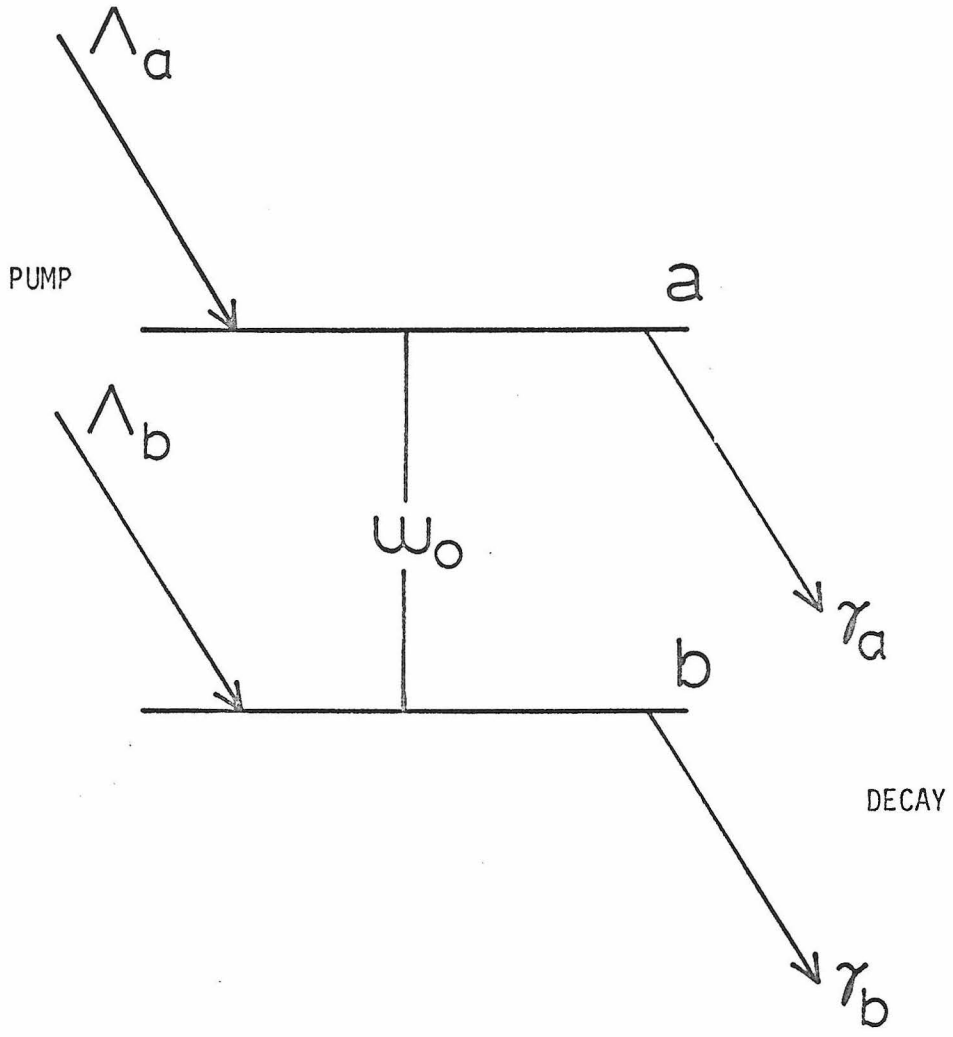

Fig. 2.1 Energy diagram of two-level system

With the substitutions (2.1.25) and (2.1.26), Eqs. (2.2.11) and (2.2.12) reduce to

$$\frac{df}{dt} = -\vec{\gamma} \cdot \vec{S} + \Lambda_o \, e^{\Gamma_o t} \tag{2.2.15}$$

$$\frac{d\vec{S}}{dt} = (\vec{\omega} \times \vec{S}) - f\vec{\gamma} + \vec{\Lambda} e^{\Gamma_o t} \tag{2.2.16}$$

Expression for $\vec{\omega}$

Assuming that the unperturbed Hamiltonian is diagonalized, $\vec{\omega}_o$ in Eq. (2.1.29) has only one nonzero component:

$$\vec{\omega}_o = \mathrm{Tr}[H_o \vec{\sigma}]/\hbar$$

$$= (0,0,\omega_o) \tag{2.2.17}$$

where

$$\omega_o = \frac{1}{\hbar}(E_a - E_b) \tag{2.2.18}$$

The perturbed part of the Hamiltonian of atoms moving with velocity v is different from that of atoms moving with another velocity. If we assume that the transition is electric dipole with $\Delta m = 0$, we get the perturbation[1],

$$V_{ab}(v,z,t) = -\mu_{ab} \, E(v,z,t) \tag{2.2.19}$$

μ_{ab} is the matrix element between the two states for the component of dipole moment along the electric field. $E(v,z,t)$ is the electromagnetic field as seen from a coordinate system fixed to atoms moving with velocity v. If μ_{ab} is made real by a proper choice of phase of the wave functions, each component of $\vec{\omega}_p$ is given by Eq.

(2.1.18) as

$$\omega_{p_1} = \mathrm{Tr}[V\sigma_1]/\hbar = \frac{V_{ab} + V_{ba}}{\hbar} = -\frac{2\mu_{ab}}{\hbar} E(v,z,t)$$

$$\omega_{p_2} = \mathrm{Tr}[V\sigma_2]/\hbar = \frac{i(V_{ab} - V_{ba})}{\hbar} = 0$$

$$\omega_{p_3} = 0 \qquad (2.2.20)$$

The time and space coordinates of the moving frame are described by the following Galilean transformation:

$$z = z' + vt'$$

$$t = t' \qquad (2.2.21)$$

With these transformations, the field expressed by Eq. (2.2.5) is given by

$$\begin{aligned} E(v,z',t') &= \sum E_n(t')\, U_n(z' + vt') \\ &= \sum E_n \cos(\omega_n t')\, \sin(k_n z' + k_n v t') \\ &= \frac{1}{2} \sum E_n \mathrm{Im}[e^{ik_n z'} \{e^{i(\omega_n + k_n v)t'} \\ &\quad + e^{-i(\omega_n - k_n v)t'}\}] \end{aligned} \qquad (2.2.22)$$

where we assume $\phi_n = 0$. The notation "Im" refers to the imaginary part of the quantity in the square brackets. Finally we get the following:

$$\vec{\omega}_p = (\omega_{p_1}, 0, 0)$$

where

$$\omega_{pl} = -\frac{\mu_{ab}}{\hbar} \sum E_n \, \mathrm{Im}[e^{ik_n z'} \{e^{i(\omega_n + k_n v)t'} + e^{-i(\omega_n - k_n v)t'}\}] \tag{2.2.23}$$

Zero order approximation

From Eqs. (2.1.32) and (2.1.33) we have

$$\frac{df^{(0)}}{dt} = -\vec{\gamma}\cdot\vec{S}^{(0)} + \Lambda_o e^{\Gamma_o t} \tag{2.2.24}$$

$$\frac{d\vec{S}^{(0)}}{dt} = \vec{\omega}_o \times \vec{S}^{(0)} - f^{(0)}\vec{\gamma} + \vec{\Lambda} e^{\Gamma_o t} \tag{2.2.25}$$

in which we drop primes, since there is no possibility of confusion. With the help of Eqs. (2.2.13) and (2.2.14), the following explicit forms can be derived from the above:

$$\begin{aligned}
\dot{f}^{(0)} &= -\gamma S_3^{(0)} + \Lambda_o e^{\Gamma_o t} \\
\dot{S}_1^{(0)} &= -\omega_o S_2^{(0)} \\
\dot{S}_2^{(0)} &= \omega_o S_1^{(0)} \\
\dot{S}_3^{(0)} &= -\gamma f^{(0)} + \Lambda e^{\Gamma_o t}
\end{aligned} \tag{2.2.26}$$

where

$$\gamma = \frac{\gamma_a - \gamma_b}{2} \tag{2.2.27}$$

$$\Lambda = \Lambda_a - \Lambda_b \tag{2.2.28}$$

Equations (2.2.26) are solved with arbitrary initial conditions. If we choose

$$\begin{aligned}
\vec{S}(0) &= (A_1, A_2, A_3) \\
f(0) &= B
\end{aligned} \tag{2.2.29}$$

the solutions are

$$S_1^{(0)}(t) = \sqrt{A_1^2 + A_2^2}\,\sin(\phi + \omega_o t)$$

$$S_2^{(0)}(t) = \sqrt{A_1^2 + A_2^2}\,\cos(\phi + \omega_o t) \qquad (2.2.30)$$

$$S_3^{(0)}(t) = \frac{\Lambda - \gamma B}{\gamma}\sinh(\gamma t) + A_3\cosh(\gamma t) + \frac{\Gamma_o\Lambda - \gamma\Lambda_o}{\Gamma_o^2 - \gamma^2}\,e^{\Gamma_o t}$$
$$+ \frac{\Gamma_o\Lambda - \gamma\Lambda_o}{2\gamma}\left(\frac{e^{-\gamma t}}{\gamma+\Gamma_o} + \frac{e^{\gamma t}}{\gamma-\Gamma_o}\right) \qquad (2.2.31)$$

$$f^{(0)}(t) = \left(B - \frac{\Lambda}{\gamma}\right)\cosh(\gamma t) - A_3\sinh(\gamma t) + \frac{\Gamma_o\Lambda_o - \gamma\Lambda}{\Gamma_o^2 - \gamma^2}\,e^{\Gamma_o t}$$
$$+ \frac{\Gamma_o\Lambda - \gamma\Lambda_o}{2\gamma}\left(\frac{e^{-\gamma t}}{\gamma+\Gamma_o} - \frac{e^{\gamma t}}{\gamma-\Gamma_o}\right) \qquad (2.2.32)$$

where $\phi = \tan^{-1}\dfrac{A_1}{A_2}$. Since $\Gamma_o > \gamma$, we may neglect all terms without the time-dependence $e^{\Gamma_o t}$.* Then we have

---

* ρ_o and $\vec{r}$ have physical significance rather than f and $\vec{S}$ themselves. Since ρ_o and $\vec{r}$ are given by

$$\rho_o = f\,e^{-\Gamma_o t'} \quad \text{and} \quad \vec{r} = \vec{S}\,e^{-\Gamma_o t},$$

only the leading terms with $e^{\Gamma_o t}$ time-dependence in Eqs. (2.2.30) to (2.2.32) remain appreciable when t is very large.

$$S_1^{(0)} = S_2^{(0)} = 0$$

$$S_3^{(0)} = \overline{N}\, e^{\Gamma_o t}$$

$$f^{(0)} = \overline{M}\, e^{\Gamma_o t} \tag{2.2.33}$$

where

$$\overline{N} = \frac{\Gamma_o \Lambda - \gamma \Lambda_o}{\Gamma_o^2 - \gamma^2} = \frac{\Lambda_a}{\gamma_a} - \frac{\Lambda_b}{\gamma_b}$$

$$\overline{M} = \frac{\Gamma_o \Lambda_o - \gamma \Lambda}{\Gamma_o^2 - \gamma^2} = \frac{\Lambda_a}{\gamma_a} + \frac{\Lambda_b}{\gamma_b} \tag{2.2.34}$$

$\overline{N}$ is usually called an excitation density, and is equal to the population inversion. $\overline{M}$ is the sum of the number of atoms in the upper and lower states when there is no perturbing field.

First order approximation

To the first order in the perturbation λV, we get the following from Eqs. (2.1.34) and (2.1.35):

$$\dot{f}^{(1)} = -\gamma S_3^{(1)}$$

$$\dot{S}_1^{(1)} = -\omega_o S_2^{(1)}$$

$$\dot{S}_2^{(1)} = -\omega_{p1} S_3^{(0)} + \omega_o S_1^{(1)}$$

$$\dot{S}_3^{(1)} = \omega_{p1} S_2^{(0)} - \gamma f^{(1)} \tag{2.2.35}$$

The solutions that have the time-dependence $e^{\Gamma_o t}$ are derived in Appendix E. They are given by:

$$S_1^{(1)} = -\frac{\omega_o \bar{N} \mu_{ab} e^{\Gamma_o t}}{\hbar} \sum E_n \, \mathrm{Im}[D(\omega_n + k_n v)$$

$$\times e^{ik_n z + i(\omega_n + k_n v)t} + D(-\omega_n + k_n v) e^{ik_n z - i(\omega_n - k_n v)t}] \quad (2.2.36)$$

$$S_2^{(1)} = -\frac{\bar{N} \mu_{ab} e^{\Gamma_o t}}{\hbar} \sum E_n \, \mathrm{Im}[g(\omega_n + k_n v)$$

$$\times e^{ik_n z + (\omega_n + k_n v)t} + g(-\omega_n + k_n v) e^{ik_n z - i(\omega_n - k_n v)t}] \quad (2.2.37)$$

$$S_3^{(1)} = 0 \quad , \quad f^{(1)} = 0 \quad (2.2.38)$$

where

$$D(\omega) = [(\Gamma_o + i\omega)^2 + \omega_o^2]^{-1} \quad (2.2.39)$$

$$g(\omega) = (\Gamma_o + i\omega)[(\Gamma_o + i\omega)^2 + \omega_o^2]^{-1} \quad (2.2.40)$$

These solutions are evaluated in a frame moving with velocity v. We get the following expression in the rest frame:

$$S_1^{(1)} = -\frac{\omega_o \bar{N} \mu_{ab}}{\hbar} e^{\Gamma_o t} \sum E_n \, \mathrm{Im}[D(\omega_n + k_n v) e^{ik_n z + i\omega_n t}$$

$$+ D(-\omega_n + k_n v) e^{ik_n z - i\omega_n t}] \quad (2.2.41)$$

$$S_2^{(1)} = -\frac{\bar{N} \mu_{ab}}{\hbar} e^{\Gamma_o t} \sum E_n \, \mathrm{Im}[g(\omega_n + k_n v) e^{ik_n z + i\omega_n t}$$

$$+ g(-\omega_n + k_n v) e^{ik_n z - i\omega_n t}] \quad (2.2.42)$$

$$S_3^{(1)} = 0 \quad , \quad f^{(1)} = 0 \tag{2.2.43}$$

So far we have calculated $\vec{S}$ and f only for the class of atoms moving with velocity v. To get a collective $\vec{S}$ and f, we have to sum up the contributions from atoms with all possible velocities. We may assume that the velocity profile of the excitation density has the Maxwell distribution. Then the normalized weighting function is given by

$$W(v) = \frac{1}{u\sqrt{\pi}} e^{-v^2/u^2} \tag{2.2.44}$$

where u^2 is the mean squared velocity of atoms. Since the polarization is written as

$$P = \mu_{ab}(\rho_{ab} + \rho_{ba}) = \mu_{ab} S_1$$

the macroscopic polarization to first order in the field is

$$P^{(1)} = \mu_{ab} e^{-\Gamma_o t} \int_{-\infty}^{\infty} S_1^{(1)} W(v)\, dv \tag{2.2.45}$$

This integral is carried out (in Appendix F), with the result

$$P^{(1)} = -\frac{\bar{N} \mu_{ab}^2 \sqrt{\pi}}{\hbar k_n u} \sum E_n \{ \mathrm{Im}[\underset{\sim}{W}(\zeta_n^+)] \cos \omega_n t + \mathrm{Re}[\underset{\sim}{W}(\zeta_n^+)] \sin \omega_n t \} \sin k_n z \tag{2.2.46}$$

"Re" designates the real part in the square brackets, ζ and $\underset{\sim}{W}$ are defined by

$$\zeta_n^{\pm} = (\pm\omega_o - \omega_n + i\Gamma_o)/k_n u \tag{2.2.47}$$

and

$$\underset{\sim}{W}(\zeta) = \frac{i}{\pi}\int_{-\infty}^{\infty}\frac{e^{-s^2}}{\zeta - s}\,ds$$

$$= e^{-\zeta^2}\,\mathrm{erfc}(-i\zeta) \qquad (2.2.48)$$

where erfc is a complementary error function. Substituting Eq. (2.2.46) into Eq. (2.2.2), one finds the following equation for the nth normal mode:

$$k_n^2 \cos\omega_n t - \omega_n\mu_o\sigma \sin\omega_n t - \omega_n^2\,\mu_o\varepsilon_o\cos\omega_n t$$

$$= -\frac{\mu_o\overline{N}\,\mu_{ab}^2\omega_n^2\sqrt{\pi}}{\hbar\, k_n u}\left\{\mathrm{Im}[\underset{\sim}{W}(\zeta_n^+)]\cos\omega_n t + \mathrm{Re}[\underset{\sim}{W}(\zeta_n^+)]\sin\omega_n t\right\} \qquad (2.2.49)$$

By equating sine and cosine terms on both sides of the above equation, we get

$$\frac{1}{Q_n} = \frac{\overline{N}\,\mu_{ab}^2\sqrt{\pi}}{\varepsilon_o\hbar k_n u}\,\mathrm{Re}[\underset{\sim}{W}(\zeta_n^+)] \qquad (2.2.50)$$

$$\frac{k_n^2}{\omega_n^2} = \mu_o\varepsilon_o - \frac{\mu_o\overline{N}\,\mu_{ab}^2}{\hbar\, k_n u}\,\mathrm{Im}[\underset{\sim}{W}(\zeta_n^+)] \qquad (2.2.51)$$

with

$$Q_n = \varepsilon_o\omega_n/\sigma \qquad (2.2.52)$$

These results might be useful for calculating the threshold pumping and the dispersion relation near the threshold. Special cases of the above results would be the following two situations:

(1) The medium is homogeneously broadened,

(2) The medium is inhomogeneously broadened.

In case (1) we let $u \to 0$, so that the Maxwell distribution function becomes a delta function. In this limit, the polarization is given by

$$P^{(1)} \cong -\frac{2\omega_o \bar{N} \mu_{ab}^2}{\hbar} \sum_n E_n \sin k_n z \{\mathrm{Re}[D(\omega_n)] \cos \omega_n t - \mathrm{Im}[D(\omega_n)] \sin \omega_n t\} \tag{2.2.53}$$

Then expressions (2.2.50) and (2.2.51) reduce to

$$\frac{1}{Q_n} \cong \frac{\bar{N} \mu_{ab}^2}{\hbar \varepsilon_o} \frac{\Gamma_o}{(\omega_n - \omega_o)^2 + \Gamma_o^2} \tag{2.2.54}$$

$$\frac{k_n^2}{\omega_n^2} \cong \mu_o \varepsilon_o - \frac{\mu_o \bar{N} \mu_{ab}^2}{\hbar} \frac{\omega_n - \omega_o}{(\omega_n - \omega_o)^2 + \Gamma_o^2} \tag{2.2.55}$$

When the Doppler broadening is dominant, the thermal motion of an atom during its natural decay time carries it through many optical wavelengths. Thus we might take $k_n u \gg 1/\Gamma_o$. In this limit $\mathrm{erfc}(-i\zeta^+)$ may be set equal to unity, and $\underset{\sim}{W}(\zeta^+)$ is simplified to

$$\underset{\sim}{W}(\zeta^+) = \exp\{-\frac{(\omega_o - \omega_n)^2}{k_n^2 u^2}\} [1 + 2i \frac{\Gamma_o(\omega_n - \omega_o)}{k_n^2 u^2} + \ldots] \tag{2.2.56}$$

This gives the polarization,

$$p(1) \cong -\frac{\bar{N}\,\mu_{ab}^2\sqrt{\pi}}{\hbar\, k_n u}\sum_n E_n \sin k_n z \exp\frac{(\omega_n-\omega_o)^2}{k_n^2 u^2}$$

$$\times \quad [\sin \omega_n t + \frac{2\Gamma_o(\omega_n-\omega_o)}{k_n^2 u^2}\cos \omega_n t] \qquad (2.2.57)$$

From Eqs. (2.2.50) and (2.2.51) we get the following:

$$\frac{1}{Q_n} \cong \frac{\bar{N}\,\mu_{ab}^2\sqrt{\pi}}{\varepsilon_o \hbar k_n u}\exp\{-\frac{(\omega_n-\omega_o)^2}{k_n^2 u^2}\} \qquad (2.2.58)$$

$$\frac{k_n^2}{\omega_n^2} \cong \mu_o\varepsilon_o - \frac{2\mu_o\bar{N}\,\mu_{ab}^2\sqrt{\pi}}{\hbar}\frac{\Gamma_o(\omega_n-\omega_o)}{(k_n u)^3}\exp\{-\frac{(\omega_n-\omega_o)^2}{k_n^2 u^2}\} \qquad (2.2.59)$$

These results are equivalent to those previously obtained by Lamb[7] and other authors.

2.3 Infinite Order Solution for the Geometrical Representation

The density matrix has been found for the zero and first order in the field. When the intensity of a field increases, higher order perturbation theory is necessary. In this section we will develop further the method described in Section 2.2 to an infinite order approximation. The solution is given in an operator form which can be extended to any kind of Hamiltonian with the form given by Eq. (2.1.5).

The differential equations for the zero order approximation are found from Eq. (2.2.26) to be

$$\dot{f}^{(0)} = -\gamma S_3^{(0)} + \Lambda_o e^{\Gamma_o t}$$

$$\dot{S}_1^{(0)} = -\omega_o S_2^{(0)}$$

$$\dot{S}_2^{(0)} = \omega_o S_1^{(0)}$$

$$\dot{S}_3^{(0)} = -\gamma f^{(0)} + \Lambda e^{\Gamma_o t} \qquad (2.3.1)$$

Similar to Eq. (2.2.35) we have the following recursion relations for the nth order approximation:

$$\dot{f}^{(n)} = -\gamma S_3^{(n)}$$

$$\dot{S}_1^{(n)} = -\omega_o S_2^{(n)}$$

$$\dot{S}_2^{(n)} = \omega_o S_1^{(n)} - \omega_{p1} S_3^{(n-1)}$$

$$\dot{S}_3^{(n)} = \omega_{p1} S_2^{(n-1)} - \gamma f^{(n)} \qquad (2.3.2)$$

where

$$\omega_p = -\frac{2\mu_{ab}}{\hbar} E(v,z,t)$$

Differentiating both sides of the above equations with respect to time, we get

$$\left[\frac{d^2}{dt^2} - \gamma^2\right] f^{(n)} = -\gamma \omega_{p1} S_2^{(n-1)}$$

$$\left[\frac{d^2}{dt^2} + \omega_o^2\right] S_1^{(n)} = \omega_o \omega_{p1} S_3^{(n-1)}$$

$$\left[\frac{d^2}{dt^2} + \omega_o^2\right] S_2^{(n)} = - \frac{d}{dt} \left[\omega_{p1} S_3^{(n-1)}\right]$$

$$\left[\frac{d^2}{dt^2} - \gamma^2\right] S_3^{(n)} = \frac{d}{dt} \left[\omega_{p1} S_2^{(n-1)}\right] \qquad (2.3.3)$$

Defining an operator[10]

$$D = d/dt \qquad (2.3.4)$$

Eqs. (2.3.3) are formally written by*

$$f^{(n)} = - \frac{\gamma}{D^2 - \gamma^2} \omega_{p1} S_2^{(n-1)} \qquad (2.3.5)$$

$$S_1^{(n)} = \frac{1}{D^2 + \omega_o^2} \omega_o \omega_{p1} S_3^{(n-1)} \qquad (2.3.6)$$

$$S_2^{(n)} = - \frac{D}{D^2 + \omega_o^2} \omega_{p1} S_3^{(n-1)} \qquad (2.3.7)$$

$$S_3^{(n)} = \frac{D}{D^2 - \gamma^2} \omega_{p1} S_2^{(n-1)} \qquad (2.3.8)$$

in which the operator $1/(D+a)$ designates the operation

---

*For those readers who may wonder about the meaning of $1/D$ in Eq. (2.3.5), it is not rigorous to discuss the solutions for differential equations, using this operator D. But so long as one is concerned with steady state solutions, one will find that the results given by using this operator D are the same as the results obtained by using the Laplace transformation. (See Appendix G). We use this operator D because we think the physical phenomenon can be grasped much more easily than by using the Laplace transform method.

$$\frac{1}{D+a}\, g(t) \;\rightarrow\; \int_{-\infty}^{t} g(t')\, e^{at'}\, dt'$$

$g(t)$ is an arbitrary function. Substitution of Eqs. (2.3.7) into (2.3.8) yields

$$S_3^{(n)} = -\frac{D}{D^2-\gamma^2}\,\omega_{pl}\,\frac{D}{D^2+\omega_o^2}\,\omega_{pl}\,S_3^{(n-2)} \tag{2.3.9}$$

which will give

$$S_3^{(2n)} = \left[-\frac{D}{D^2-\gamma^2}\,\omega_{pl}\,\frac{D}{D^2+\omega_o^2}\,\omega_{pl}\right]^n S_3^{(0)} \tag{2.3.10}$$

$$S_3^{(2n+1)} = \left[-\frac{D}{D^2-\gamma^2}\,\omega_{pl}\,\frac{D}{D^2+\omega_o^2}\,\omega_{pl}\right]^n S_3^{(1)} \tag{2.3.11}$$

The solution S_3 which is given by the infinite sum of $S_3^{(n)}$, can be written in the following form:

$$S_3 = \sum_0^\infty \left[-\frac{D}{D^2-\gamma^2}\,\omega_{pl}\,\frac{D}{D^2+\omega_o^2}\,\omega_{pl}\right]^n (S_3^{(0)} + S_3^{(1)})$$

$$= \left[1 + \frac{D}{D^2-\gamma^2}\,\omega_{pl}\,\frac{D}{D^2+\omega_o^2}\,\omega_{pl}\right]^{-1} (S_3^{(0)} + S_3^{(1)}) \tag{2.3.12}$$

With the help of the above expression, we get

$$S_1 = S_1^{(0)} + \frac{\omega_o}{D^2+\omega_o^2}\,\omega_{pl}\,S_3 \tag{2.3.13}$$

$$S_2 = S_2^{(0)} - \frac{D}{D^2+\omega_o^2}\,\omega_{pl}\,S_3 \tag{2.3.14}$$

$$f = -\frac{\gamma}{D} S_3 \tag{2.3.15}$$

Using these results for f and $\vec{S}$, one can compute the expectation value of an operator $\tilde{O}$ in accordance with

$$\begin{aligned} \langle \tilde{O} \rangle &= Tr[\tilde{O}\rho] \\ &= \frac{1}{2} \rho_o \, Tr[\tilde{O}] + \frac{1}{2} \vec{r} \, Tr[\tilde{O}\vec{\sigma}] \end{aligned} \tag{2.3.16}$$

where

$$\rho_o = f e^{-\Gamma_o t}$$

$$\vec{r} = \vec{S} e^{-\Gamma_o t}$$

Sharp brackets $\langle \rangle$ denote the expectation value of the operator inside the brackets.

Let us choose for this operator $\tilde{P}$ the polarization which is given by

$$P = \begin{pmatrix} 0 & \mu_{ab} \\ \mu_{ba} & 0 \end{pmatrix}$$

In terms of $S_1^{(0)}$, $S_3^{(0)}$ and $S_3^{(1)}$, Eq. (2.3.16) reduces to

$$\begin{aligned} \langle \tilde{P} \rangle &= \mu_{ab} S_1 \, e^{-\Gamma_o t} \\ &= \mu_{ab} \, e^{-\Gamma_o t} \left\{ S_1^{(0)} + \frac{\omega_o}{D^2 + \omega_o^2} \omega_{p1} \left[1 + \frac{D}{D^2 - \gamma^2} \right. \right. \\ &\quad \left. \left. \cdot \omega_{p1} \frac{D}{D^2 + \omega_o^2} \omega_{p1} \right]^{-1} (S_3^{(0)} + S_3^{(1)}) \right\} \end{aligned} \tag{2.3.17}$$

This expression provides the formal solution for the polarization which is calculated to infinite order. These results are obtained only for the special case where we assumed that the pumping and decay matrices are diagonal, and also that the matrix element μ_{ab} is real. An interested reader (if extant) would derive the generalized formula quite easily.

2.4 An Exact Solution for the Geometrical Representation

In the last section we treated the interaction between atoms and a field as a perturbation and obtained a formal solution to infinite order approximation. In this section we shall solve the equation of motion (2.2.8) without using any perturbation technique. Since the polarization of the medium is a nonlinear function of the field, we have higher harmonics of the fundamental mode both in space and time. A physical interpretation will be given for the solution.

First we apply the result of the last section and then the exact solution will be discussed. The exact solution requires a great deal of mathematical manipulation[11,12,13], yet it gives almost the same results derived from the rotating wave approximation (RWA) or rate equation approximation (REA). In the case of the Xe 3.51μ transition the comparison of numerically calculated results of exact solution with that of RWA or REA shows that RWA and REA are sufficient for practical purposes.

(A) Rotating wave approximation (RWA)

We assume the electromagnetic field is monochromatic and single mode,

$$E(z,t) = E_0 \cos \omega t \sin kz \qquad (2.4.1)$$

Since the dependence of macroscopic polarization on the field is non-linear, higher Fourier components of expression (2.4.1) will appear. In RWA we neglect all the terms except the fundamental mode*.

The standing wave expressed by the above equation can be split into four complex waves with the same amplitude as

$$E(z,t) = \frac{E_0}{4i} \{e^{i\omega t + ikz} - e^{i\omega t - ikz} + e^{-i\omega t + ikz} - e^{-i\omega t - ikz}\} \qquad (2.4.2)$$

We may assign the following physical meanings to each wave, as often the case in quantum electrodynamics[14,15]:

(1) The operator associated with $e^{i\omega t}$ corresponds to a photon (not normalized) creation, while $e^{-i\omega t}$ corresponds to annihilation of the photon.

(2) $e^{i\omega t - ikz}$ is a creation of photon with wave number k, and $e^{-i\omega t - ikz}$ is an annihilation of photon with wave number $-k$.

In a moving frame, expression (2.4.2) is rewritten by a proper Galilean transformation as

---

*Higher Fourier components of the polarization are not resonant with passive cavity modes and thus far less effective.

$$E(v,z,t) = \frac{E_o}{4i}\{e^{i(\omega+kv)t + ikz} - e^{i(\omega-kv)t - ikz}$$

$$+ e^{-i(\omega-kv)t + ikz} - e^{-i(\omega+kv)t - ikz}\} \qquad (2.4.3)$$

We have the following from Eq. (2.3.12):

$$S_3 = \sum_{m=0}^{\infty} [-\frac{D}{D^2 - \gamma^2}\omega_{pl}\frac{D}{D^2 + \omega_o^2}\omega_{pl}]^m (S_3^{(0)} + S_3^{(1)}) \qquad (2.4.4)$$

where

$$\omega_{pl} = -\frac{2\mu_{ab}}{\hbar} E(v,z',t') \qquad (2.4.5)$$

We already know from Eq. (2.2.33) that $S_3^{(1)} = 0$ and $S_3^{(0)} = \overline{N} e^{\Gamma_o t}$. Combining these with Eq. (2.4.4), S_3 is simplified to*

$$S_3 = \overline{N} e^{\Gamma_o t} \sum_{m=0}^{\infty} [-\frac{D + \Gamma_o}{(D+\Gamma_o)^2 - \gamma^2}\omega_{pl}\frac{D + \Gamma_o}{(D+\Gamma_o)^2 + \omega_o^2}\omega_{pl}]^m$$

$$= \overline{N} e^{\Gamma_o t} \sum [-\mathcal{D}(D)\omega_{pl} L^+(D)\omega_{pl}]^m \qquad (2.4.6)$$

where

$$\mathcal{D}(D) = \frac{1}{2}(\frac{1}{D+\gamma_a} + \frac{1}{D+\gamma_b}) \qquad (2.4.7)$$

---

*We use the relation

$$D(e^{\Gamma_o t} g(t)) = e^{\Gamma_o t}(D + \Gamma_o) g(t)$$

where $g(t)$ is an arbitrary function of t.

$$L^{\pm}(D) = \frac{1}{2}\left(\frac{1}{D+\Gamma_o - i\omega_o} \pm \frac{1}{D+\Gamma_o + i\omega_o}\right) \tag{2.4.8}$$

The mth stage of the approximation $\langle P\rangle_m$ for the macroscopic polarization is given by Eq. (2.3.17) as

$$\langle P\rangle_m = \frac{\overline{N}\mu_{ab}}{i} L^{-}(D)\ \omega_{p1}[-\mathcal{D}(D)\ \omega_{p1} L^{+}(D)\ \omega_{p1}]^m \tag{2.4.9}$$

By substituting the expression (2.4.3) into the above relation we find

$$\langle P\rangle_m = (-1)^m \frac{\overline{N}\mu_{ab}}{i} \sum L^{-}(D)\omega_{p1}(2m+1)\ \ \mathcal{D}(D)\omega_{p1}(2m)L^{+}(D)$$

$$\omega_{p1}(2m-1)\ \cdots\ \cdots\ \mathcal{D}(D)\ \omega_{p1}(2)\ L^{+}(D)\omega_{p1}(1) \tag{2.4.10}$$

where the summation in the above expression is taken for all possible combinations of $\omega_{p1}(n)$, $(n=1,\cdots,2m+1)$ from the following four quantities

$$\frac{E_o}{4i} e^{i(\omega+kv)t + ikz}, \qquad -\frac{E_o}{4i} e^{i(\omega-kv)t - ikz},$$

$$\frac{E_o}{4i} e^{-i(\omega-kv)t + ikz}, \qquad -\frac{E_o}{4i} e^{-i(\omega+kv)t - ikz}$$

Choosing

$$\omega_{p1}(1) = \frac{E_o}{4i} e^{i(\omega+kv)t + ikz}$$

$$\omega_{p1}(2) = \frac{E_o}{4i} e^{-i(\omega-kv)t + ikz}$$

$$\omega_{p1}(3) = -\frac{E_o}{4i} e^{-i(\omega+kv)t - ikz}$$

we may interpret this as a process where a photon $\omega_{p1}(1)$ is emitted first, $\omega_{p1}(2)$ is absorbed second, and finally the absorption of $\omega_{p1}(3)$ occurs. The diagram of this process is shown in Fig. 2.2. After the annihilation of $\omega_{p1}(2)$, the momentum and energy are changed by amounts of $2k$ and $-2kv$ (in units of $\hbar$) respectively*.

In Fig. 2.2 the diagram for $m=2$ is also shown as an example. If we allow only the conserving process (which means the changes in momentum and energy are zero) after the absorption or emission of ω_{p1} (even integer) photon, Eq. (2.4.6) is simplified to

$$S_3 = \bar{N} e^{\Gamma_o t} \sum_0^\infty \left[- \frac{\mu_{ab}^2 E_o^2 \Gamma_o^2}{4\hbar^2 \gamma_a \gamma_b} \left\{ \frac{1}{\Gamma_o^2 + (\omega-\omega_o+kv)^2} + \frac{1}{\Gamma_o^2 + (\omega-\omega_o-kv)^2} \right\} \right]^m \tag{2.4.11}$$

We may call this a rotating wave approximation (RWA). Then the amplitude of the field E_o is given by the following integral equation:

$$\frac{1}{Q} = \frac{\bar{N}\mu_{ab}^2}{\varepsilon_o \hbar\, u\sqrt{\pi}} \int_{-\infty}^{\infty} \frac{\Gamma_o}{\Gamma_o^2 + (\omega-\omega_o+kv)^2} \times \frac{e^{-v^2/u^2}}{1 + \frac{\mu_{ab}^2 E_o^2 \Gamma_o^2}{4\hbar^2 \gamma_a \gamma_b} \left\{ \frac{1}{\Gamma_o^2+(\omega-\omega_o+kv)^2} + \frac{1}{\Gamma_o^2+(\omega-\omega_o-kv)^2} \right\}} dv \tag{2.4.12}$$

---

*The conservation of momentum, i.e., the alteration of the velocity of an atom due to the emission or absorption of a photon becomes important if the relative linewidth $\Delta\nu/\nu_o$ is of the order or less than $\hbar\nu/Mc^2$, M = mass of the atom.

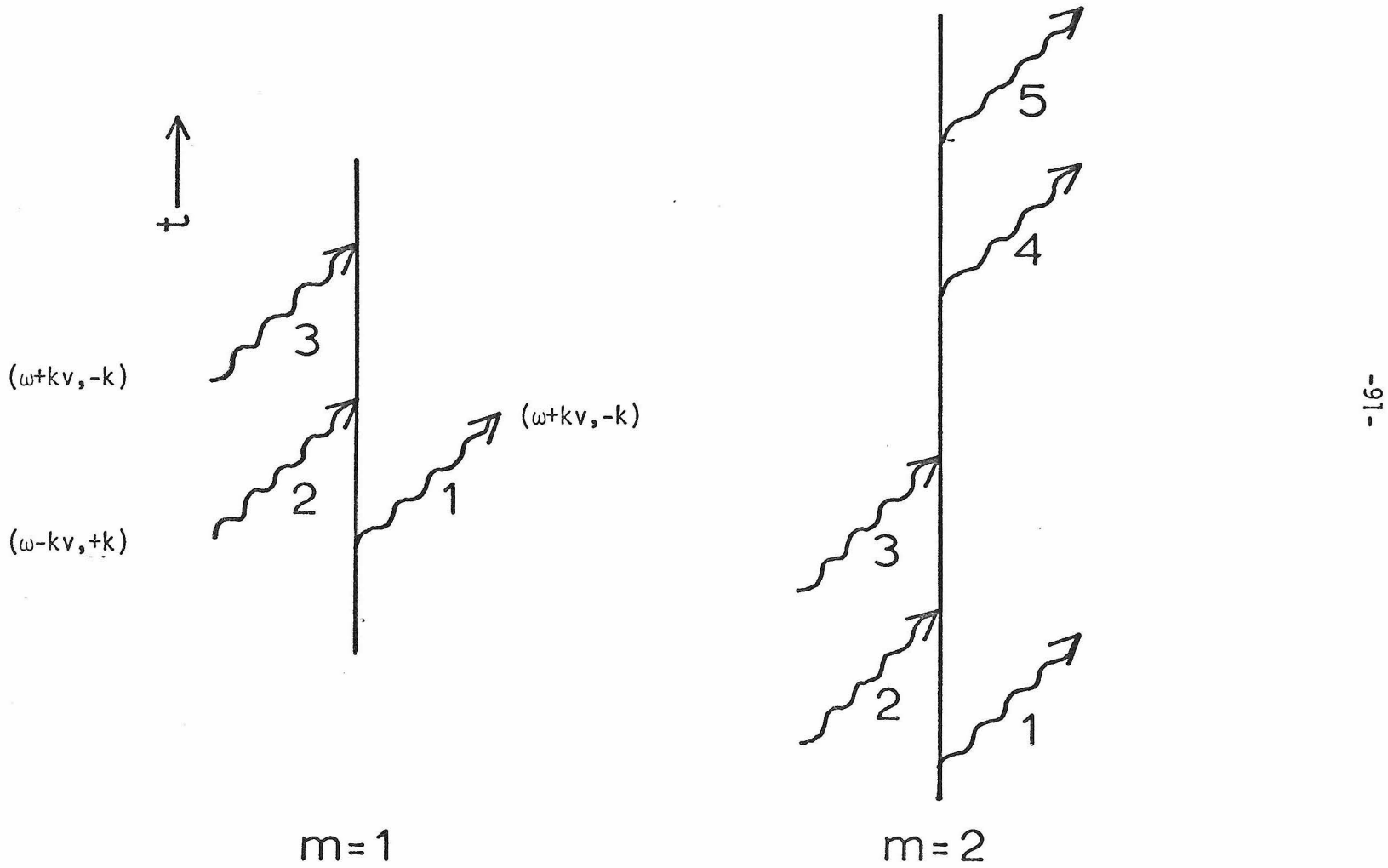

Fig. 2.2 Diagram of the interaction between an atom and three photons (left) and five photons (right). Inside the parenthesis denotes the energy and wave number of photon.

where Q is the figure of merit of the resonator. The above relation is equivalent to the result obtained in Sec. 1.2 by using REA. Details will be discussed in Sec. 2.6.

(B) Exact solution

As mentioned before, we have to take all the processes of absorption and emission into account to get an exact solution. To find this, it is more convenient to go back to the original expression for $\vec{S}$ and f given by Eqs. (2.2.15) and (2.2.16) as

$$\dot{f} = -\vec{\gamma}\cdot\vec{S} + \Lambda_o e^{\Gamma_o t}$$

$$\dot{\vec{S}} = \vec{\omega}\times\vec{S} - \vec{\gamma}\cdot f + \vec{\Lambda} e^{\Gamma_o t} \tag{2.4.13}$$

with the same algebraic manipulation as in Sec. 2.3 we obtain the following equation:

$$S_3 = \overline{N} e^{\Gamma_o t} - \frac{D}{D^2-\gamma^2}\omega_{P1}\frac{D}{D^2+\omega_o^2}\omega_{P1} S_3 \tag{2.4.14}$$

We may assume (Appendix H)

$$S_3 = \overline{N} e^{\Gamma_o t}\sum_{n=-\infty}^{\infty} A_n e^{2ink(z+vt)} \tag{2.4.15}$$

where A_n is the Fourier coefficient. The recursion relation for A_n is given by

$$A_n = \delta_{n,o} + \frac{\mu_{ab}^2 E_o^2}{16\hbar^2}\mathcal{D}(2iknv)[(A_{n+1}-A_n)\{L^+(\omega+(2n+1)kv) + L^+(\omega-(2n+1)kv)\} - (A_n - A_{n-1})\{L^+(\omega+(2n-1)kv) + L^+(\omega-(2n-1)kv)\}] \tag{2.4.16}$$

If $\frac{\mu_{ab}^2 E_o^2}{16\hbar^2} |\mathcal{D} \cdot L^+|$ is much smaller than unity, we may assume $|A_o| >> |A_1| >> |A_2| >> \cdots$. In this case we get Eq. (2.4.11) again. In the general case, we have to resort to a numerical calculation (see Appendix I). Using these coefficients A_n , we find that the polarization is given by

$$P = \frac{\overline{N}\mu_{ab}^2 E_o}{\hbar\, u\sqrt{\pi}} \mathrm{Im}\left[e^{i\omega t} \int_{-\infty}^{\infty} \frac{A_o - A_1}{\Gamma_o - i(\omega-\omega_o-kv)} e^{-v^2/u^2}\, dv\right] \sin kz \qquad (2.4.17)$$

The relation corresponding to Eq. (2.4.12) is

$$\frac{1}{Q} = \frac{\overline{N}\mu_{ab}^2}{\varepsilon_o \hbar\, u\sqrt{\pi}} \mathrm{Re}\left[\int_{-\infty}^{\infty} \frac{A_o - A_1}{\Gamma_o - i(\omega-\omega_o-kv)} e^{-v^2/u^2}\, dv\right] \qquad (2.4.18)$$

The calculated intensity for Xe 3.51μ transition is shown in Fig. 2.3 for various normalized pumping density $\bar{n} = \overline{N}/\overline{N}_T$. We took the parameters $\gamma_a/\Gamma_o = 6.4 \times 10^{-2}$ and $\gamma_b/\gamma_o = 1.94$. The discrepancy between the exact solution and RWA is the largest at line center where the medium is saturated by the oppositely traveling two waves at the same time. Deviations from the exact solutions are less than 5% at line center. As the relative excitation density $\bar{n}$ decreases, this discrepancy becomes smaller. The convergence of the computed solutions are checked to a part in a thousand.

Thus we can conclude the REA and RWA give a satisfactory agreement with the exact solution. In the following sections we use only RWA.

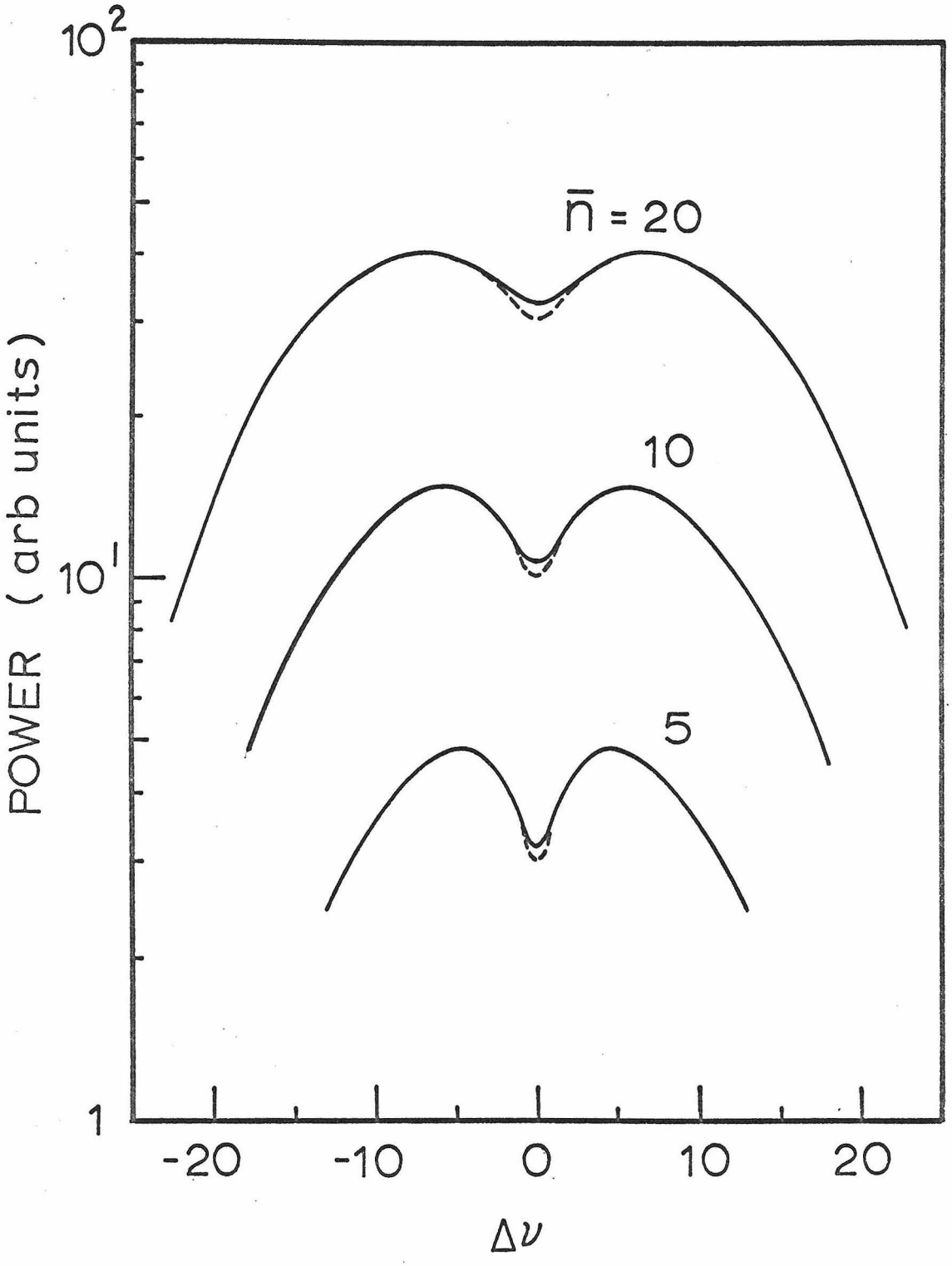

Fig. 2.3 Output power from a standing wave laser. Solid line is exact solution. Broken line is RWA.

2.5 A Multi-Mode Laser (narrow band random signal)

Up to this point we have been involved in a laser field with only one mode. It has been assumed that the field is sinusoidal both in time and in space, and that the amplitude and phase are constant. In this section we treat a field with many modes. According to Close[16], a higher order nonlinear process generates new spectral components by parametric modulation. However, this is incompatible with self-consistent field theory, i.e., whenever there are originally two modes oscillating in a laser, a third, a fourth, ... modes will appear due to this modulation effect. Nevertheless, in an actual laser we observe an electromagnetic field with finite number of modes which has fluctuations both in amplitude and in phase[17,18]. We can avoid this self-contradiction by treating the spectrum of the field as a narrow band random signal[19].

An actual laser has mechanical and statistical disturbances which give rise to a finite radiation bandwidth. Among the intrinsic line broadening mechanisms are: thermal noise, vacuum fluctuation fields, and spontaneous emission[20]. In this section the field is treated mainly as a random process. We do not treat a field with a deterministic phase and amplitude to which the phase-locking of modes may be related. We will present the limitation of the REA in this section.

The field is assumed to be expressed as

$$E(t,z) = \sum_n E_n(t) \cos(\omega_n t + \phi_n(t)) \sin k_n z \qquad (2.5.1)$$

$E_n(t)$ is a real amplitude of the field, ω_n is the frequency, $\phi_n(t)$ is the phase and k_n is the wave number of the nth mode. $E_n(t)$ and $\phi_n(t)$ are slowly varying functions of time in comparison with $\cos \omega_n t$. With a simple trigonometric manipulation, Eq. (2.5.1) is rewritten as

$$E(t,z) = \frac{1}{2} \sum_n E_n(t) \{e^{i\phi_n(t)} + e^{-i\phi_n(t)}\} \cos \omega_n t \sin k_n z$$

$$+ \frac{i}{2} \sum_n E_n(t) \{e^{i\phi_n(t)} - e^{-i\phi_n(t)}\} \sin \omega_n t \sin k_n z \quad (2.5.2)$$

Assuming $E_n(t)$ is square integrable (even if it is not, it is still possible to use the Fourier analysis technique[19]), we may describe $E_n(t)\, e^{i\phi_n(t)}$ by a proper Fourier transformation as

$$E_n(t)\, e^{i\phi_n(t)} = \int_{-\infty}^{\infty} f_n(\beta)\, e^{-i\beta t}\, d\beta \quad (2.5.3)$$

Since $E_n(t)\, e^{i\phi_n(t)}$ determines the linewidth of the mode, which is known to be very small[21], $f_n(\beta)$ is appreciable only around $\beta = 0$.

On the other hand we can consider the function $f_n(\beta)$ to be a random variable*. To distinguish this from conventional non-random processes, we use the tilde notation. Formally we may write,

---

*If the width $\Delta\beta$ of the significant region of the spectral density $f_n(\beta)$ is small compared to the center frequency ω_n , the process with this characteristic is called a narrow band random process[19].

$$\tilde{E}_n(t)\, e^{i\tilde{\phi}_n(t)} = \int_{-\infty}^{\infty} \tilde{f}_n(\beta)\, e^{i\beta t}\, d\beta \qquad (2.5.4)$$

For the time being we treat the deterministic process. From Eqs. (2.5.2) and (2.5.3) we have the following:

$$E(t,z) = \frac{1}{2} \sum \{ \int f_n(\beta)\, e^{-i\beta t}\, d\beta + \int f_n^*(\beta)\, e^{i\beta t}\, d\beta \}$$

$$\times \cos \omega_n t \sin k_n z + \frac{i}{2} \sum \{ \int f_n(\beta)\, e^{-i\beta t}\, d\beta$$

$$- \int f_n^*(\beta)\, e^{i\beta t}\, d\beta \} \sin \omega_n t \sin k_n z \qquad (2.5.5)$$

With the above expression the macroscopic polarization of the medium has to be constructed. However, in this case the task is more difficult than that of the previous cases. We have to calculate

$$\left[- \frac{D + \Gamma_o}{(D+\Gamma_o)^2 - \gamma^2}\, \omega_{pl}\, \frac{D + \Gamma_o}{(D+\Gamma_o)^2 + \omega_o^2}\, \omega_{pl} \right]^N \qquad (2.5.6)$$

where $N = 1,2,\ldots$

$$\omega_{pl} = - \frac{2\mu_{ab}}{\hbar} E(t,z)$$

$$= \frac{i\mu_{ab}}{2\hbar} \sum_n \left[\int f_n(\beta)\, e^{-i\beta t}\, d\beta\, e^{i(\omega_n t + k_n z)} - \text{c.c.} \right.$$

$$\left. - \int f_n(\beta)\, e^{-i\beta t}\, d\beta\, e^{i(\omega_n t - k_n z)} + \text{c.c.} \right] \qquad (2.5.7)$$

In Section 2.4 we made the quantity (2.5.6) time independent by using

RWA. In the case where the field has many modes, expression (2.5.6) is no longer time independent. With a proper Galilean transformation, $z = z' + vt'$ and $t = t'$, we have Eq. (2.5.8) on the next page. The operator D in Eq. (2.5.8) operates on the whole quantity that comes on the right.

We make the following assumptions to simplify the calculations:

(i) Since $f_n(\beta)$ is appreciable only around $\beta = 0$, the integral

$$\iint_{-\infty}^{\infty} f_n(\beta)\, f_m^*(\beta')\, e^{-i(\beta-\beta')t}\, d\beta\, d\beta'$$

has a much narrower spectral width than any intermode spacing $\Delta\omega_{n',m'}$ $(n' \neq m')$.

(ii) $f_n(\beta)$ approaches to zero very rapidly as β departs from zero. We can thus set $\beta = 0$ in $\mathcal{D}$ or L^+ inside the integral in Eq. (2.5.8).

With these assumptions, quantity (2.5.6) is shown to have at least one term which is proportional to

$$\exp\{it \sum_{j=1} \Delta\omega_{n_j,m_j}\}$$

$\Delta\omega_{n_j,m_j}$ is the difference between the angular frequencies of n_jth and m_jth modes. n_j and m_j are arbitrary. The Nth stage approximation for the polarization is proportional to $L^-(D)\, \omega_{p1}[-\mathcal{D}(D)\, \omega_{p1}\, L^+(D)\, \omega_{p1}]^N$. There is at least one term in this quantity with time dependence $\exp it(\omega_\ell + \sum_{j=1}^{N} \Delta\omega_{n_j,m_j})$. The polarization and the field given by Eq. (2.5.5), satisfy the wave equation,

$$- \frac{D + \Gamma_o}{(D+\Gamma_o)^2 - \gamma^2}\,\omega_{pl}\,\frac{D + \Gamma_o}{(D+\Gamma_o)^2 + \omega_o^2}\,\omega_{pl}$$

$$= -\frac{\mu_{ab}^2}{16\hbar^2}\sum_{n,m}\Big[e^{i(\Delta\omega_{n,m} + \Delta k_{n,m}v)t' + i\Delta k_{n,m}z'}\int_{-\infty}^{\infty}\!\!\int f_n(\beta)\, f_m^*(\beta')\, e^{-i(\beta-\beta')t'}$$

$$\times\, \mathcal{D}(D + i(\Delta\omega_{n,m} + \Delta k_{n,m}v - \beta + \beta'))\,\{L^+(D + i(\omega_n - \beta + k_n v)) + L^+(D - i(\omega_m - \beta' + k_m v))\}\, d\beta\, d\beta'$$

$$+ e^{i(\Delta\omega_{n,m} - \Delta k_{n,m}v)t' - i\Delta k_{n,m}z'}\int_{-\infty}^{\infty}\!\!\int f_n(\beta)\, f_m^*(\beta')\, e^{-i(\beta-\beta')t'}$$

$$\times\, \mathcal{D}(D + i(\Delta\omega_{n,m} - \Delta k_{n,m}v - \beta + \beta'))\,\{L^+(D + i(\omega_n - \beta - k_n v)) + L^+(D - i(\omega_m - \beta' - k_m v))\, d\beta\, d\beta'\}\,\Big] \quad (2.5.8)$$

where

$$\Delta\omega_{n,m} = \omega_n - \omega_m \quad , \quad \Delta k_{n,m} = k_n - k_m \quad (2.5.9)$$

$$\mathcal{D}(D) = \frac{1}{2}\left(\frac{1}{D + \gamma_a} + \frac{1}{D + \gamma_b}\right) \quad (2.5.10)$$

and

$$L^{\pm}(D) = \frac{1}{2}\left(\frac{1}{D + \Gamma_o - i\omega_o} \pm \frac{1}{D + \Gamma_o + i\omega_o}\right) \quad (2.5.11)$$

$$-\nabla^2 E + \mu_o \sigma \frac{\partial E}{\partial t} + \mu_o \varepsilon_o \frac{\partial^2 E}{\partial t^2} = -\mu_o \frac{\partial^2 P}{\partial t^2} \tag{2.5.12}$$

then the electromagnetic field should have a term which is written, within a constant, as

$$\exp it(\omega_\ell + \sum_{j=1}^{N} \Delta\omega_{n_j,m_j})$$

Thus, we have

$$\omega_k = \omega_\ell + \sum_{j=1}^{N} \Delta\omega_{n_j,m_j} \tag{2.5.13}$$

If the modes are not spaced equally, it is impossible to find a proper combination of k and ℓ which satisfies Eq. (2.5.13). In other words, we cannot construct a self-consistent field unless each mode is spaced in arithmetical progression.

We do not carry out the calculations for a field which has a deterministic amplitude and phase. We now treat a field as a random variable. We have neglected the spontaneous term, which gives rise to the fluctuations both in phase and in amplitude. This phenomenological fluctuation may be described as a random process. We assume that this is a stationary and ergodic process* and that there is no correlation between two different modes. Then we have

---

*Stationary means that the ensemble average is independent of origin of time, and ergodic means that the ensemble average is the same as the time average over individual members of the ensemble.

$$\overline{\tilde{E}_n(t)\, e^{i\tilde{\phi}_n(t)}\, (\tilde{E}_m(t)\, e^{i\tilde{\phi}_m(t)})^*} = \overline{\tilde{E}_n^2(t)}\, \delta_{n,m} \tag{2.5.14}$$

where the bar denotes the ensemble average. From Eq. (2.5.4), the above expression is rewritten as

$$\int_{-\infty}^{\infty}\int \overline{\tilde{f}_n(\beta)\, \tilde{f}_m^*(\beta')}\, e^{-i(\beta-\beta')t}\, d\beta\, d\beta' = \overline{\tilde{E}_n^2(t)}\, \delta_{n,m}$$

$$= \langle \tilde{E}_n^2(t) \rangle\, \delta_{n,m} \tag{2.5.15}$$

Angle brackets denote the time average.

In an actual laser, the noise spectrum of the oscillator due to amplitude fluctuations is much smaller than that due to phase fluctuations, except when a laser is operated near threshold[20]. Therefore, we may assume that $\tilde{E}_n(t)$ is much more slowly varying than $e^{i\tilde{\phi}_n(t)}$. In this case we may replace the time average of $\tilde{E}_n^2(t)$ by its instantaneous value. That is,

$$\overline{E_n^2(t)} = \langle E_n^2(t) \rangle$$

$$= \tilde{E}_n^2(t) \tag{2.5.16}$$

Under this assumption, the ensemble average of the quantity (2.5.6) is, for $N = 1$,

$$\overline{-\mathcal{D}(D)\, \tilde{\omega}_{p1}\, L^+(D)\, \tilde{\omega}_{p1}}$$

$$= -\frac{\mu_{ab}^2}{4\hbar^2 \gamma_a \gamma_b} \sum_n \tilde{E}_n^2(t)\, L(\omega_n, v) \tag{2.5.17}$$

where

$$L(\omega_n, v) = \frac{\Gamma_o^2}{\Gamma_o^2 + (\omega_n - \omega_o + k_n v)^2} + \frac{\Gamma_o^2}{\Gamma_o^2 + (\omega_n - \omega_o - k_n v)^2} \qquad (2.5.18)$$

In calculating the Nth term of the polarization series, the following expression appears:

$$\tilde{f}_{n_1}(\beta_1)\, \tilde{f}^*_{m_1}(\beta_1')\, \tilde{f}_{n_2}(\beta_2)\, \tilde{f}^*_{m_2}(\beta_2') \cdots \tilde{f}_{n_N}(\beta_N)\, \tilde{f}^*_{m_N}(\beta_N')$$

If we take the ensemble average of the above, correlations exist not only between adjacent terms but also between any two non-adjacent terms. Let us examine the case

$$\tilde{f}_{n_1} \cdots \tilde{f}_{n_p}\, \tilde{f}^*_{m_p} \cdots \underbrace{\tilde{f}_{n_q}\, \tilde{f}^*_{m_q} \cdots \tilde{f}_{n_r}\, \tilde{f}^*_{m_r}} \cdots \tilde{f}^*_{m_N} \qquad (2.5.19)$$

where correlations occur between $\tilde{f}_{n_q}$ and $\tilde{f}^*_{m_r}$, $(n_q = m_r)$ but not between $\tilde{f}_{n_r}$ and $\tilde{f}^*_{m_r}$ $(n_r \neq m_r)$. Then $\Delta\omega_{n_r,m_r}$ and $\Delta k_{n_r,m_r}$ do not vanish, and we have a factor $\mathcal{D}(i(\Delta\omega_{n_r,m_r} + v\Delta k_{n_r,m_r}))$ in Eq. (2.5.8). If we assume that

$$\Delta\omega_{n,m} >> \gamma_a \quad \text{and} \quad \gamma_b \qquad (2.5.20)$$

for $n \neq m$, we have

$$|\mathcal{D}(i(\Delta\omega_{n_r,m_r} + v\Delta k_{n_r,m_r}))| << |\mathcal{D}(0)|$$

Thus, we may neglect the contribution from the terms which have the correlation as described in (2.5.19). Therefore we have to take into consideration only the terms expressed in the form

$$\tilde{f}_{n_1}\tilde{f}^{*}_{n_1}\tilde{f}_{n_2}\tilde{f}^{*}_{n_2}\cdots\cdots,\ \tilde{f}_{n_N}\tilde{f}^{*}_{n_N}$$

If the fluctuations of the quantity $\tilde{E}_n(t)$ are very small, we may approximate (Appendix J),

$$\overline{\{\tilde{E}_n^2(t)\}^N} \cong \overline{\{\tilde{E}_n^2(t)\}}^N$$

$$\cong \{\tilde{E}_n^2(t)\}^N \tag{2.5.21}$$

Thus we get,

$$\overline{[-\mathcal{D}(D)\ \tilde{\omega}_{pl}\ L^{+}(D)\ \tilde{\omega}_{pl}]^N}$$

$$\cong \{-\frac{\mu_{ab}^2}{4\hbar^2\ \gamma_a\gamma_b}\sum_n \tilde{E}_n^2(t)\ L(\omega_n,v)\}^N \tag{2.5.22}$$

where we neglect the operation D on $\tilde{E}_n^2(t)$. The polarization is given by Eq. (2.3.17) as

$$\tilde{P} = \frac{\overline{N}\ \mu_{ab}^2\omega_o}{i\hbar\ u\sqrt{\pi}}\int_{-\infty}^{\infty}\sum_{m=0}^{\infty} L^{-}(D)\tilde{\omega}_{pl}[-\mathcal{D}(D)\tilde{\omega}_{pl}$$

$$\cdot\ L^{+}(D)\tilde{\omega}_{pl}]^m\ e^{-v^2/u^2}\ dv \tag{2.5.23}$$

The Maxwell's wave equation is

$$\frac{\partial^2}{\partial z^2}\tilde{E} + \mu_o\sigma\frac{\partial}{\partial t}\tilde{E} + \frac{1}{c_o^2}\frac{\partial^2}{\partial t^2}\tilde{E} = -\mu_o\frac{\partial^2}{\partial t^2}\tilde{P} \tag{2.5.24}$$

The left hand side of the above relation is written as

$$\frac{1}{2}\sum_n \Big[\int_{-\infty}^{\infty}\Big\{k_n^2 + i\mu_o\sigma(\omega_n-\beta) - \frac{(\omega_n-\beta)^2}{c_o^2}\Big\}\tilde{f}_n(\beta)\, e^{-i\beta t}d\beta\, e^{i\omega_n t} + \text{c.c.}\Big] \sin k_n z \qquad (2.5.25)$$

If we take the ensemble average of the above, it vanishes because $\tilde{f}_n(\beta) = 0$. If we calculate the ensemble average after multiplying by $\tilde{E}_\ell(t)\, e^{i\tilde{\phi}_\ell(t)}$, we have the following

$$\Big\{k_\ell^2\tilde{E}_\ell^2(t) - \frac{\omega_\ell^2}{c_o^2}\tilde{E}_\ell^2(t)\Big\}\cos\omega_\ell t \sin k_\ell z - \omega_\ell\mu_o\sigma\,\tilde{E}_\ell^2(t)\sin\omega_\ell t \sin k_\ell z$$

$$= \frac{\bar{N}\,\mu_{ab}^2\,\mu_o\,\omega_\ell^2}{\hbar\, u\sqrt{\pi}} \sin k_\ell z\, \tilde{E}_\ell^2(t)$$

$$\int_{-\infty}^{\infty} \frac{-\Gamma_o\sin\omega_\ell t + (\omega_\ell - \omega_o + k_\ell v)\cos\omega_\ell t}{\Gamma_o^2 + (\omega_\ell - \omega_o + k_\ell v)^2}\, \frac{e^{-v^2/u^2}}{1+\tilde{B}(v)}\, dv \qquad (2.5.26)$$

where

$$\tilde{B}(v) = \frac{\mu_{ab}^2}{4\hbar^2\,\gamma_a\gamma_b}\sum_n \tilde{E}_n^2(t)\, L(\omega_n, v) \qquad (2.5.27)$$

Thus, we have

$$\frac{1}{Q} = \frac{\bar{N}\,\mu_{ab}^2}{\varepsilon_o\hbar\, u\sqrt{\pi}}\int_{-\infty}^{\infty}\frac{\Gamma_o}{\Gamma_o^2 + (\omega_\ell - \omega_o + kv)^2}\,\frac{e^{-v^2/u^2}}{1+\tilde{B}(v)}\,dv \qquad (2.5.28)$$

and

$$k_\ell^2 - \frac{\omega_\ell^2}{c_o^2} = \frac{\bar{N}\mu_{ab}^2\mu_o\omega_\ell^2}{\hbar\, u\sqrt{\pi}}\int\frac{(\omega_\ell - \omega_o + kv)}{\Gamma_o^2 + (\omega_\ell - \omega_o + kv)^2}\,\frac{e^{-v^2/u^2}}{1+\tilde{B}(v)}\,dv \qquad (2.5.29)$$

Expression (2.5.28) is the threshold condition, while Eq. (2.5.29)

gives the dispersion relation. These are the same relations that the REA gives in Chapter I, if we assume

$$I(\nu) = \sum_n I_{\nu_n} \delta(\nu - \nu_n)$$

We finish this section recalling that Eqs. (2.5.28) and (2.5.29) are valid only when the following conditions are satisfied:

(i) Each mode of the laser oscillation can be regarded as a random function.

(ii) There is no correlation between two different modes.

(iii) The mode spacing is much greater than γ_a and γ_b.

If one of the above three conditions is not fulfilled, expressions (2.5.28) and (2.5.29) do not hold. In this section we do not discuss the case where the intermode spacing $\Delta\omega_{n,m}$ $(n \neq m)$ is comparable to γ_a and γ_b.

2.6 A Standing Wave Laser

We have shown in the previous two sections that either the rotation wave approximation (RWA), or the rate equation approximation, is a good substitution for an exact solution, and that they are capable of describing a laser field even though the spectrum is a narrow band random signal. In this section, using the RWA, we make a closer investigation than we did in Chapter I of a standing wave laser.

First it is shown that the RWA gives the same integral equation for the field intensity as the REA does. Secondly, the dispersion

relation is discussed. The shift of the lasing frequency is given as a function of the change of cavity length. Finally, the measured depth and width of the Lamb dip are discussed and it is pointed out that the plane wave one-dimensional model is inadequate to describe the field.

(A) Theory

When a laser is operating well above threshold, the noise contributions due to spontaneous emission and thermal or quantum fluctuations are negligibly small[20,21]. Thus, we may take the electromagnetic field in the form

$$E(z,t) = E_0 \cos \omega t \sin kz \tag{2.6.1}$$

where E_0 is the time-independent amplitude.

(i) Relation between RWA and REA

From the above expression for the field in the RWA* the macroscopic polarization is written as (see Appendix K),

$$P(z,t) = \frac{\bar{N} \mu_{ab}^2 E_0}{\hbar u \sqrt{\pi}} \sin kz \int_{-\infty}^{\infty} \frac{-\Gamma_0 \sin \omega t + (\omega-\omega_0+kv) \cos \omega t}{\Gamma_0^2 + (\omega-\omega_0+kv)^2} \times \frac{e^{-v^2/u^2}}{1 + I_0 L(\omega,v)} dv \tag{2.6.2}$$

where I_0 is the normalized intensity given by

*If we include the terms which have the time dependence $e^{\pm 2i\omega t}$, the factors of these turn out to be a factor of $\sim 1/\omega$ smaller than the leading ones. The term proportional to $e^{\pm 2ikz}$ correspond to processes in which momentum is not conserved (see Section 2.4).

$$I_o = \frac{\mu_{ab}^2 E_o^2}{4\hbar^2 \gamma_a \gamma_b} \tag{2.6.3}$$

and

$$L(\omega,v) = \frac{\Gamma_o^2}{\Gamma_o^2 + (\omega-\omega_o+kv)^2} + \frac{\Gamma_o^2}{\Gamma_o^2 + (\omega-\omega_o- kv)^2} \tag{2.6.4}$$

Substituting expressions (2.6.1) and (2.6.2) into the Maxwell wave equation

$$-\frac{\partial^2}{\partial z^2} E + \mu_o\sigma \frac{\partial}{\partial t} E + \frac{1}{c_o^2}\frac{\partial^2}{\partial t^2} E = -\mu_o \frac{\partial^2}{\partial t^2} P \tag{2.6.5}$$

we find the following relations by equating sine and cosine terms on both sides:

$$\frac{1}{Q} = \frac{\overline{N}\,\mu_{ab}^2}{\varepsilon_o \hbar\, u\sqrt{\pi}} \int \frac{\Gamma_o}{\Gamma_o^2 + (\omega-\omega_o+kv)^2} \frac{e^{-v^2/u^2}}{1 + I_o\, L(\omega,v)} \tag{2.6.6}$$

$$k^2 - \frac{\omega^2}{c_o^2} = \frac{\mu_o\omega^2\, \overline{N}\mu_{ab}^2}{\hbar\, u\sqrt{\pi}} \int \frac{\omega-\omega_o+ kv}{\Gamma_o^2 + (\omega-\omega_o+kv)^2} \frac{e^{-v^2/u^2}}{1 + I_o L(\omega,v)} \tag{2.6.7}$$

where we use the relation $\sigma = \varepsilon_o\omega/Q$. The upper equation determines the amplitude E_o , while the lower one describes the dispersion relation. The expression (2.6.6) is equivalent to Eq. (1.2.11) which was derived from the REA. The identity may be shown by the substitutions

$$\Gamma_o = \pi\Delta\nu_N$$

$$\gamma_a = A_3$$

$$\gamma_b = A_2$$

$$B_{32} = \frac{\mu_{ab}^2}{4\hbar^2 c_o}$$

$$\alpha = \frac{\varepsilon_o \omega}{2Qc_o} \tag{2.6.8}$$

(ii) Output power

We may introduce the threshold pumping density $\bar{N}_T$ at line center as

$$\bar{N}_T = \frac{\varepsilon_o h\, u\sqrt{\pi}}{Q\mu_{ab}^2} \left\{ \int_{-\infty}^{\infty} \frac{\Gamma_o e^{-v^2/u^2}}{\Gamma_o^2 + k^2 v^2}\, dv \right\}^{-1} \tag{2.6.9}$$

For an arbitrary pumping density and detuning $\Delta\omega \equiv \omega - \omega_o$, the amplitude of the field is obtained from the integral equation

$$\bar{n} \int \frac{\Gamma_o}{\Gamma_o^2 + (\omega-\omega_o+kv)^2} \frac{e^{-v^2/u^2}}{1 + I_o\, L(\omega,v)}\, dv$$

$$= \int \frac{\Gamma_o\, e^{-v^2/u^2}}{\Gamma_o^2 + (\omega-\omega_o+kv)^2}\, dv \tag{2.6.10}$$

where $\bar{n}$ is the normalized density given by

$$\bar{n} = \bar{N}/\bar{N}_T \tag{2.6.11}$$

The above integral may be evaluated when the medium has a very large Doppler width and the laser is operated at line center. By a simple contour integral we have

$$\bar{n}^2 = 1 + \frac{\mu_{ab}^2\, E_o^2}{2\hbar^2 \gamma_a\, \gamma_b} \tag{2.6.12}$$

with the help of Eqs. (2.6.8), relation (2.6.12) is approximated by

$$I = \frac{2\pi\hbar\nu^3 A_2 A_3}{c_o^2 A_{32}} (\bar{n}^2 - 1)$$

$$\propto \begin{cases} \bar{n} - 1 & \text{for } \bar{n} \simeq 1 \\ \bar{n}^2 & \text{for } \bar{n} \gg 1 \end{cases} \qquad (2.6.13)$$

We have solved the integral equation (2.6.10) numerically with an IBM computer. The parameters were taken to be those appropriate for the Xe 3.27 μm line ($\Delta\nu_D$ = 100 MHz, $\Delta\nu_N$ = 3.68 MHz). Figure 2.4 is a theoretical plot of the depth of the Lamb dip vs. the excitation density.

(iii) Dispersion relation

Equation (2.6.7) gives the dispersion relation. Defining a function*

$$F(\bar{n},\omega) = \frac{\int \frac{\omega-\omega_o+kv}{\Gamma_o^2 + (\omega-\omega_o+kv)^2} \frac{e^{-v^2/u^2}}{1 + I_o L(\omega,v)} dv}{\int \frac{\Gamma_o}{\Gamma_o^2 + (\omega-\omega_o+kv)^2} \frac{e^{-v^2/u^2}}{1 + I_o L(\omega,u)} dv} \qquad (2.6.14)$$

---

* Some readers may wonder why F is a function of $\bar{n}$ and ω, instead of E_o and ω. However, as can be easily seen from Eq. (2.6.10), only two out of three quantities, namely $\bar{n}$, ω, and E_o, are independent. We may thus take $\bar{n}$ and ω as independent variables in Eq. (2.6.10) and also (2.6.14).

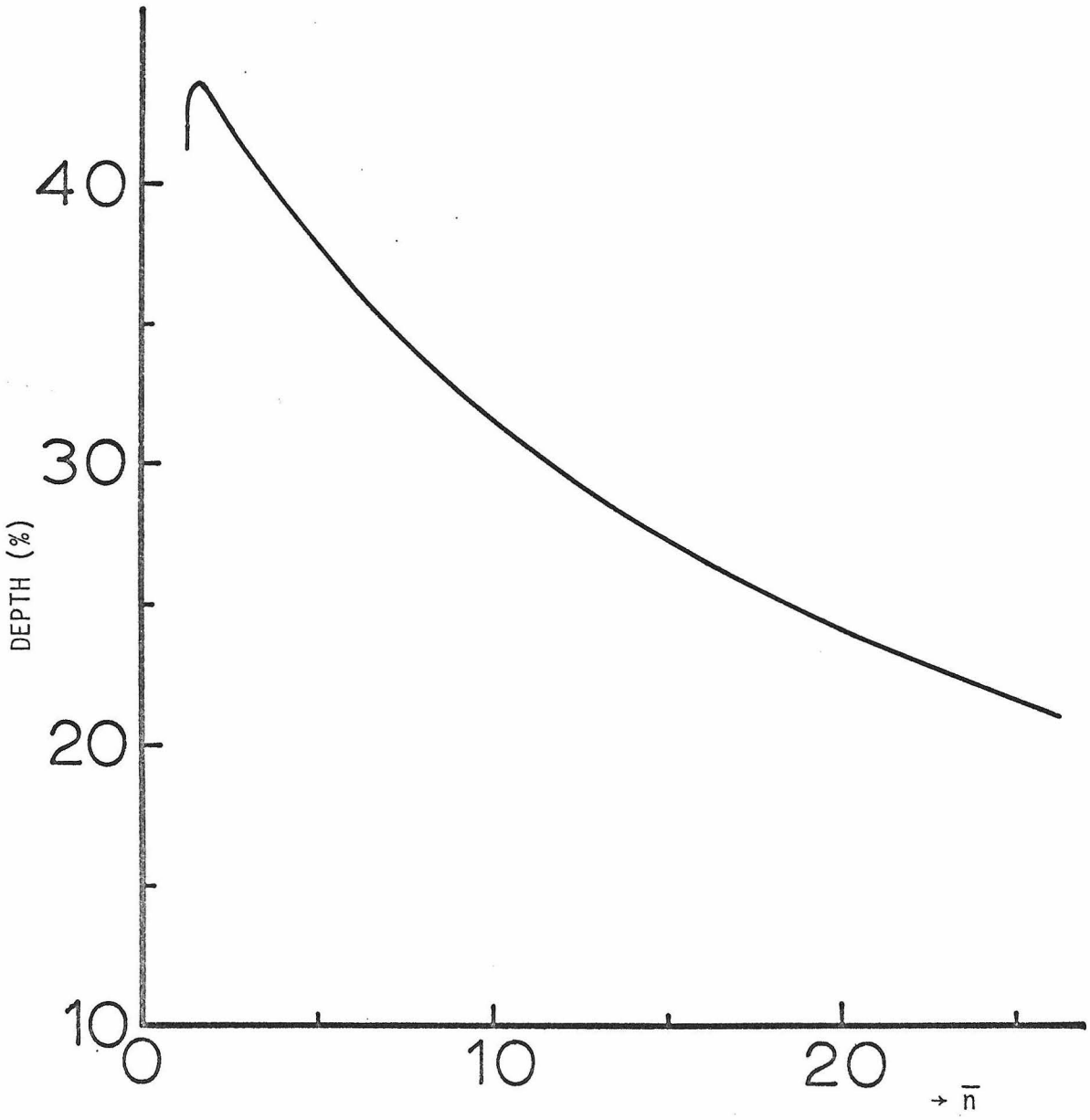

Fig. 2.4 Theoretical depth of the Lamb dip vs. the normalized pumping density.

We have the following relation from Eqs. (2.6.6) and (2.6.7):

$$\omega = \frac{kc_o}{\sqrt{1 + F/Q}} \tag{2.6.15}$$

The numerically calculated values of $F(\bar{n},\omega)$ are plotted in Fig. 2.5 for $\bar{n} = 2$ and 6. (Again the parameters are for Xe 3.27 μm line). Note that $F(\bar{n},\omega)$ has a different sign around line center from that of the wings. This causes the slope of the dispersion curve $\partial\omega/\partial k$ to be greater than c_o at resonance. The exact solution in Section 2.4 gives a similar dispersion relation[12].

Next we discuss the frequency shift due to the change of the cavity length. Defining $\Delta\omega$ and Δk as the deviations of ω and k from the values at line center, we have the following from Eq. (2.6.15):

$$\Delta k = \frac{\omega_o + \Delta\omega}{c_o}\sqrt{1 + \frac{1}{Q}F(\bar{n},\omega_o + \Delta\omega)} - \frac{\omega_o}{c_o} \tag{2.6.16}$$

Since kL is equal to a large integer times π, a small change ΔL in the cavity length L, gives rise to the variation in the wave number as

$$\Delta k = -\frac{k}{L}\Delta L \tag{2.6.17}$$

By equating Δk in Eqs. (2.6.16) and (2.6.17), we have

$$\frac{\Delta L}{L} = -(1 + \frac{\Delta\omega}{\omega_o})\sqrt{1 + \frac{1}{Q}F(\bar{n},\omega_o + \Delta\omega)} + 1 \tag{2.6.18}$$

where we put $k = \omega_o/c_o$. The quality factor Q of the cavity is on the order of 10^7, thus we may expand the square root in the above expression as

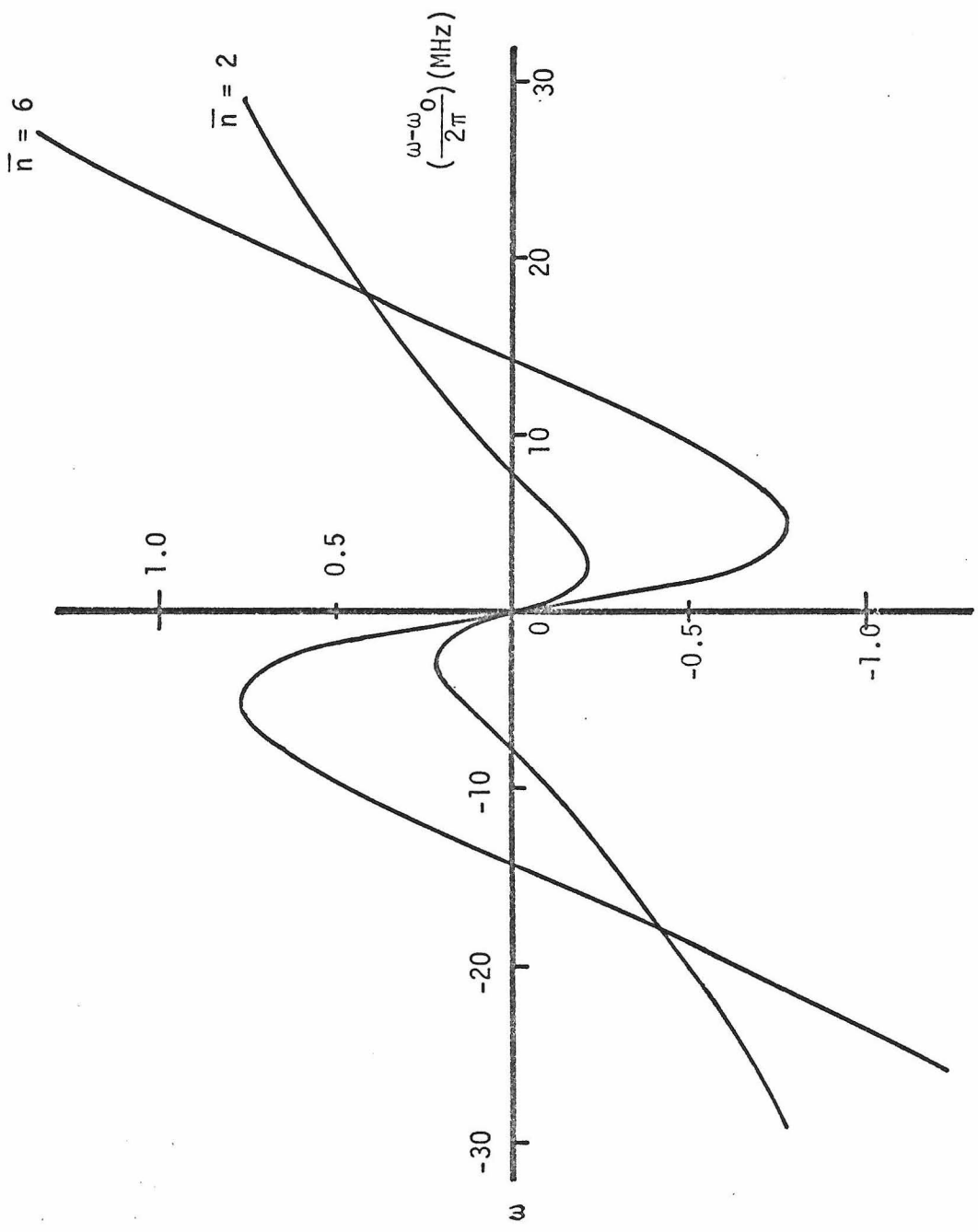

Fig. 2.5 Computed value of $F(\bar{n},\omega)$

$$\frac{\Delta L}{L} \simeq -\frac{\Delta\omega}{\omega_o} - \frac{1}{2Q} F(\bar{n}, \omega_o + \Delta\omega) \qquad (2.6.19)$$

Equations (2.6.18) or (2.6.19) give the frequency shift due to the change of the cavity length.

The numerically calculated full width at half maximum $\Delta\nu_{FWHM}$ of the Lamb dip is shown in Fig. 2.6.

The full scanning distance of the mirror at half maximum of the Lamb dip ΔL_{FDHM} is given by Eq. (2.6.18) as

$$\frac{\Delta L_{FDHM}}{2L} = -\left(1 + \frac{\Delta\nu_{FWHM}}{2\nu_o}\right) \sqrt{1 + \frac{1}{Q} F(\bar{n}, 2\pi\nu_o + \pi\Delta\nu_{FWHM})} + 1 \qquad (2.6.20)$$

In Fig. 2.7 is plotted ΔL_{FDHM} (in unit $c_o/\lambda L$ MHz) vs. $\bar{n}$ for various quality factors. The behavior of the ΔL_{FDHM} depends strongly on Q.

One may use the relation[22]

$$\Delta\nu_{FWHM} \simeq -\frac{c_o}{\lambda L} \Delta L_{FDHM} \qquad (2.6.21)$$

when the quality factor satisfies*

$$Q >> \frac{\nu_o}{\Delta\nu_{FWHM}} \qquad (2.6.22)$$

---

*From Eq. (2.6.19) the necessary condition to satisfy Eq. (2.6.21) is given by

$$\frac{\Delta\omega}{\omega_o} >> \frac{1}{2Q} F(\bar{n}, \omega_o + \Delta\omega)$$

Since $F(\bar{n}, \omega_o + \Delta\omega)$ is the order of unity for $\Delta\omega \sim \pi\Delta\nu_{FWHM}$, we get the relation (2.6.22).

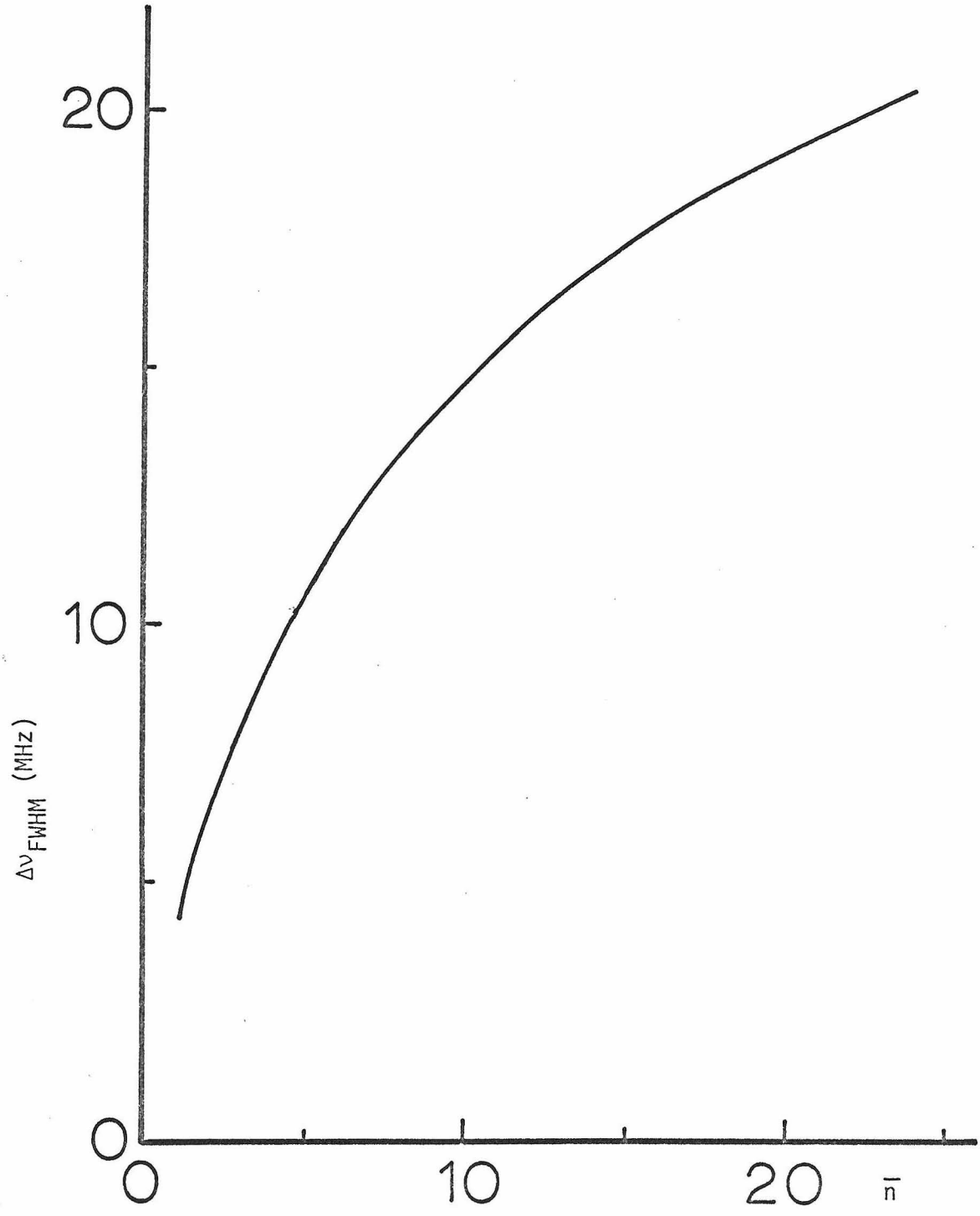

Fig. 2.6 Theoretical FWHM of Lamb dip for Xe 3.27μ transition vs. normalized pumping density.

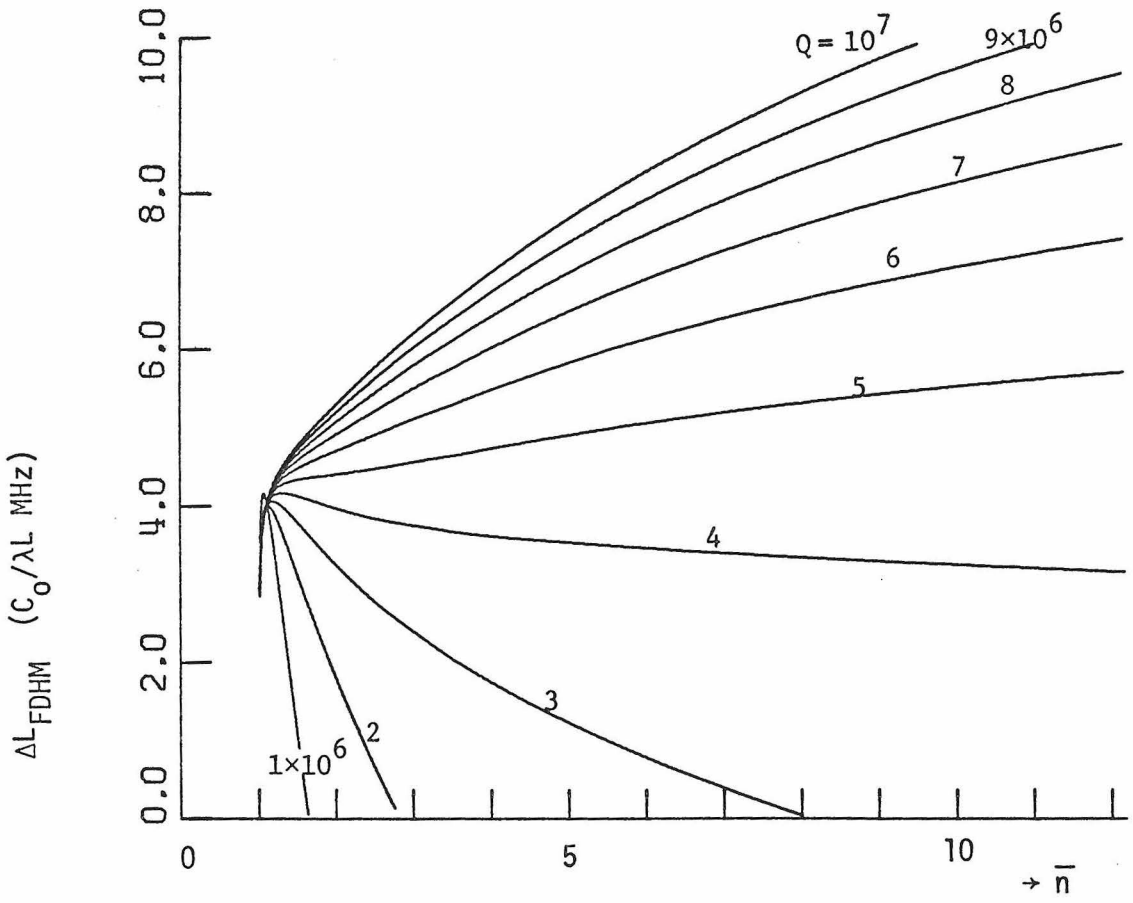

Fig. 2.7 Computed full scanning distance of the mirror at the half maximum of the Lamb dip vs. $\bar{n}$, for various values of Q .

(B) Experiment

(i) Measurement of the power output at line center

The experiments were conducted using the Xe 3.51μ transition. The cavity was 125 cm long with the discharge section 110 cm long and 5.5 mm in diameter. The excitation was done by d.c. discharge. The flat gold mirrors had reflectance of about 60% and 80%. To avoid vibration of the mirrors, the laser cavity was set up on a stable iron table which was isolated from the floor by air cushions.

One of the mirrors was scanned by a piezo-electric transducer to which about 6 cycles/min sawtooth voltage was applied. The distance of the translation was around 5 μm. The output was chopped by a 200 Hz mechanical chopper and was guided to a PbS detector followed by a PAR lock-in amplifier, model HR-8 (see Fig. 2.8). The output power was measured at the deepest point of the Lamb dip (which is believed to occur at the line center). The results are shown in Figs. 2.9 and 2.10 for near threshold and far above threshold, respectively.

Although Eqs. (2.6.13) are obtained under the standing wave assumption, these relations give good agreement with our experiments.

(ii) Measurement on the Lamb dip

The experiment was done with Xe 136 isotope[23]. The cavity was 75 cm long with a 50 cm discharge section. The diameter of the tube was 2.5 mm. The pressure of Xe gas was kept at about 5×10^{-3}Torr by a liquid nitrogen trap. We used a highly reflecting silver-coated mirror at one end of the cavity. At the other end was a gold coated mirror with a reflection of approximately 60%.

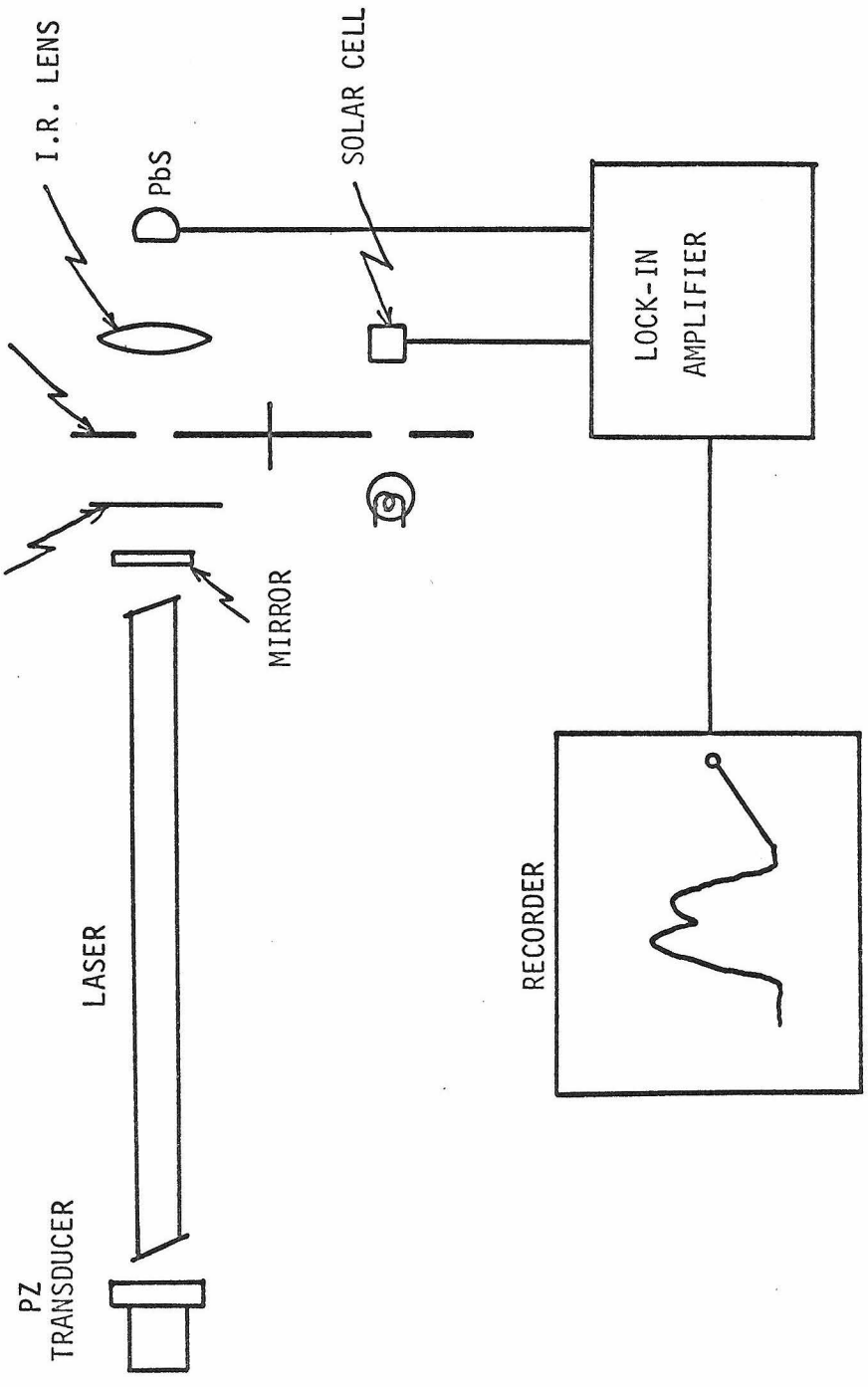

Fig. 2.8 Setup for measurement of the output power at line center

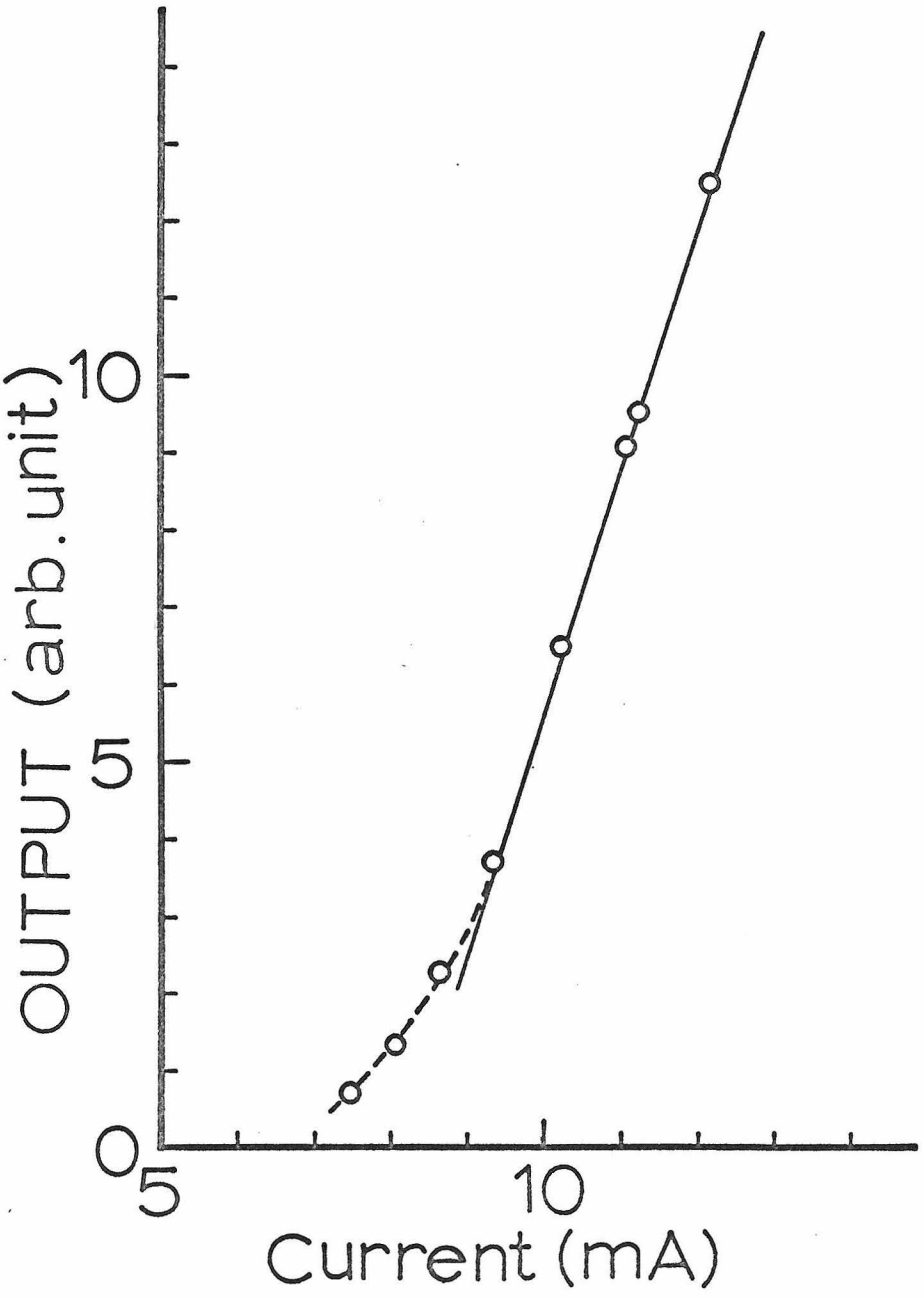

Fig. 2.9 Experimental output power vs. excitation current near the threshold at $\omega = \omega_0$

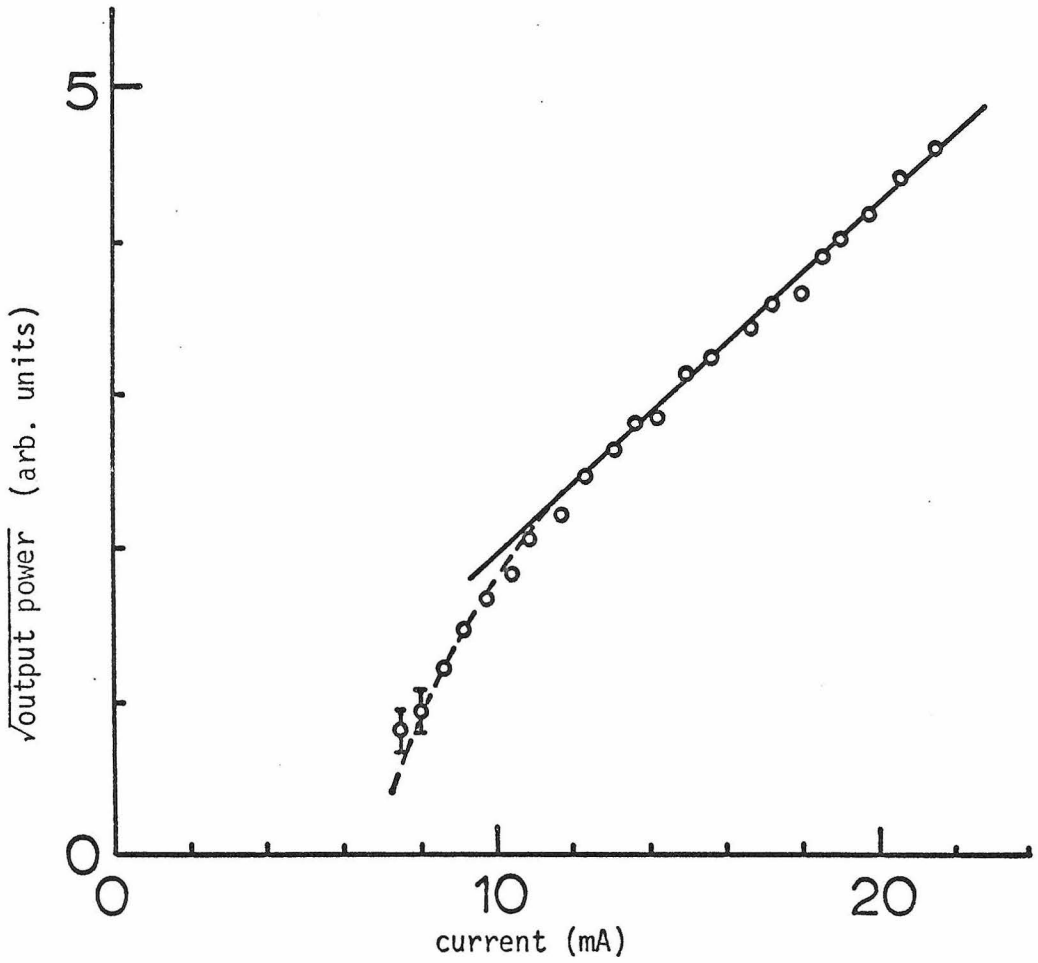

Fig. 2.10 Experimental output power above threshold $\bar{n} \gg 1$ at line center

Under these conditions both the 3.51μ and 3.27μ transitions occur simultaneously. Above a certain pumping current, peaks with different periods could be observed, as we scanned the mirror. If we put a filter (3.50μ with passband ±0.1μ) in the beam, only one peak could be seen. We did not, at first, know the wavelength of the second peak, so we set up the experiment shown in Fig. 2.11. The PbS detector is more sensitive to this unknown line than to the 3.51μ transition. A liquid nitrogen cooled Ge:Au detector responds to the unknown line and the 3.51μ line. We split the output from the laser into two beams. One went directly to the PbS detector, and the other beam passed through the 3.51μ filter and went to the Ge:Au detector. By this method we could separate the two peaks. The mirror was scanned over many wavelengths mechanically. The signals from the two detectors were amplified and recorded on a two-channel recorder simultaneously (Fig. 2.12). We counted 485.9 peaks for the unknown line and 453.5 peaks for the 3.508μ transition. This gives the wavelength

$$\lambda_{unknown} = 3.508 \times \frac{453.5}{485.9}$$

$$= 3.274\mu$$

Using this 3.27μ line[24] we measured the depth and width of the Lamb dip.

To avoid the vibrations, as mentioned before, the cavity was set up on a very stable iron table. The experiments were done mainly between Saturday nights and Sunday mornings. The mirror was scanned over about 5 μm by a piezo-electric transducer. The typical output for

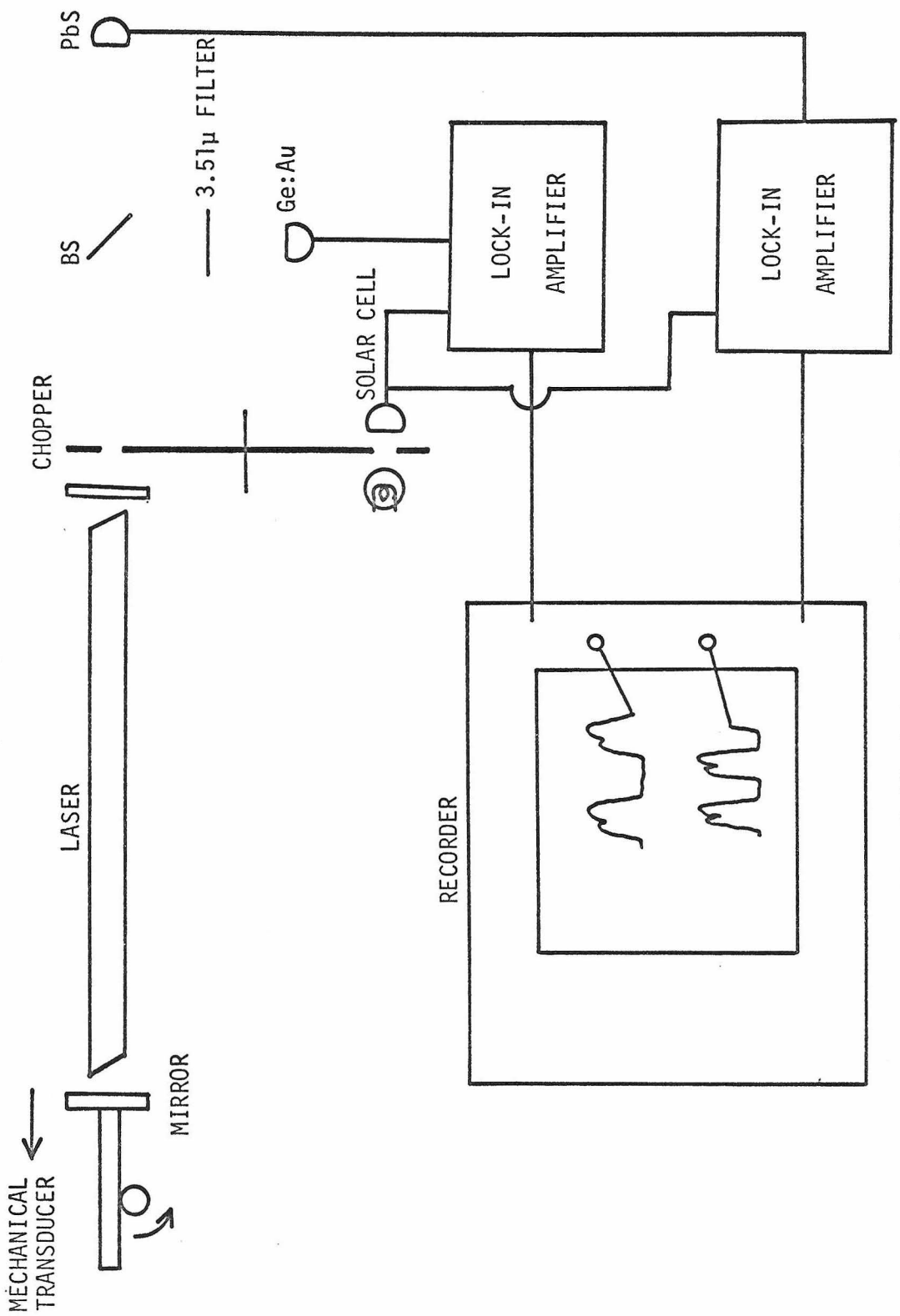

Fig. 2.11 Set-up for deciding the wavelength

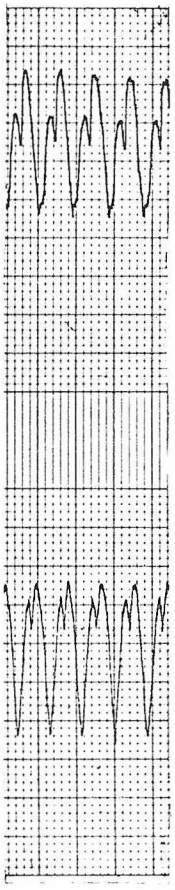

3.51μ output from Ge:Au detector

3.27μ output from PbS detector

increasing L

Fig. 2.12 Two separated signals from Xe laser

a pumping of 8.5 mA is shown in Fig. 2.13. The horizontal line is the voltage applied to the transducer. It took approximately 1 min. to scan the mirror once.

The measured depth of the Lamb dip (in %) is shown in Fig. 2.14. The fractional depth of the dip falls down to approximately 25% at a pumping current of 10 mA. The numerical calculations predict that the normalized pumping density $\bar{n} = \bar{N}/\bar{N}_T$ should be around 20, when the depth goes down to about 25%. The pumping current of 10 mA is twice the threshold current. If we take the normalized excitation density $\bar{n}$ is proportional to the pumping current, the observed decrease of the depth is larger than predicted by the theory (see Fig. 2.4).

The experimental full scanning distance at half maximum ΔL_{FDHM} vs. pumping current is plotted in Fig. 2.15. The measured ΔL_{FDHM} has a minimum at 8 mA. Neither of the curves shown in Fig. 2.7 seems to fit the data.

The observation that the depth of the Lamb dip at a given pumping is larger than predicted by the theory of this section can be explained if we assume that the effective quality factor of the cavity Q_{eff} increases with the pumping*.

---

*In the following section it will be shown that the radius of the curvature of the phase front R increases with the pumping density $\bar{N}$ (see Fig. 2.19), and that the diffraction loss due to the diverging wave is proportional to $2k/R$ (see Eq. (2.7.14)). Thus the quality factor Q (effective Q_{eff} in plane wave model in this section) increases with $\bar{N}$.

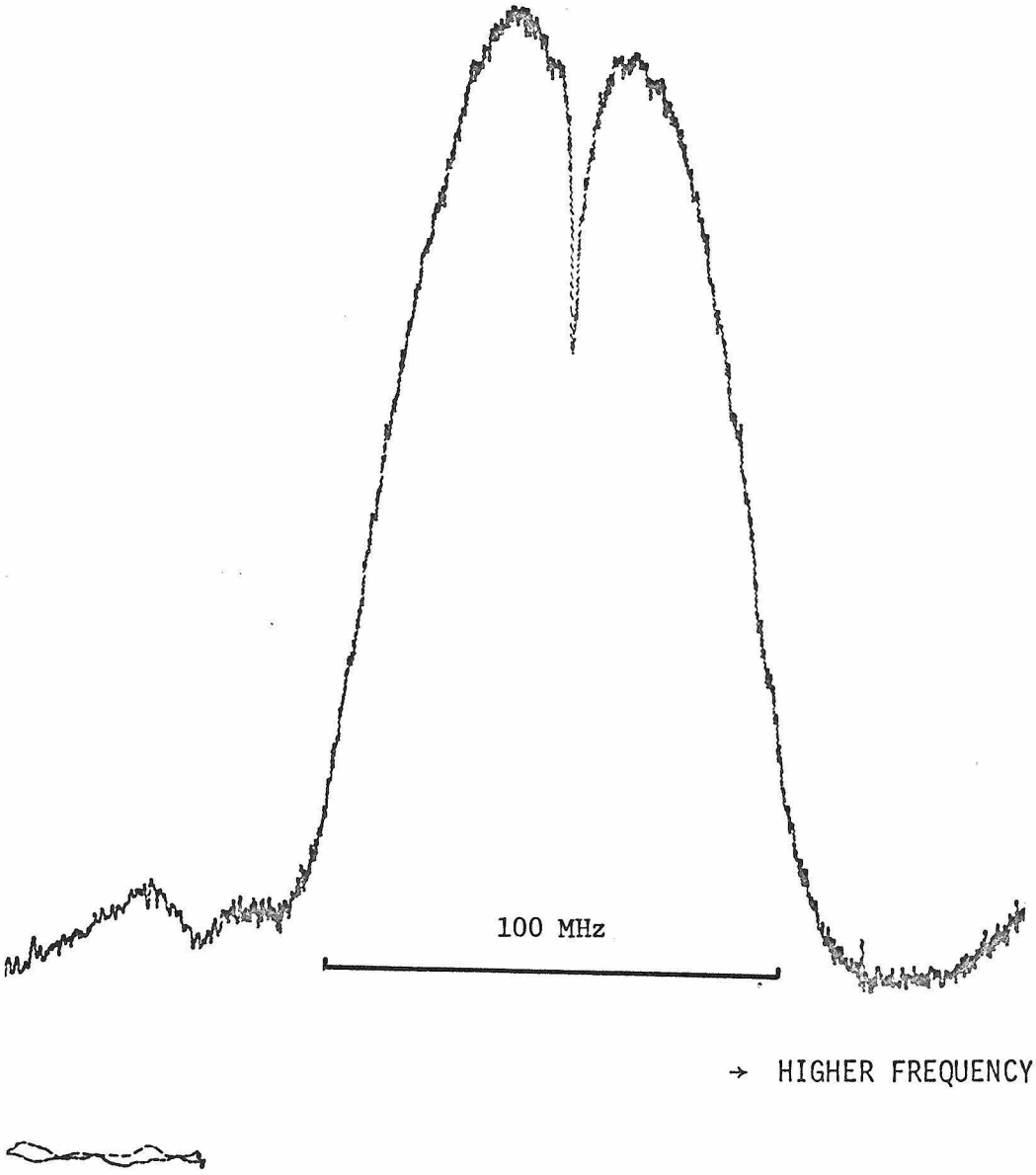

Fig. 2.13 A typical output power vs. scanned distance of the mirror, at excitation current 8.5 mA.

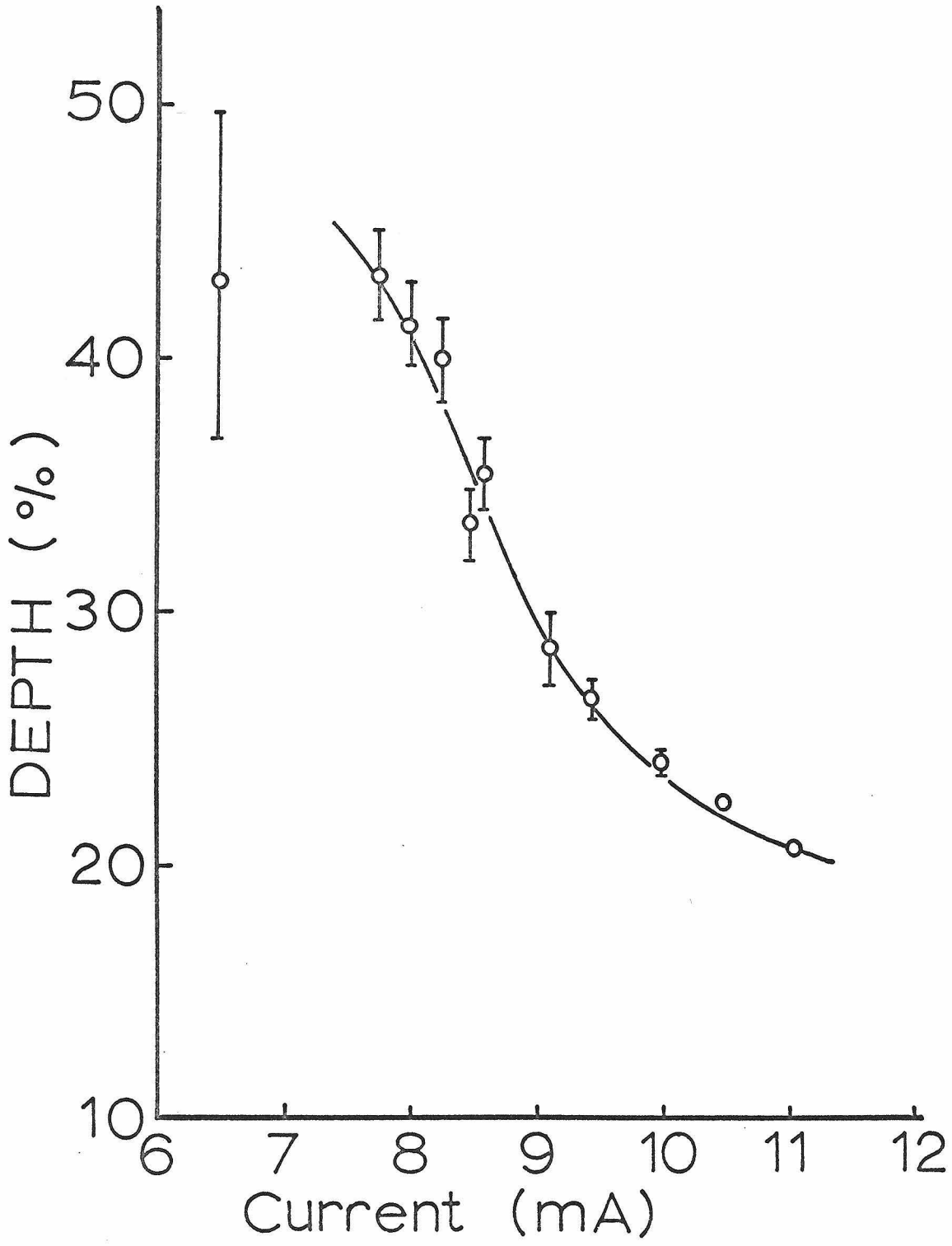

Fig. 2.14 Measured depth of the Lamb dip

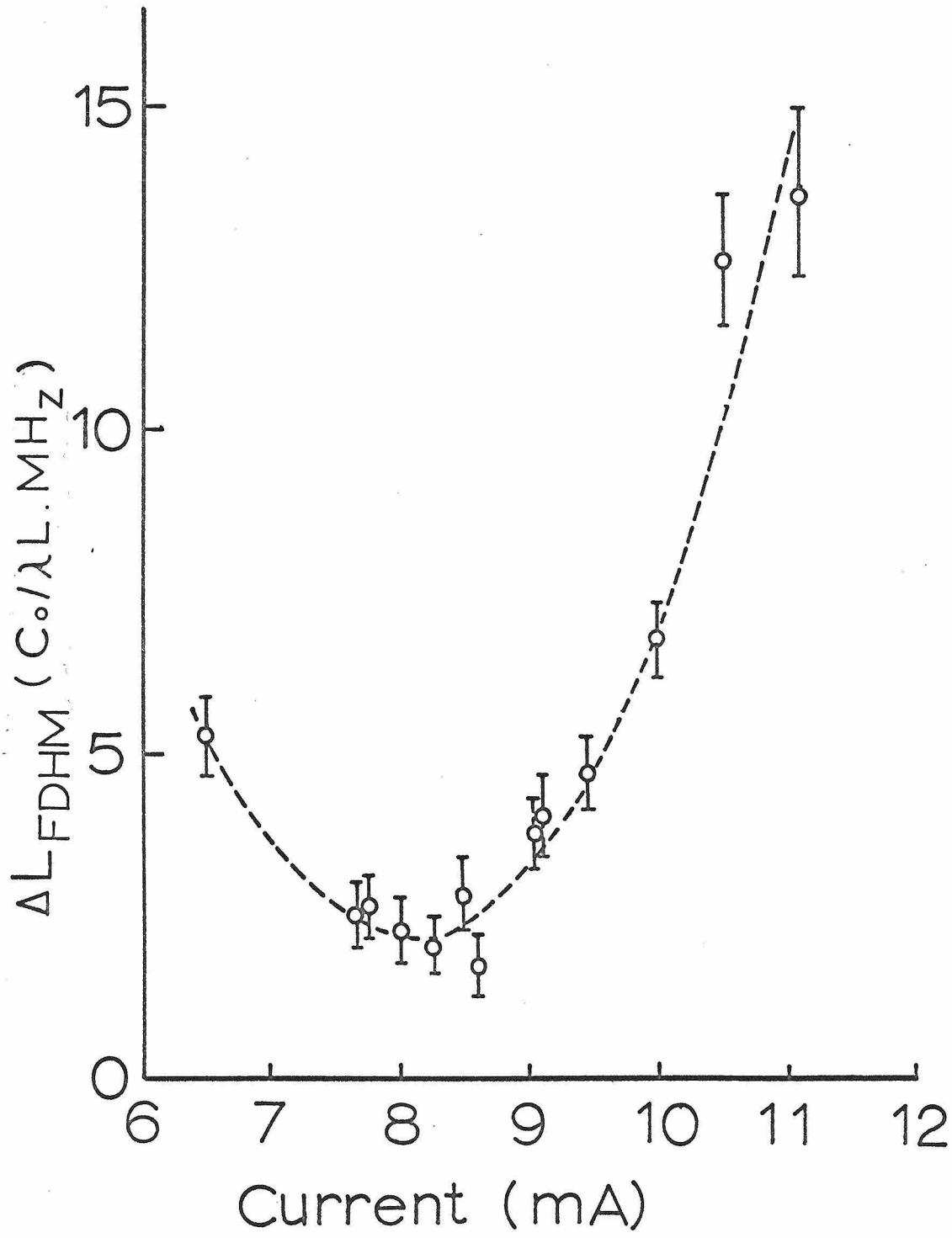

Fig. 2.15 Experimental full scanning distance at half maximum of the Lamb dip. Open circles are the data.

Under this assumption, the increase of Q_{eff} gives rise to the decrease of the effective excitation density $\overline{N}_T$ for a given pumping current. Then, the normalized excitation density $\overline{n} = \overline{N}/\overline{N}_T$ is not a linear function in $\overline{N}$. Thus the pumping current of 10 mA corresponds to $\overline{n}$ larger than 2 and the observed rapid decrease of the depth is explained qualitatively.

In Fig. 2.7 we have to use different curves for various $\overline{n}$. If we assume that Q takes a value of $1 \sim 2 \times 10^6$ for $\overline{n} = 1$, and that Q increases with the pumping current, ΔL_{FDHM} decreases first and increases after $Q \gtrsim 4 \times 10^6$.

(C) Conclusion

The experimental results for the output power at line center fit the theory, Eq. (2.6.13), satisfactorily. However, the measurement of the width and depth of the Lamb dip do not agree with the plane wave model. A qualitative agreement is provided, if we take into account the three-dimensional features of the modes. This point is taken up in detail in the next section.

2.7 A Radial Profile of a Laser

So far we have treated a field using a plane wave one-dimensional model. In an actual laser the beam extends only a finite distance in the radial direction, and cannot be described by a plane wave. The amplitude of the electromagnetic field has a gradient along the transverse direction and, moreover, the phase front has a finite radius of curvature. Therefore, under some circumstances, especially in a

capillary waveguide laser, the matching of the beam wavefront to the end mirrors becomes important. In this section we extend the RWA method to the three-dimensional model.

Many authors have analyzed the problem of the radial profile in a laser field. Two main approaches can be distinguished. The first one[25,26,27] is to assume that the index of refraction is quadratic in r. That is,

$$n(r) = n_0 + n_2 r^2 + \cdots$$

where r is the radial distance from the cylindrical axis. In a medium with this variation of the index of refraction, a ray matrix formalism[25] is of practical value. With this tool, often referred to as an ABCD law, the beam radius and phase front curvature are described. However, this method neglects saturation effects and does not give a self-consistent solution for the field.

The second one is often employed to treat the self-focusing effects[28,29,30]. An index of refraction is assumed in this case as

$$n = n_0 + n_2 E^2 + \cdots$$

A solution for the field is obtained self consistently, although the r dependence of n_0 and n_2 is neglected.

(A) Theory

In our approach to this problem, we use the RWA. It will be shown that the beam radii and the radii of curvature of the phase front vary as a function of pumping and frequency.

The laser field has a radial profile due to the fact that

(i) The electromagnetic field must satisfy the boundary conditions at the wall.

(ii) The excitation density is not uniform in the transverse direction.

If we pay attention to the field near the axis only, we may neglect the boundary condition at the wall. We use the following simplified model:

(i) The mirrors have flat surfaces with 100% reflectance.

(ii) The cavity is filled with an active medium.

(iii) The loss is uniformly distributed.

(iv) The wave has a spherical wavefront with Gaussian radial profile[25] (see Fig. 2.16).

(v) The amplitude, the radius of curvature of the phase front and the beam radius are constant along the cavity length.

Under these assumptions the electromagnetic field may be assumed to have the form

$$E(z,r,t) = E_0 \, e^{-r^2/w_0^2} \cos(\omega t - \frac{k}{2R} r^2) \sin kz \qquad (2.7.1)$$

where E_0 is a time independent amplitude, r is the distance in the transverse direction, w_0 is $\frac{1}{e}$ radius of the beam, ω is the angular frequency of the field, k is the wave number along the axis, and R is the radius of curvature of the phase front. The sign convention for R is taken so that positive and negative R indicate diverging and converging waves respectively.

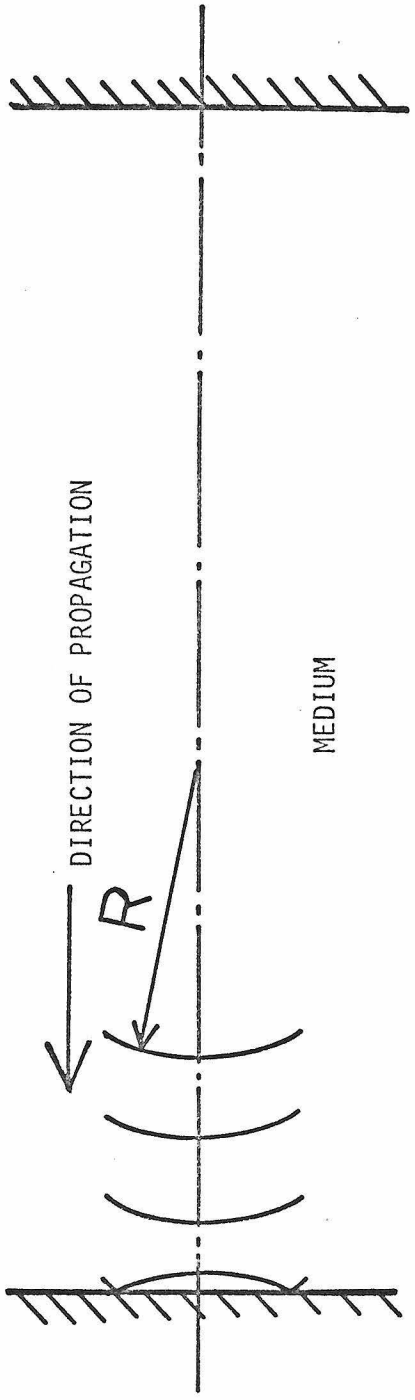

Fig. 2.16 Simple three-dimensional model of a laser

The Maxwell wave equation in cylindrical coordinates is given by

$$-\frac{1}{r}\frac{\partial}{\partial r}\left(r\frac{\partial}{\partial r}E\right)-\frac{\partial^2}{\partial z^2}E+\mu_o\sigma\frac{\partial}{\partial t}E+\frac{1}{c_o^2}\frac{\partial^2}{\partial t^2}E$$

$$=-\mu_o\frac{\partial^2}{\partial t^2}P \qquad (2.7.2)$$

where we took $\partial E/\partial\phi = 0$.

Using the following definitions:

$$C(z,r,t) = \cos(\omega t - \frac{k}{2R}r^2)\sin kz \qquad (2.7.3)$$

$$S(z,r,t) = \sin(\omega t - \frac{k}{2R}r^2)\sin kz \qquad (2.7.4)$$

the left hand side of Eq. (2.7.2) is given by

$$E_o[(k^2-\frac{\omega^2}{c_o^2}+\frac{4}{w_o^2})\,C(z,r,t)-(\frac{2k}{R}+\mu_o\sigma\omega)\,S(z,r,t)]$$

$$+r^2E_o[\{-\frac{8}{w_o^4}-\frac{1}{w_o^2}(k^2-\frac{\omega^2}{c_o^2})+\frac{k^2}{R^2}\}\,C(z,r,t)$$

$$+(\frac{6}{w_o^2}\frac{k}{R}+\frac{\mu_o\sigma\omega}{w_o^2})\,S(z,r,t)]+r^4E_o[\;\cdots\cdots \qquad (2.7.5)$$

It has been shown that the pumping, or the density of the population inversion in a gas discharge has a zero order Bessel function profile[31,32]. That is,

$$\bar{N}(r) = \bar{N}_o J_o(\frac{a_o}{b}r) \qquad (2.7.6)$$

where a_o is the first zero of the Bessel function, b is the radius

of the discharge tube and $\overline{N}_0$ is the excitation density on the axis.

Next we have to calculate the polarization. In the frame fixed to an atom with velocity (v_x,v_y,v_z) at (x,y,z), the time and space coordinates are given by the following Galilean transformation:

$$\begin{aligned} x &= x' + v_x t' \\ y &= y' + v_y t' \\ z &= z' + v_z t' \\ t &= t' \end{aligned}$$

With these new coordinate systems, the field (2.7.1) is approximated by

$$E(z',r',t') \cong E(r') \cos(\omega t' - \frac{k}{2R}\{\vec{r}'^2 + 2\vec{r}' \cdot \vec{v}_\perp t'\}) \sin k(z' + v_z t') \qquad (2.7.7)$$

where we used the approximation*,

$$(x' + v_x t')^2 + (y' + v_y t')^2 \cong \vec{r}'^2 + 2\vec{r}' \cdot \vec{v}_\perp t' \qquad (2.7.8)$$

and the substitution

$$\begin{aligned} \vec{r}' &= (x',y') \\ \vec{v}_\perp &= (v_x,v_y) \\ E(r) &= E_0 e^{-r^2/w_0^2} \end{aligned} \qquad (2.7.9)$$

---

*Since the time interval Δt between excitation and de-excitation of an atom is of order $\sim 1/\pi\Delta\nu_N$, the distance $\Delta\ell$ traveled by an atom during this time interval Δt is $v\Delta t$, where v is the velocity of the atom. For most atoms, we may take $x',y' >> \Delta\ell$, therefore we have the relation (2.7.8). Even when $\vec{r}'$ goes to zero, Eq. (2.7.8) is valid, because a transverse component of the motion does not cause an atom near the axis to see any phase shift of the field due to the finite curvature of the phase front.

Using the expression (2.7.7), we find the polarization in exactly the same way as we did in Section 2.6:

$$P(z,r,t) = \frac{\bar{N}_o \mu_{ab}^2 J_o(a_o r/b)\, E(r)}{\hbar\, u^3 \pi^{3/2}} \iiint_{-\infty}^{\infty} \frac{-\Gamma_o S(z,r,t) + (\omega-\omega_o - \frac{k}{R}\vec{r}\cdot\vec{v}_\perp + kv_z)\, C(z,r,t)}{\Gamma_o^2 + (\omega-\omega_o - \frac{k}{R}\vec{r}\cdot\vec{v}_\perp + kv_z)^2}$$

$$\times \left[1 + \frac{\mu_{ab}^2 E^2(r)}{4\hbar^2 \gamma_a \gamma_b} L(\omega - \frac{k}{R}\vec{r}\cdot\vec{v}_\perp, v_z)\right]^{-1} e^{-\frac{1}{u^2}(v_x^2 + v_y^2 + v_z^2)} \times dv_x dv_y dv_z \qquad (2.7.10)$$

This polarization and the electromagnetic field (2.7.1) should satisfy the wave equation (2.7.2). To find the self-consistent field, we expand P and E in power series of r and compare term by term on both sides of the wave equation. We go up to quadratic term, however we neglect $kr^2/2R$ in $C(z,r,t)$ and $S(z,r,t)$ in the expressions (2.7.5) and (2.7.10) as explained in Appendix L.

The zeroth order polarization P_o in r is written as

$$P_o = \frac{\bar{N}_o \mu_{ab}^2 E_o}{\hbar\, u\sqrt{\pi}} \int_{-\infty}^{\infty} \frac{-\Gamma_o S(z,0,t) + (\omega-\omega_o + kv_z) C(z,0,t)}{\Gamma_o^2 + (\omega-\omega_o + kv_z)^2} \frac{e^{-v_z^2/u^2}}{[1 + I_o\, L(\omega, v_z)]}\, dv_z \qquad (2.7.11)$$

where

$$I_o = \frac{\mu_{ab}^2 E_o^2}{4\hbar^2 \gamma_a \gamma_b}$$

This is the same expression as given in the previous section.

The polarization to first order in r vanishes and to second order in r, the polarization P_2 is

$$P_2 = \frac{\bar{N}_o \mu_{ab}^2 E_o}{\hbar u\sqrt{\pi}} \left\{ -\frac{a_o^2}{4b^2} - \frac{1}{w_o^4} \right\} \int \frac{-\Gamma_o S(z,0,t) + (\omega-\omega_o+kv_z)C(z,0,t)}{\Gamma_o^2 + (\omega-\omega_o+kv_z)^2}$$

$$\times \frac{e^{-v_z^2/u^2}}{1+I_o\, L(\omega,v_z)}\, dv_z - \frac{2}{w_o^4} \frac{\bar{N}_o \mu_{ab}^2 E_o}{\hbar u\sqrt{\pi}}$$

$$\times \int \frac{-\Gamma_o S(z,0,t) + (\omega-\omega_o+kv_z)\, C(z,0,t)}{\Gamma_o^2 + (\omega-\omega_o+kv_z)^2} \frac{I_o\, L(\omega,v_z) e^{-v_z^2/u^2}}{\{1+I_o\, L(\omega,v_z)\}^2}\, dv_z$$

$$+ P_{phase} \qquad (2.7.12)$$

where P_{phase} is the quadratic term in r which arises from the Doppler shift due to the transverse motion of atoms across the spherical phase front (see Appendix M). This term is approximately a factor of $|b/R|$ smaller than the others. (The absolute value sign is employed because R can take a negative value). Assuming $|b/R| \ll 1$, we neglect P_{phase} from now on.*

Thus we have obtained explicit expressions for both sides of the Maxwell equation (2.7.2). Comparing each factor of S and C in the power series, we get the following four equations from Eqs. (2.7.5),

---

*However, this term may become important when the laser tube has a very small inner diameter.

(2.7.11) and (2.7.12):

$$\frac{4}{w_o^2} + k^2 - \frac{\omega^2}{c_o^2} = \omega^2 A \int \frac{\omega-\omega_o+ kv_z}{\Gamma_o^2 + (\omega-\omega_o+ kv_z)^2} \frac{e^{-v_z^2/u^2}}{1 + I_o\, L(\omega,v_z)}\, dv_z \quad (2.7.13)$$

$$\frac{2k}{R} + \mu_o\sigma\omega = \omega^2 A \int \frac{\Gamma_o}{\Gamma_o^2 + (\omega-\omega_o+ kv_z)^2} \frac{e^{-v_z^2/u^2}}{1 + I_o\, L(\omega,v_z)}\, dv_z \quad (2.7.14)$$

$$\frac{8}{w_o^4} + \frac{1}{w_o^2}\left(k^2 - \frac{\omega^2}{c_o^2}\right) - \frac{k^2}{R^2} = \omega^2 A \left(\frac{a_o^2}{4b^2} + \frac{1}{w_o^2}\right)$$

$$\times \int \frac{\omega-\omega_o+ kv_z}{\Gamma_o^2 + (\omega-\omega_o+ kv_z)^2} \frac{e^{-v_z^2/u^2}}{1 + I_o\, L(\omega,v_z)}\, dv_z$$

$$- \frac{2}{w_o^2}\omega^2 A \int \frac{\omega-\omega_o+ kv_z}{\Gamma_o^2 + (\omega-\omega_o+ kv_z)^2} \frac{I_o\, L(\omega,v_z) e^{-v_z^2/u^2}}{\{1 + I_o\, L(\omega,v_z)\}^2}\, dv_z \quad (2.7.15)$$

and

$$\frac{1}{w_o^2}\left(\frac{6k}{R} + \mu_o\sigma\omega\right) = \omega^2 A\left(\frac{a_o^2}{4b^2} + \frac{1}{w_o^2}\right)$$

$$\times \int \frac{\Gamma_o}{\Gamma_o^2 + (\omega-\omega_o+ kv_z)^2} \frac{e^{-v_z^2/u^2}}{1 + I_o\, L(\omega,v_z)}\, dv_z$$

$$- \frac{2}{w_o^2}\omega^2 A \int \frac{\Gamma_o}{\Gamma_o^2 + (\omega-\omega_o+ kv_z)^2} \frac{I_o\, L(\omega,v_z) e^{-v_z^2/u^2}}{\{1 + I_o\, L(\omega,v_z)^2\}^2}\, dv_z \quad (2.7.16)$$

where $A = \dfrac{\mu_o \overline{N}_o \mu_{ab}^2}{\hbar\, u\sqrt{\pi}}$.

Equations (2.7.13) and (2.7.14) correspond to the expression (2.6.6) and (2.6.7), but are slightly different. The dispersion relation (2.7.13) has an extra term $4/w_o^2$. When w_o goes to infinity, i.e., the plane wave limit, the dispersion is the same as in the one-dimensional case (Section 2.6). For a finite size beam, the phase velocity at line center is greater than C_o.

Equation (2.7.14) gives the amplitude of the field corresponding to the expression (2.6.6). The intensity of the field increases as $1/R$ decreases. In the case of a converging wave, which has negative $1/R$, less energy escapes than for the diverging wave with $1/R > 0$. Thus, the intensity is larger for smaller $1/R$.

We have four equations (2.7.13) to (2.7.16) for four unknowns, w_o, k, E_o and R. It is impossible to find analytical solutions satisfying the four equations simultaneously. Before solving these numerically, we wish to see how these four quantities behave on line center at threshold. By putting $E_o = 0$ and $\omega = \omega_o$, Eqs. (2.7.13) to (2.7.16) are

$$\frac{4}{w_o^2} + k^2 - \frac{\omega_o^2}{C_o^2} = 0 \tag{2.7.17}$$

$$\frac{2k}{R} + \mu_o \sigma \omega_o = \omega_o^2 A \int \frac{\Gamma_o e^{-v_z^2/u^2}}{\Gamma_o^2 + k^2 v_z^2} dv_z \tag{2.7.18}$$

$$\frac{8}{w_o^4} + \frac{1}{w_o^2}\left(k^2 - \frac{\omega_o^2}{C_o^2}\right) - \frac{k^2}{R^2} = 0 \tag{2.7.19}$$

$$\frac{1}{w_o^2}\left(\frac{6k}{R} + \mu_o \sigma \omega_o\right) = \omega_o^2 A \left(\frac{a_o^2}{4b^2} + \frac{1}{w_o^2}\right) \int_{-\infty}^{\infty} \frac{\Gamma_o e^{-v_z^2/u^2}}{\Gamma_o^2 + k^2 v_z^2} dv_z \tag{2.7.20}$$

Thus, from Eqs. (2.7.17) to (2.7.20) we obtain

$$\frac{k}{R} = \frac{a_o^2}{8b^2}\left[1 + \sqrt{1 + \frac{8b^2\omega_o^2}{a_o^2 c_o^2 Q}}\right] \tag{2.7.21}$$

$$\cong \begin{cases} \dfrac{a_o k}{4b}\sqrt{\dfrac{2}{Q}} & \text{for } Q \ll Q_o \\ \dfrac{a_o^2}{4b^2} & \text{for } Q \gg Q_o \end{cases} \tag{2.7.22}$$

where we have used the approximation $k \cong \omega_o/C_o$, and the substitution

$$Q_o = \frac{32\pi^2 b^2}{a_o^2 \lambda^2} \tag{2.7.23}$$

The curvature and spot size are given by

$$R \cong \begin{cases} \dfrac{4b}{a_o}\sqrt{\dfrac{Q}{2}} & \text{for } Q \ll Q_o \\ \dfrac{8\pi b^2}{\lambda a_o^2} & \text{for } Q \gg Q_o \end{cases} \tag{2.7.24}$$

and

$$w_o \cong \begin{cases} 2\sqrt{\dfrac{b\lambda}{\pi a_o}}\left(\dfrac{Q}{2}\right)^{1/4} & \text{for } Q \ll Q_o \\ 2\sqrt{2}\,\dfrac{b}{a_o} = 1.18b & \text{for } Q \gg Q_o \end{cases} \tag{2.7.25}$$

(B) Numerical calculation

For an arbitrary pumping density and detuning, we have to solve Eqs. (2.7.13) to (2.7.16) simultaneously. We used an IBM computer for numerical calculations. The results are shown in Figs. 2.17 to 2.22.

We took the parameters appropriate to Xe 3.51 μm line.

Figure 2.17 is the threshold excitation density at resonance vs. the quality factor for various diameters of tubes. These thresholds were obtained from Eqs. (2.7.13) to (2.7.16) for four unknowns, w_0, k, R and $\bar{N}_0$ (instead of E_0), by putting $E_0 = 0$. Q_0 given by Eq. (2.7.23) is approximately $Q_0 \simeq 4b^2 \times 10^6$, where b is given in mm. It is seen in the figure that the threshold pumping density becomes independent of the quality factor Q when $Q > Q_0$.

The radius of curvature of the phase front vs. Q is plotted in Fig. 2.18. As the diameter of the tube is made smaller, R decreases and the term 2k/R in Eq. (2.7.14) becomes more important. The threshold pumping of the high-Q cavity is determined by the radius of the tube.

Figure 2.19 is the curvature of the wave front at line center vs. $\bar{n}$ for various Q . As can be seen, the radius of curvature increases as Q and $\bar{n}$ become larger.

The calculated values of various quantities, intensity R and w_0 , are shown in Figs. (2.20) to (2.22). These are computed for a tube with a diameter of 2.5 mm and $Q = 10^6$. Figure 2.20 is the computed power against detuning for $\bar{n} = 1.05$, 1.5, and 3.0 . At the Lamb dip, the power falls down almost to one-tenth of its peak value. Asymmetries can be seen around $\Delta\nu = 0$: the low frequency peak is smaller than the high frequency peak for $\bar{n} = 1.05$, but as the pumping increases the reverse becomes true.

Figure 2.21 shows the radius of curvature of the phase front calculated for $\bar{n} = 3$. Solid lines are diverging waves and dashed

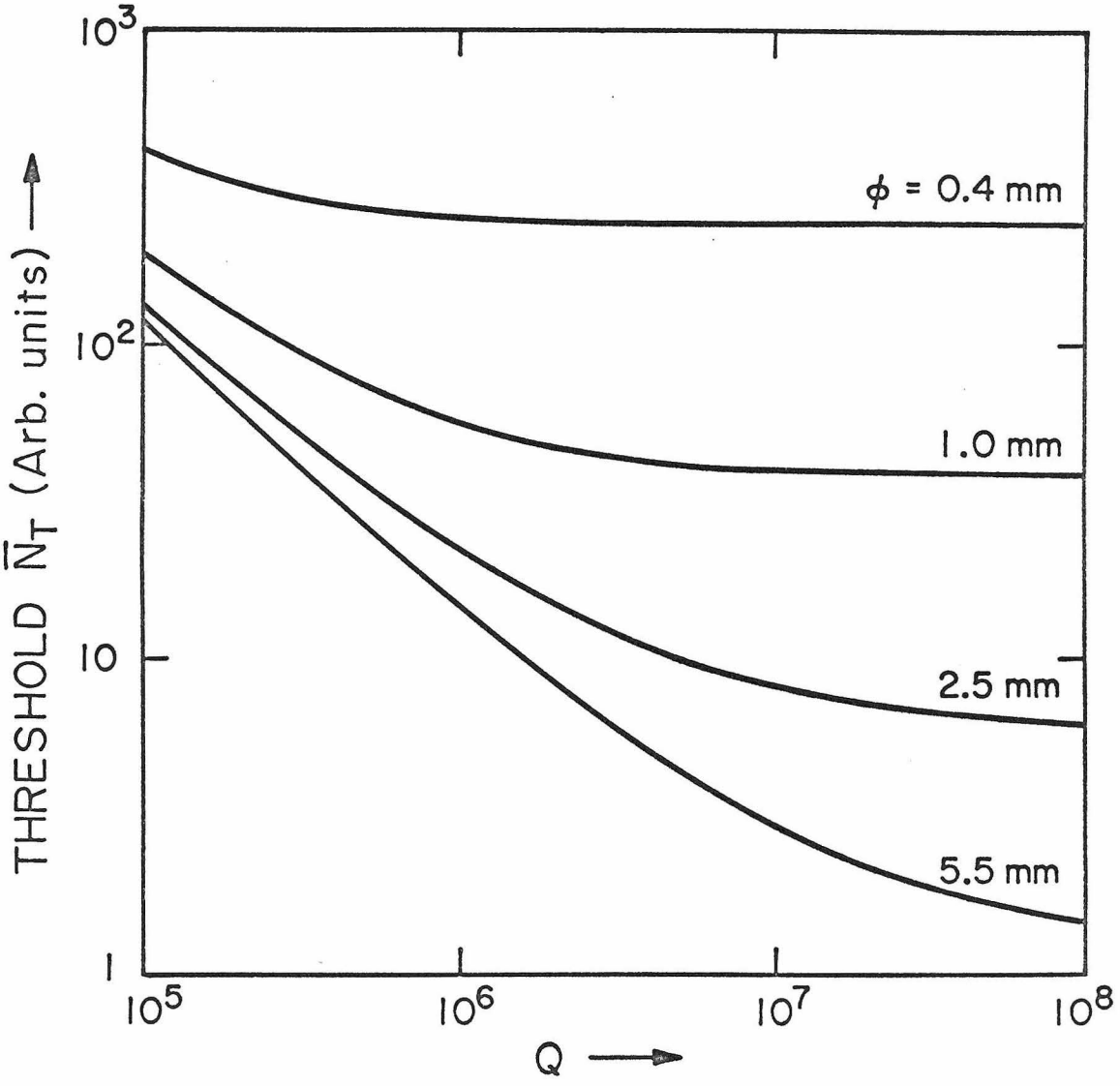

Fig. 2.17 Threshold excitation density vs. Q for various diameter of tubes

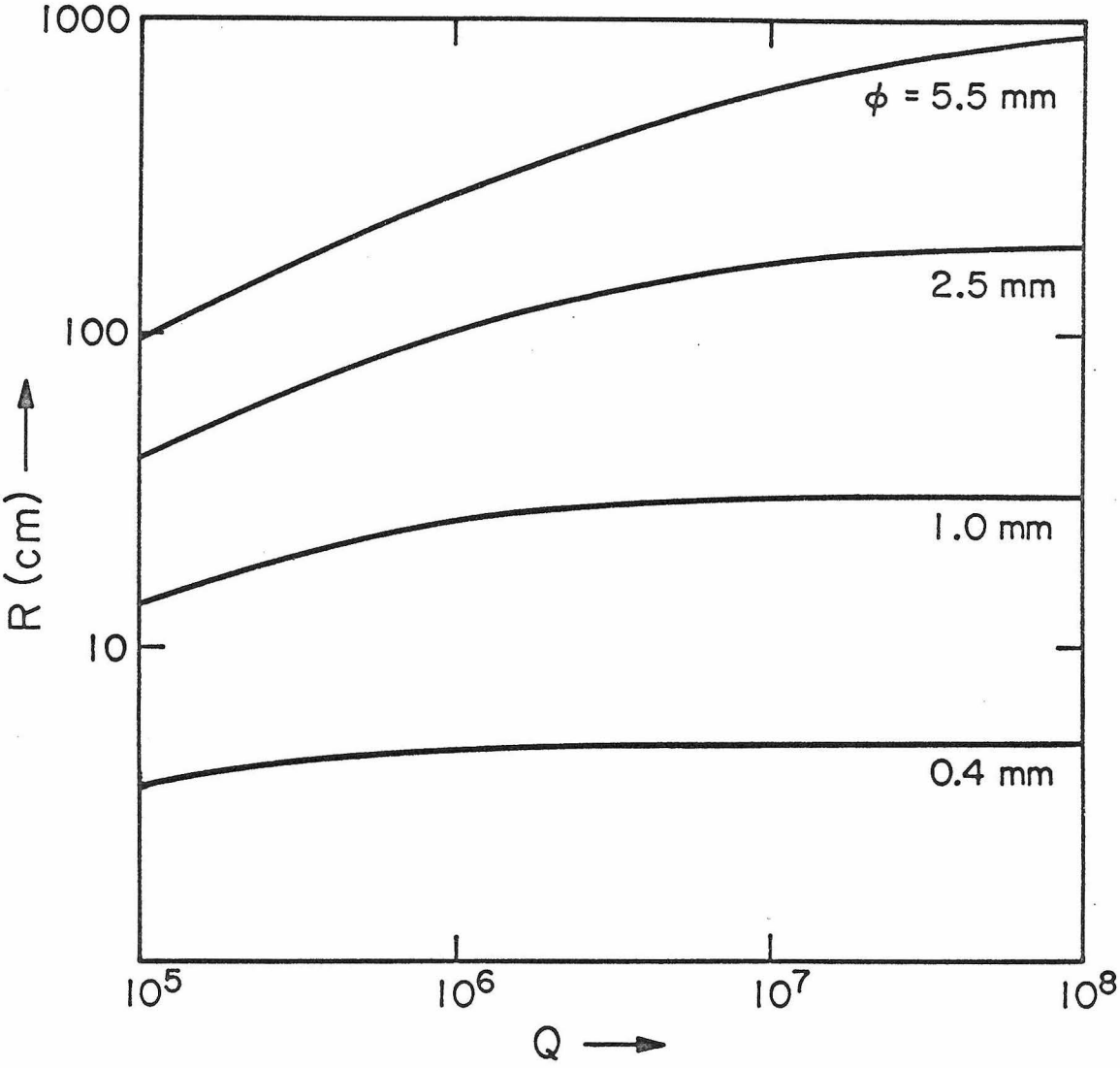

Fig. 2.18 The radius of curvature of the phase front vs. Q for various tube diameters at threshold

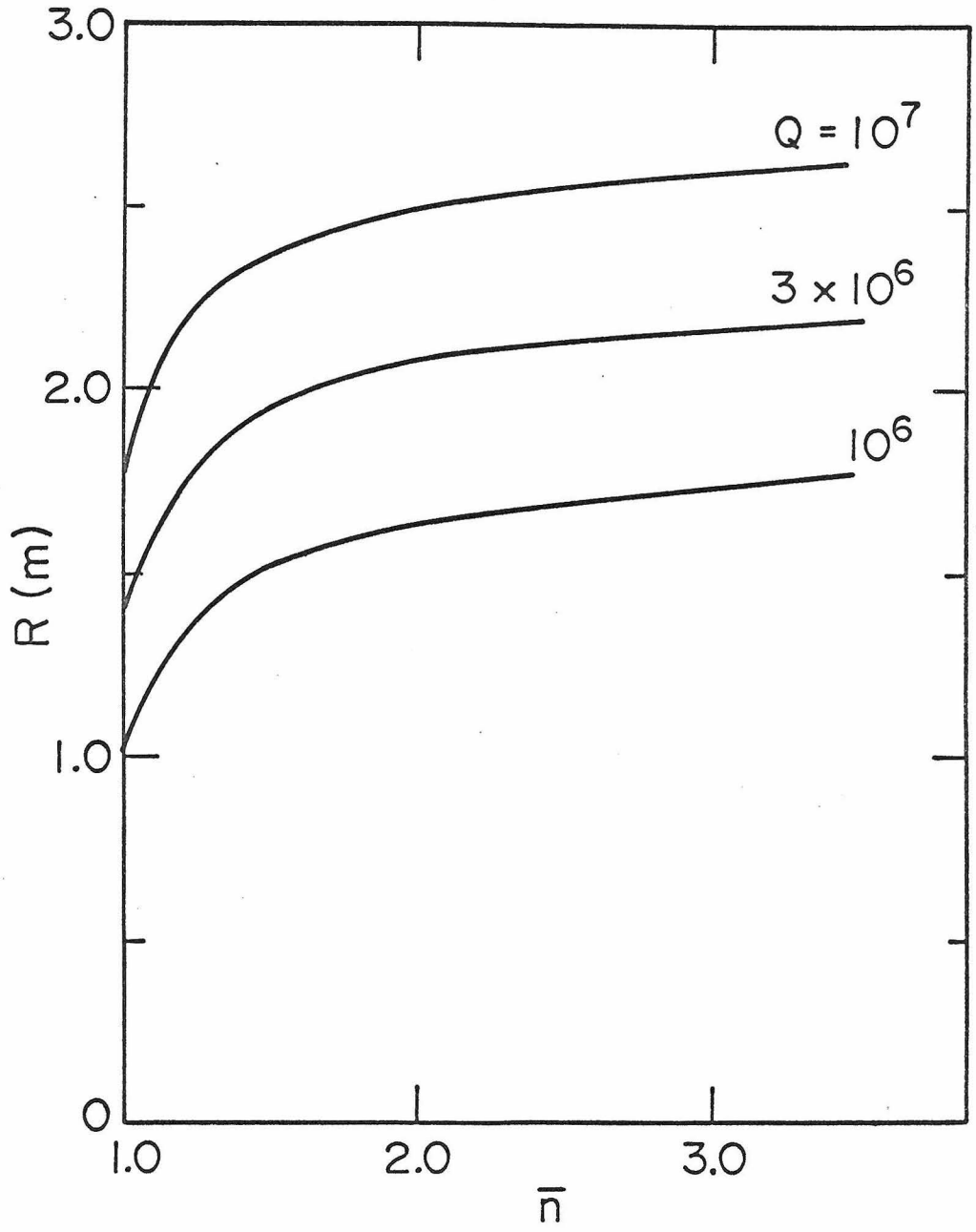

Fig. 2.19 Curvature of the phase-front vs. normalized excitation density for various Q .

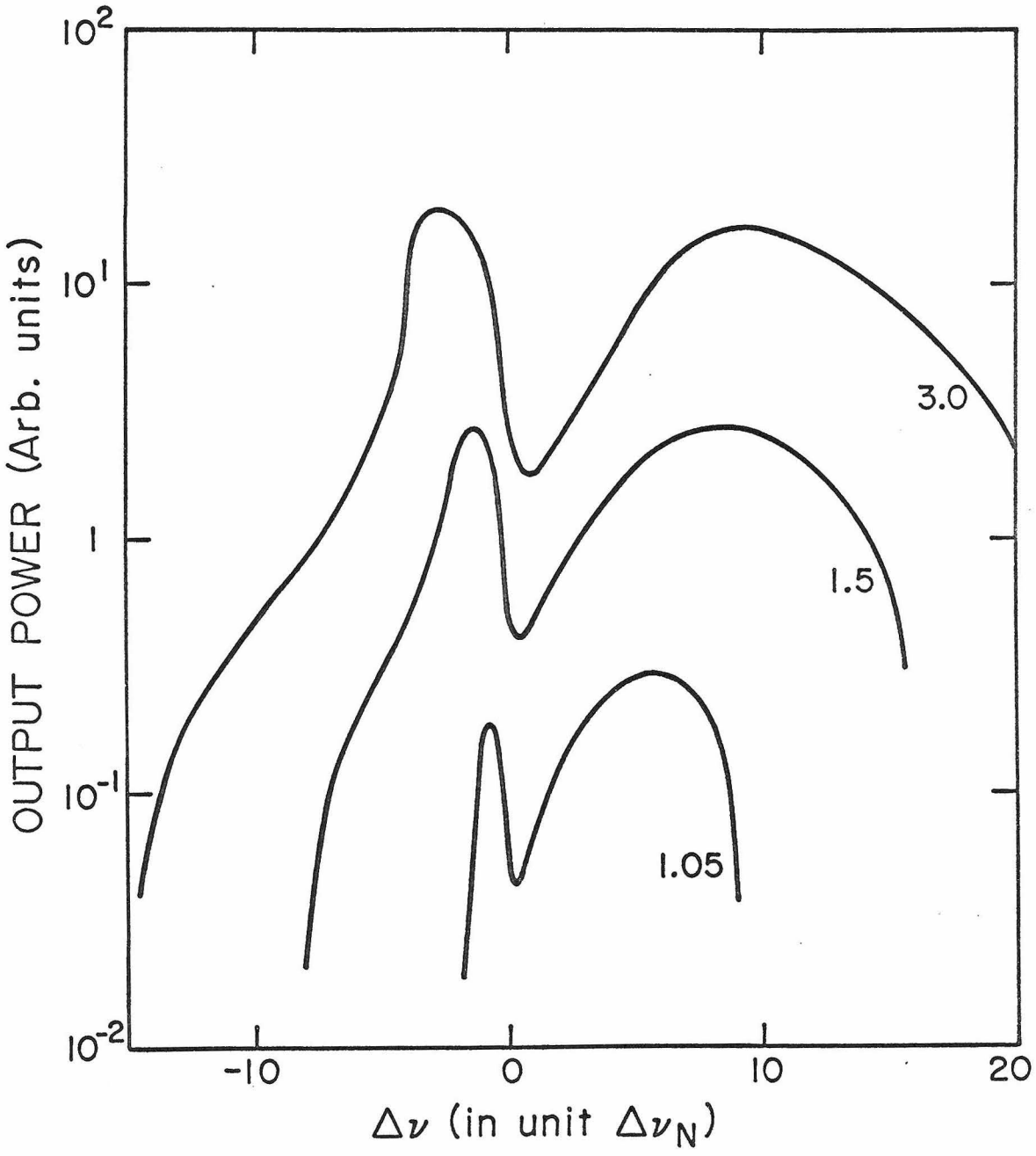

Fig. 2.20. Output power vs. detuning for various pumping density $\bar{n}$

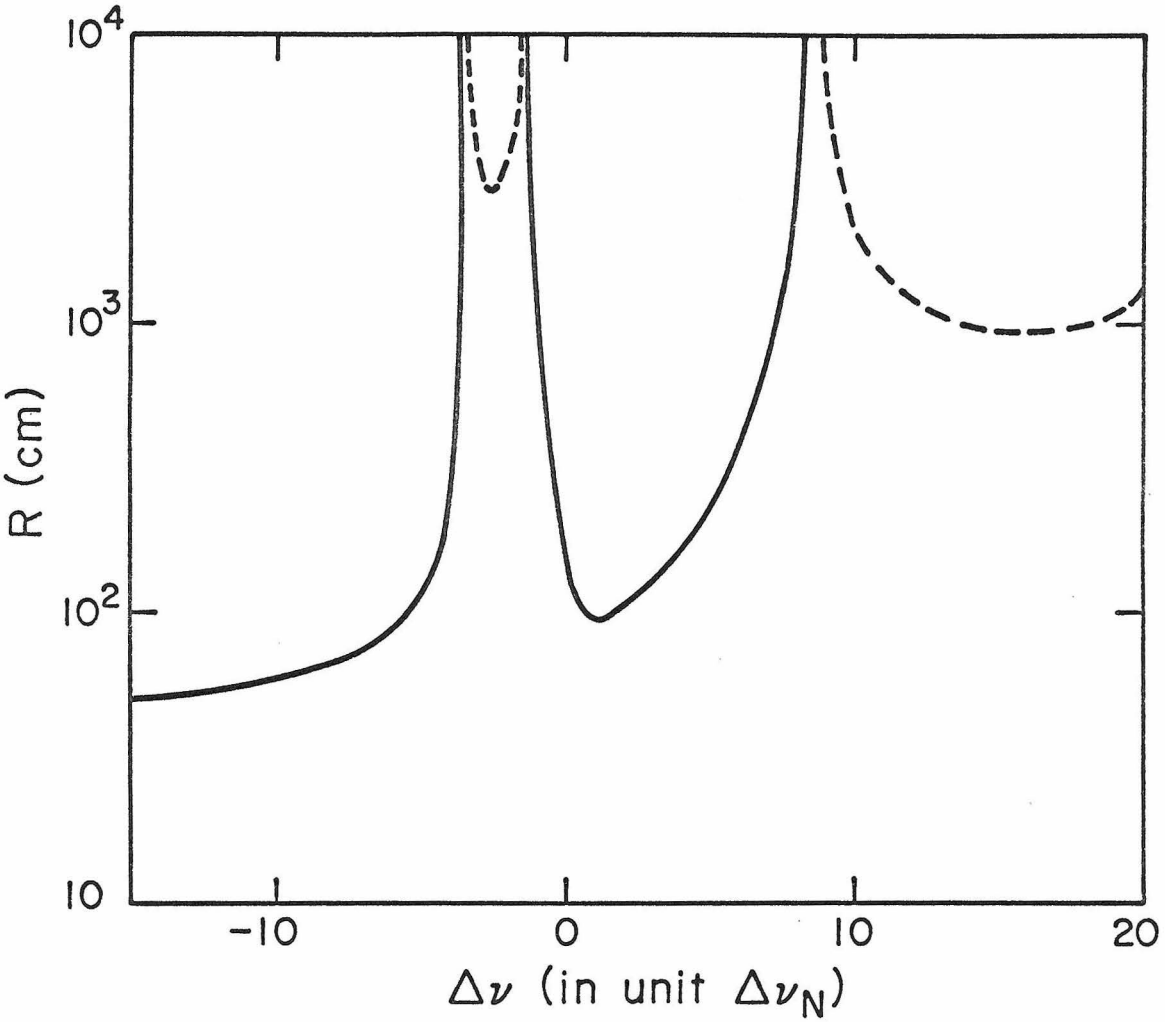

Fig. 2.21 Radius of phase front vs. $\Delta\nu$ for $\bar{n} = 3$; solid lines and dashed lines correspond to positive and negative values of R respectively.

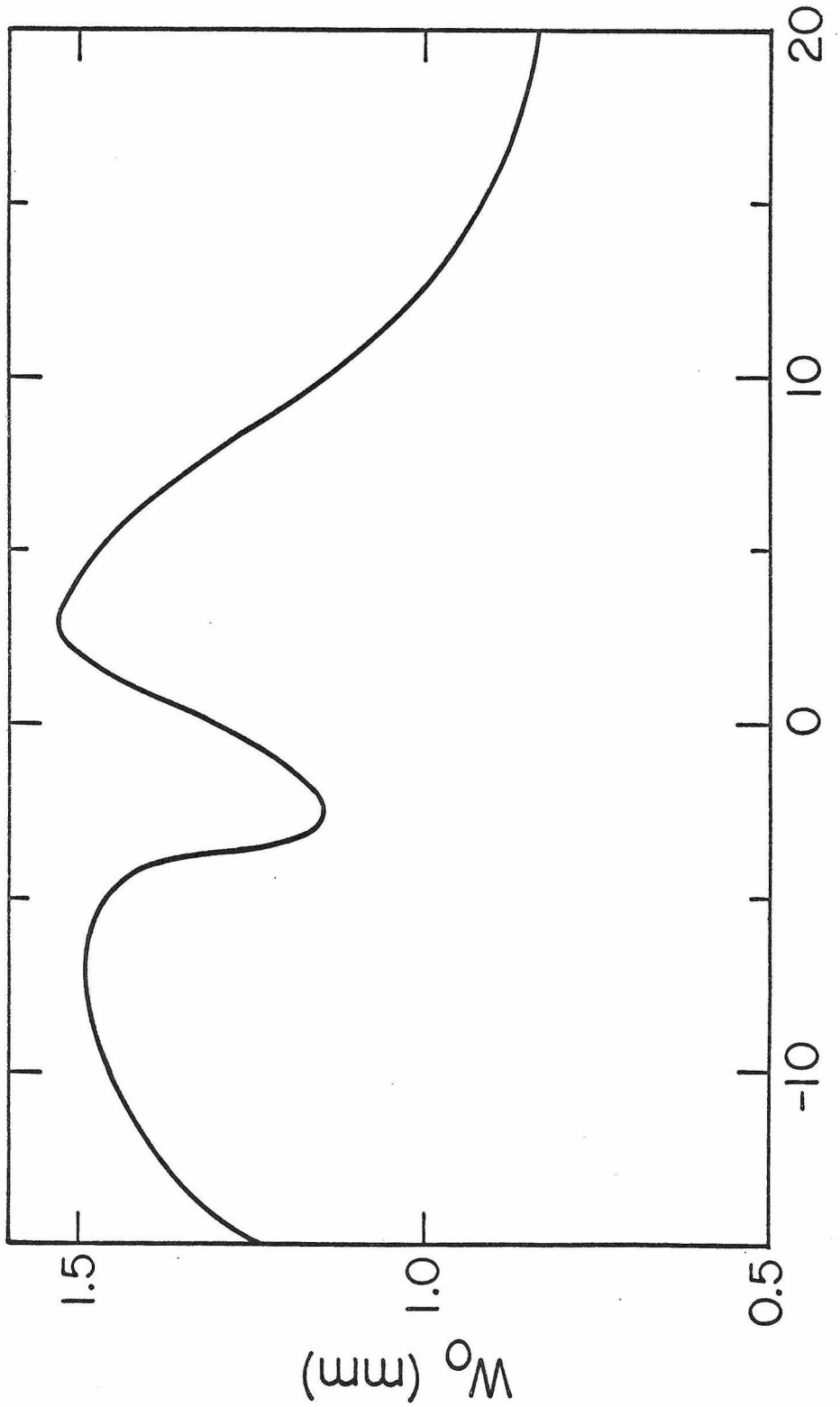

Fig. 2.22 Beam radius vs. $\Delta\nu$ for $\bar{n} = 3$

lines are converging waves.

Figure 2.22 is the computed beam waist w_o (in mm) vs. detuning for $\bar{n} = 3$.

(C) Experiment on the measurement of beam size

We measured the beam radii of the high frequency and low frequency peaks at various distances from the laser window. The experiments were conducted using the Xe 3.27 μm line. The cavity was 75 cm long with discharge section of 55 cm and an inner diameter of 2.5 mm. One end mirror was a highly reflective silvered flat surface, and the other one had about 60% reflectance obtained with a gold coated flat surface. The pressure was kept around 5×10^{-3}Torr with a liquid nitrogen trap.

The experimental set-up is shown in Fig. 2.23. The laser beam was chopped mechanically at 200 Hz and then split into two. One of the beams was incident on an 0.25 ×0.25 mm PbS detector 1 which was scanned to measure the beam radius. The other one was focused on a PbS detector 2 for monitoring the output power from the laser. We scanned one end mirror over a distance of 5 μm by a piezo-electric transducer with an applied sawtooth voltage. The signals from the detectors were recorded simultaneously. The output power of low frequency and high frequency peaks were compared between the monitoring signal and the signal from detector 1. Detector 1 was displaced about 0.25 mm across the beam after every 10 scanning of the piezo-electric transducer. The measurements were performed at a normalized pumping density $\bar{n} \sim 3$. The data were fitted to a Gaussian beam profile by a computer. The experimental half-width of

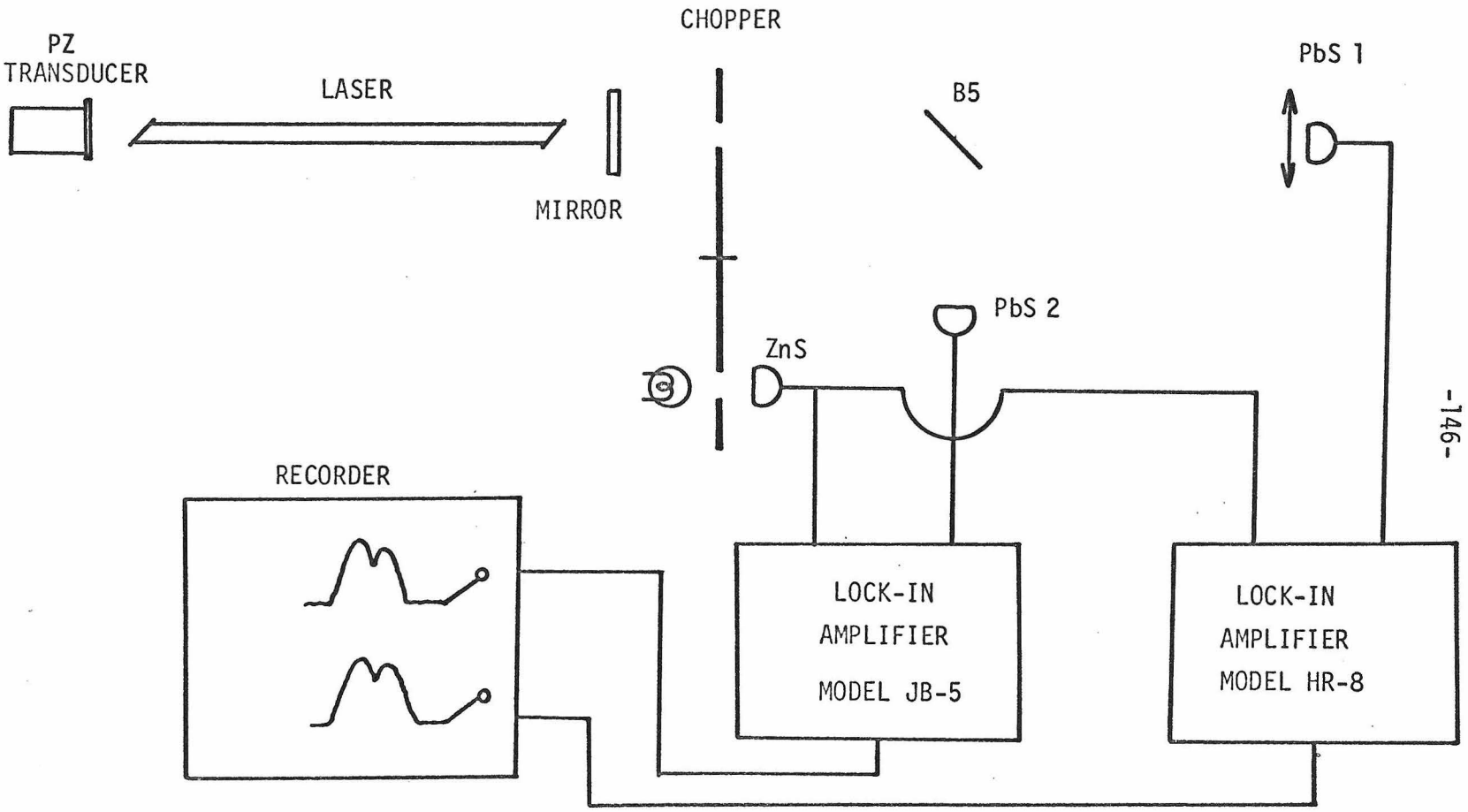

Fig. 2.23 Set-up for measurement of beam size

the beam radii at half maximum are plotted in Fig. 2.24 as a function of the distance from the cavity window. Open circles and cross marks correspond to the high and low frequency peaks respectively. The beam radii corresponding to the two peaks are different.

We observed an asymmetry of the output power as a function of detuning. Figure 2.25 shows the output power vs. voltage applied to the piezo-electric transducer (i.e., vs. mirror position). These data were taken in the experiment described in Section 2.6. In Fig. 2.13 the output has a larger peak on the low frequency side, but in Fig. 2.25, the larger peak is on the high frequency side.

(D) Conclusion

It has been shown that the three-dimensional model gives a considerably different picture of the behavior of the output power as a function of the detuning from that of the one-dimensional model. More specifically, the beam radii and the radii of curvature of the phase fronts vary with the pumping density and detuning. As a consequence there is a sizable shift of the frequency of the minimum of the Lamb dip and an asymmetry of the two-power maxima[33,34,35] on either side at the Lamb dip (see Fig. 2.20).

For a more rigorous discussion, the following improvements of our model are necessary:

(a) The boundary conditions at the dielectric walls should be taken into account in determining the field inside the tube.

(b) The field expansion should extend to higher power in r^2.

(c) We should consider the mirror loss or the geometrical loss that exists because of the free space between mirror

and active medium.

(d) The z dependence of the beam radius, the curvature of the phase front, and the field amplitude should be considered.

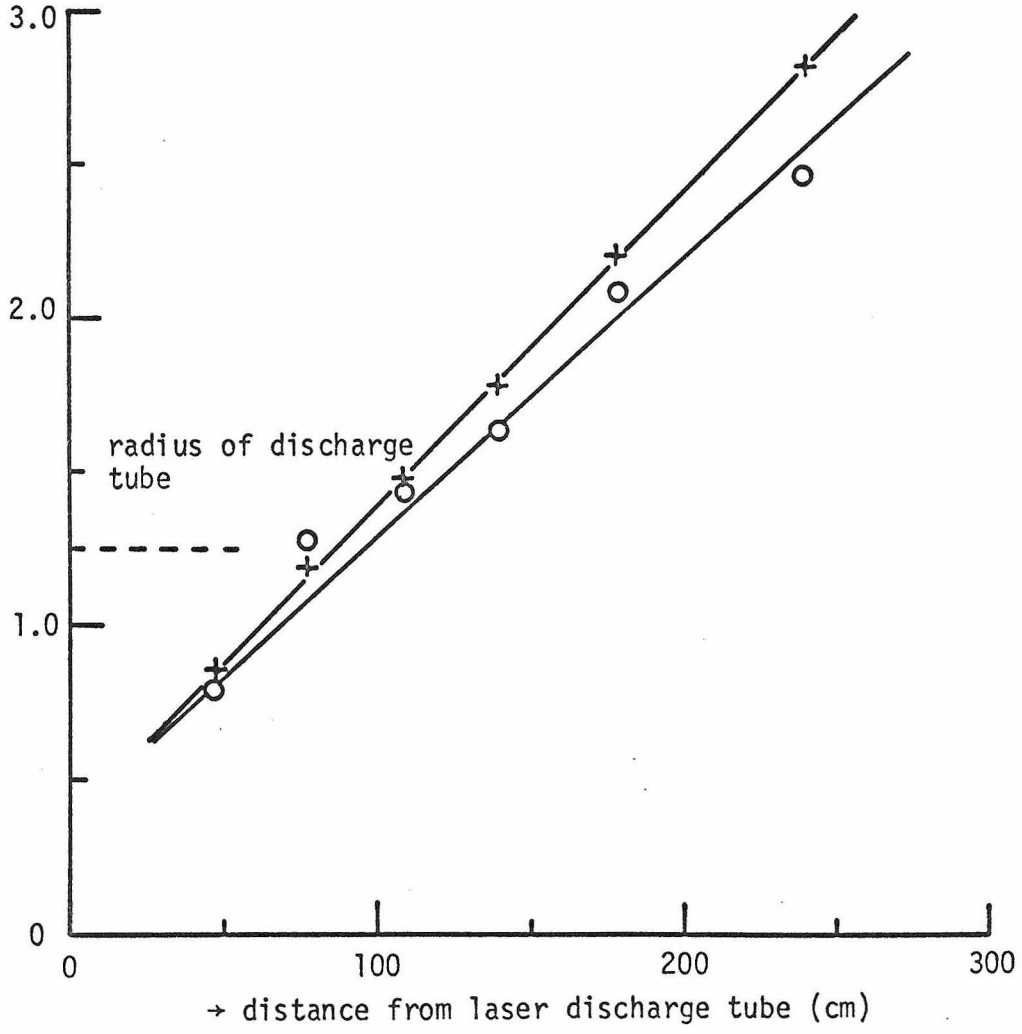

Fig. 2.24 Experimental beam waist at different positions $\bar{n} \simeq 3$.

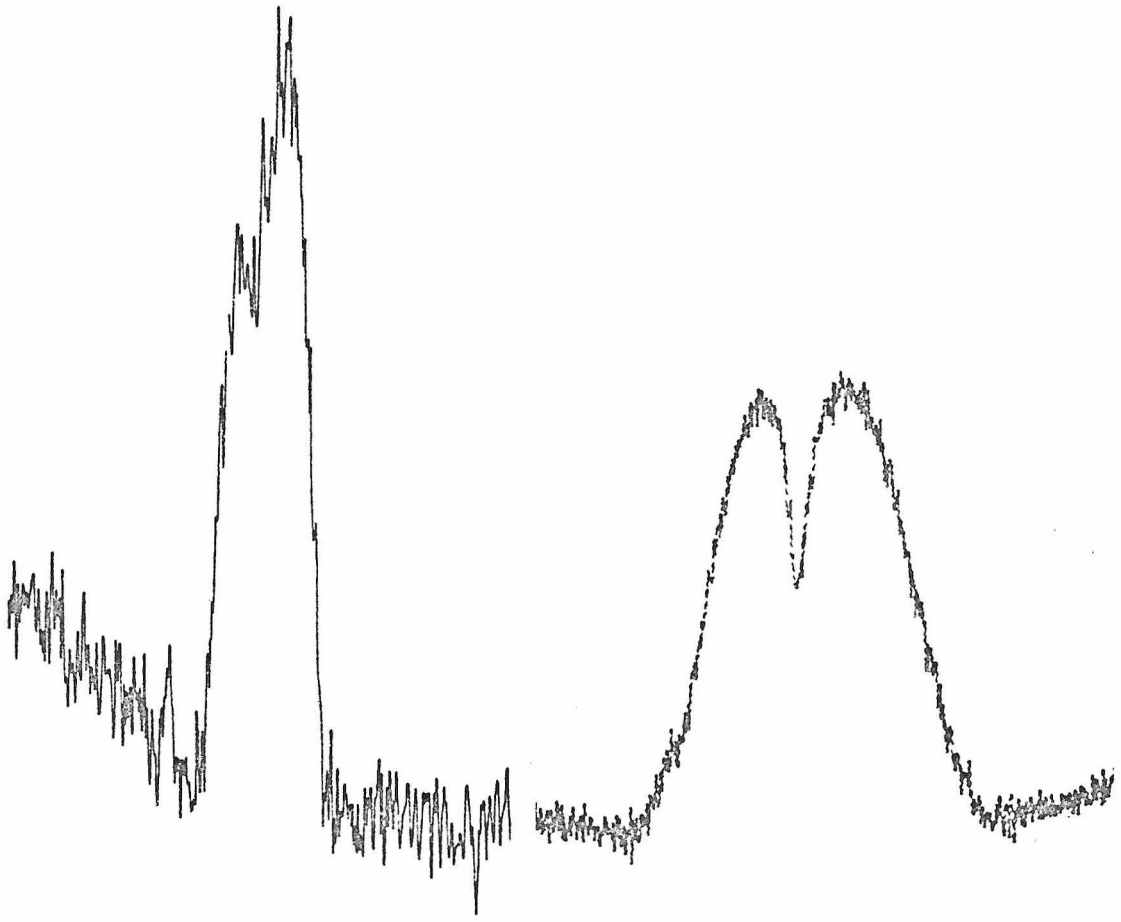

x5

5.3 mA

6.5 mA

Fig. 2.25 Output power vs. voltage applied to the PZ transducer. (The horizontal line has the same scale as in Fig. 2.13)

References for Chapter II

1. R. P. Feynman and F. L. Vernon Jr., J. Appl. Phys. 28, 49 (1957).
2. A. Merzbacher, Quantum Mechanics, John Wiley & Sons, Inc. (1966), Ch. 3, p. 29.
3. Ibid, Ch. 16.
4. Ibid, Ch. 13.
5. L. R. Wilcox and W. E. Lamb Jr., Phys. Rev. 119, 1915 (1960).
6. G. Breit and I. S. Lomen, Phys. Rev. 46, 590 (1934).
7. W. E. Lamb, Jr., Phys. Rev. 134, A1429 (1964).
8. C. H. Papas, Theory of Electromagnetic Wave Propagation, McGraw-Hill (1965), p. 1.
9. K. R. Manes and A. E. Siegman, Phys. Rev. 4, 373 (1971).
10. C. Cheng, Analysis of Linear System, Addison Wesley (1959), Ch. 2, p. 14.
11. S. Stenholm and W. E. Lamb Jr., Phys. Rev. 181, 618 (1969).
12. B. J. Feldman and M. S. Feld, Phys.Rev.A 1, 1375 (1970).
13. H. K. Holt, Phys. Rev.A 2, 233 (1970).
14. R. P. Feynman, Quantum Electrodynamics, W. A. Benjamin (1962).
15. J. J. Sakurai, Advanced Quantum Mechanics, Addison Wesley (1967).
16. D. Close, Phys. Rev. 153, 360 (1967).
17. M. Born and E. Wolf, Principles of Optics, Pergamon Press (1970), Ch. X, p. 491.
18. L. Mandel and E. Wolf, Rev. Mod. Phys. 37, 231 (1965).
19. Davenport and Root, Random Signal and Noise, McGraw Hill (1958), Ch. 8, p. 145.
20. A. Yariv, Quantum Electronics, John Wiley & Sons, Inc. (1967), Ch. 24, p. 406.

21. M. Lax, Phys. Rev. 129, 2342 (1963).

22. A. Yariv, Introduction to Optical Electronics, Holt Rinehart & Winston (1971), Ch. 4.

23. L. Casperson, Ph.D. Thesis, California Institute of Technology (1971), Ch. 3.

24. L. Allen, D. G. C. Jones and D. G. Schofield, J. Opt. Soc. Am. 59, 842 (1969).

25. H. Kogelnik, Appl. Opt. 4, 1562 (1965).

26. L. Casperson and A. Yariv, Appl. Phys. Letters 12, 355 (1968).

27. L. A. Schlie and J. T. Verdeyen, IEEE J. Quant. Elec. QE-5, 21 (1969).

28. D. Pohl, Phys. Rev. A 5, 1906 (1972).

29. R. Chiao, E. Garmire and C. H. Townes, Phys. Rev. Letters 13, 479 (1964).

30. P. L. Kelly, Phys. Rev. Letters 15, 1005 (1965).

31. J. V. Paker, Phys. Fluids 6, 1657 (1963).

32. W. R. Bennett Jr., Appl. Opt., Supplement on Chemical Lasers, (1965), p. 3.

33. A. Szöke and A. Javan, Phys. Rev. 145, 137 (1966).

34. T. Kan and G. J. Wolga, IEEE J. Quant. Elec. QE-7, 141 (1971).

35. C. Freed, Appl. Phys. Lett. 18, 458 (1971).

APPENDIX A

Equations (1.3.6) and (1.3.7) are

$$B(v,z) = B_{23}^{+}(v,\nu)\ I_{\nu}^{+}(z) + B_{23}^{-}(v,\nu)\ I_{\nu}^{-}(z) \tag{A.1}$$

$$I_{\nu}^{\pm}(z) = X^{\pm} \exp\left[\mp \alpha z \pm h\nu \int_{0}^{z}\int_{-\infty}^{\infty} \frac{B_{32}^{\pm}(v',\nu)\{A_2S_3(v') - A_3S_2(v')\}}{\{A_3A_2 + (A_3 + A_2)B(v',\xi)\}} dv'd\xi\right] \tag{A.2}$$

$X^{\pm}$ are constant. If we set $X = X^{\pm}$ in Eq. (A.2), one boundary condition $I_{\nu}^{+}(0) = I_{\nu}^{-}(0)$ is automatically satisfied. Then the problem to solve is to determine the value of X so that the other boundary condition $I_{\nu}^{-}(L)/I_{\nu}^{+}(L) = R$ is satisfied. Let

$$i_{\nu}^{\pm}(z) = \frac{I_{\nu}^{\pm}(z)}{X} \tag{A.3}$$

then the boundary condition is written in terms of i as

$$\frac{i_{\nu}^{-}(L)}{i_{\nu}^{+}(L)} = R \tag{A.4}$$

For an initial guess we may put $B(v',\xi) = 0$ in Eq. (A.2) and we will find

$$i_{\nu}^{\pm(o)}(z) = \exp\left[\mp \alpha z \pm h\nu \int_{0}^{z}\int_{-\infty}^{\infty} \frac{B_{32}^{\pm}(v',\nu)\{A_2S_3(v') - A_3S_2(v')\}}{A_3A_2} dv'd\xi\right] \tag{A.5}$$

To advance to the first interation, we may put $X = X^{(1)}$, then we have

$$B^{(1)} = \chi^{(1)}\{B_{23}^{+}(v,\nu) i_{\nu}^{+(o)}(z) + B_{23}^{-}(v,\nu)\ i_{\nu}^{-(o)}(z)\} \tag{A.6}$$

$$i_{\nu}^{\pm(1)}(z) = \exp\left[\mp \alpha z \pm h\nu \int_{0}^{z}\int_{-\infty}^{\infty} \frac{B_{32}^{\pm}(v',\nu)\{A_2S_3(v') - A_3S_2(v')\}}{A_3A_2^{+} (A_3^{+} A_2)B^{(1)}}\, dv'd\xi\right] \tag{A.7}$$

Defining functions

$$f^{(1)}(\chi^{(1)}) = i_{\nu}^{-(1)}(L) - Ri_{\nu}^{+(1)}(L) \quad , \tag{A.8}$$

we find the second iteration by Newton's method

$$\chi^{(2)} = \chi^{(1)} - \frac{f^{(1)}}{\partial f^{(1)}/\partial \chi^{(1)}} \tag{A.9}$$

The n^{th} iteration for B is written

$$B^{(n)} = \chi^{(n)}\{B_{23}^{+}(v,z)\ i_{\nu}^{+(n-1)}(z) + B_{23}^{-}(v,\nu)\ i_{\nu}^{-(n-1)}(z)\} \tag{A.10}$$

$$i_{\nu}^{\pm(n)} = \exp\left[\mp \alpha z \pm h\nu \int_{0}^{z}\int_{-\infty}^{\infty} \frac{B_{32}^{\pm}(v',\nu)\{A_2S_3(v') - A_3S_2(v')\}}{A_3A_2^{+} (A_3^{+} A_2)B^{(n)}}\, dv'd\xi\right] \tag{A.11}$$

and

$$f^{(n)}(\chi^{(n)}) = i^{-(n)}(L) - Ri^{+(n)}(L) \tag{A.12}$$

Using Eqs. (A.10) to (A.12), we find the (n+1)th iteration by

$$\chi^{(n+1)} = \chi^{(n)} - \frac{f^{(n)}}{\partial f^{(n)}/\partial \chi^{(n)}} \tag{A.13}$$

If $\chi^{(n)}$ and $i^{\pm(n)}(z)$ converge uniformly for sufficiently large

number of iterations, we may interpret

$$X = \lim_{n \to \infty} X^{(n)}$$

$$i_\nu^{\pm}(z) = \lim_{n \to \infty} i_\nu^{\pm(n)}(z) \tag{A.14}$$

and finally we can get

$$I_\nu^{\pm}(z) = X\, i_\nu^{\pm}(z) \tag{A.15}$$

In our computation, the uniform convergence can be seen after 5 or 6 iterations to be one part in a thousand.

APPENDIX B

In the Doppler limit $\varepsilon << 1$ and also when the spectrum of amplified spontaneous emission is much wider than the natural line width $\Delta\nu_N$, we can carry out the integration. Equation (1.4.35) is simply

$$g_o = \frac{\varepsilon}{\pi^{1/2}} \tag{B.1}$$

Expression (1.4.34) is rewritten

$$\tilde{B}(\beta,X) = \tilde{I}(\beta,X) + \tilde{I}(\beta,X_o - X) \tag{B.2}$$

where symmetry of the spectral profile about $\nu = \nu_o$ is assumed. From the above relation $\tilde{B}(\beta,X)$ is known to have almost the same line width as $\tilde{I}(\beta,X)$. Then one finds the following from Eq. (1.4.31) and (1.4.32):

$$\tilde{g}(y,X) = \frac{\varepsilon}{\pi^{1/2}} \frac{e^{-\varepsilon^2 y^2}}{1 + s\tilde{B}(y,X)/g_o} \tag{B.3}$$

$$\tilde{h}(y,X) = \frac{\varepsilon e^{-\varepsilon^2 y^2}}{\pi^{1/2}} \frac{1 + t\tilde{B}(y,X)/g_o}{1 + s\tilde{B}(y,X)/g_o} \tag{B.4}$$

Corresponding to Eq. (1.4.7), we have differential equations

$$\frac{\partial}{\partial X}\tilde{I}(y,X) = \tilde{h}(y,X) + \{\frac{\tilde{g}(y,X)}{g_o} - \alpha'\}\tilde{I}(y,X) \tag{B.5}$$

$$-\frac{\partial}{\partial X}\tilde{I}(y,X_o - X) = \tilde{h}(y,X_o - X) + \{\frac{\tilde{g}(y,X_o - X)}{g_o} - \alpha'\}\tilde{I}(y,X_o - X) \tag{B.6}$$

From Eq. (B.2), we have

$$\tilde{B}(\beta,X_o - X) = \tilde{B}(\beta,X) \tag{B.7}$$

Substituting the above relation into Eqs. (B.3) and (B.4), we get

$$\tilde{g}(y,X_o - X) = \tilde{g}(y,X) \tag{B.8}$$

$$\tilde{h}(y,X_o - X) = \tilde{h}(y,X) \tag{B.9}$$

By adding Eqs. (B.5) and (B.6) we find

$$\frac{\partial N^-}{\partial X} = 2\tilde{h}(y,X) + \{\frac{\tilde{g}(y,X)}{g_o} - \alpha'\} N^+ \tag{B.10}$$

and by subtracting

$$\frac{\partial N^+}{\partial X} = \{\frac{\tilde{g}(y,X)}{g_o} - \alpha'\} N^- \tag{B.11}$$

where

$$N^- = \tilde{I}(y,X) - \tilde{I}(y,X_o - X) \tag{B.12}$$

$$N^+ = \tilde{I}(y,X) + \tilde{I}(y,X_o - X) \tag{B.13}$$

We introduce the following new quantity:

$$p(y,X) = (1 + \frac{s}{g_o} N^+)^2 \tag{B.14}$$

with this, Eqs. (B.3) and (B.4) are given by

$$\tilde{g}(y,X) = \frac{\varepsilon}{\pi^{1/2}} e^{-\varepsilon^2 y^2} p^{-1/2} \tag{B.15}$$

$$\tilde{h}(y,X) = \frac{\varepsilon}{\pi^{1/2}} e^{-\varepsilon^2 y^2} p^{-1/2} \{1 + \frac{t}{s}(p^{1/2} - 1)\} \tag{B.16}$$

When $\alpha' = 0$, the calculation becomes simplified and we get the following from Eq. (B.11):

$$N^- = \frac{g_o}{\tilde{g}(y,X)} \frac{\partial N^+}{\partial X} \tag{B.17}$$

With the help of Eqs. (B.15), (B.16) and (B.17), Eq. (B.10) reduces to a second order differential equation for p

$$\frac{\partial^2 p}{\partial X^2} = 4s\, e^{-2\varepsilon^2 y^2} p^{-1/2} \{1 + \frac{t}{s}(p^{1/2} - 1)\} + 2e^{-2\varepsilon^2 y^2} p^{-1/2}(p^{1/2} - 1) \tag{B.18}$$

The above expression is written in the form

$$\frac{\partial^2 p}{\partial X^2} = ap^{-1/2} + b \tag{B.19}$$

where

$$a = 2e^{-2\varepsilon^2 y^2}(2s - 2t - 1) \tag{B.20}$$

$$b = 2e^{-2\varepsilon^2 y^2}(2t + 1) \tag{B.21}$$

The boundary conditions are

$$N^+ - N^- = 0 \quad \text{at} \quad X = X_o$$

$$N^+ + N^- = 0 \quad \text{at} \quad X = 0 \tag{B.22}$$

Equations (B.22) can be rewritten with the help of Eqs. (B.14) and (B.17)

$$2e^{-\varepsilon^2 y^2}(p^{1/2} - 1) - \frac{\partial P}{\partial X} = 0 \quad \text{at} \quad X = X_o$$

$$2e^{-\varepsilon^2 y^2}(p^{1/2} - 1) + \frac{\partial P}{\partial X} = 0 \quad \text{at} \quad X = 0 \tag{B.23}$$

Multiplying both sides of Eq. (B.18) by $\partial p/\partial X$ and integrating, one finds

$$\frac{1}{2}\left(\frac{\partial p}{\partial X}\right)^2 = 2ap^{1/2} + bp + c \tag{B.24}$$

From Eq. (B.12) we have $N^- = 0$ for $X = \frac{1}{2} X_o$. Thus,

$$\frac{\partial p}{\partial X} = \begin{cases} \sqrt{2bp + 4ap^{1/2} + c} & X > \frac{1}{2} X_o \\ -\sqrt{2bp + 4ap^{1/2} + c} & X \leq \frac{1}{2} X_o \end{cases} \tag{B.25}$$

By putting

$$f = p^{1/2} + \frac{a}{b} \tag{B.26}$$

Eq. (B.25) can be rewritten

$$\sqrt{\frac{2}{b}} \frac{f - \frac{a}{b}}{\sqrt{f^2 + c_1}} \frac{\partial f}{\partial X} = \begin{cases} 1 & X > \frac{1}{2} X_o \\ -1 & X \leq \frac{1}{2} X_o \end{cases} \tag{B.27}$$

Integrating the above expression for $X > \frac{1}{2} X_o$, we find

$$\sqrt{\frac{2}{b}} \left[\sqrt{f^2 + c_1} - \frac{a}{b} \ln\left| f + \sqrt{f^2 + c_1} \right| \right] = X + c_2 \tag{B.28}$$

in which c_1 and c_2 are the constants. From boundary conditions at $X = X_o$, Eq. (B.23), and also from the fact that $N^- = 0$ at $X = \frac{1}{2} X_o$, we have the following relation with the help of Eqs. (B.25) and (B.26):

$$e^{-\varepsilon^2 y^2} \left(f_o - \frac{a}{b} - 1\right) - \sqrt{\frac{b}{2}} \sqrt{f_o^2 + c_1} = 0 \tag{B.29}$$

$$\sqrt{f_{1/2}^2 + c_1} = 0 \qquad \text{for} \quad X = \frac{1}{2} X_o \tag{B.30}$$

in which f_o and $f_{1/2}$ denote the value of f at $X = X_o$ and $X = \frac{1}{2} X_o$ respectively. We have to solve the transcendental equation given by Eq. (B.28) with the boundary condition (B.29) and (B.30) viz.

$$\sqrt{\frac{2}{b}} \left[\sqrt{f_o^2 + c_1} - \frac{a}{b} \ell n \left| f_o + \sqrt{f_o^2 + c_1} \right| \right] = X_o + c_2 \tag{B.31}$$

$$\sqrt{\frac{2}{b}} \left[\sqrt{f_{1/2}^2 + c_1} - \frac{a}{b} \ell n \left| f_{1/2} + \sqrt{f_{1/2}^2 + c_1} \right| \right] = \frac{X_o}{2} + c_2 \tag{B.32}$$

By subtracting Eq. (B.32) from Eq. (B.31) and using the expressions (B.29) and (B.30), it can be shown that the solution of the following transcendental equation gives the value of f at $X = X_o$:

$$\frac{e^{\varepsilon^2 y^2}}{\sqrt{2t+1}} \left[\frac{(2s - 2t - 1)}{(2(2t+1)} \ell n \left\{ \frac{f_o^2 - \frac{(f_o - \frac{2s}{2t+1})^2}{2t+1}}{\left(f_o + \frac{f_o - \frac{2s}{2t+1}}{\sqrt{2t+1}} \right)^2} \right\} + \frac{f_o - \frac{2s}{2t+1}}{\sqrt{2t+1}} \right] = \frac{X_o}{2} \tag{B.33}$$

Then, the spectral intensity is given by

$$\tilde{I}(y, X_o) = N^+(y, X_o)$$

$$= \frac{g_o}{s}(f_o - \frac{a}{b} - 1)$$

$$\simeq \frac{g_o}{s} f_o$$

APPENDIX C

For a finite $\Delta\nu_N$ and $\Delta\nu_D$ we may use a computer solution. The iteration method may be suitable for numerical calculation. In the zeroth order approximation we may put $B^{(0)}(\beta,X) = 0$ in Eq. (1.4.34). From Eqs. (1.4.31) and (1.4.32) the zeroth order $\tilde{g}(y,X)$ and $\tilde{h}(y,X)$ are given by

$$\tilde{g}^{(0)}(y,X) = \frac{2\varepsilon}{\pi^{3/2}} \int_{-\infty}^{\infty} \frac{e^{-\varepsilon^2\beta^2}}{1+4(y-\beta)^2}\, d\beta \tag{C.1}$$

$$\tilde{h}^{(0)}(y,X) = \tilde{g}^{(0)}(y,X) \tag{C.2}$$

$$\tilde{I}^{(0)}(y,X) = \int_0^X \tilde{h}^{(0)}(y,\xi)\, \exp\{ \int_\xi^X (\tilde{g}^{(0)}(y,\zeta)/g_0 - \alpha')\, d\zeta\}\, d\xi \tag{C.3}$$

(Note that $g^{(0)}(y,X)$ is an even function of y as can be seen from Eq. (C.1); also that $I^{(0)}(y,X)$ is an even function of y .)

The nth order iteration will be given by (n-1)th order approximation as follows:

$$\tilde{B}^{(n)}(\beta,X) = \frac{2}{\pi} \int_{-\infty}^{\infty} \{\frac{\tilde{I}^{(n-1)}(y,X)}{1+4(y-\beta)^2} + \frac{\tilde{I}^{(n-1)}(y,X_0-X)}{1+4(y+\beta)^2}\}\, dy \tag{C.4}$$

$$\tilde{g}^{(n)}(y,X) = \frac{2\varepsilon}{\pi^{3/2}} \int_{-\infty}^{\infty} \frac{e^{-\varepsilon^2\beta^2}}{1+4(y-\beta)^2}\, \frac{d\beta}{1+\frac{s}{g_0}\tilde{B}^{(n)}(\beta,X)} \tag{C.5}$$

$$\tilde{h}^{(n)}(y,X) = \frac{2\varepsilon}{\pi^{3/2}} \int_{-\infty}^{\infty} \frac{e^{-\varepsilon^2\beta^2}}{1+4(y-\beta)^2}\, \frac{1+\frac{t}{g_0}\tilde{B}^{(n)}(\beta,X)}{1+\frac{s}{g_0}\tilde{B}^{(n)}(\beta,X)}\, d\beta \tag{C.6}$$

$$\tilde{I}^{(n)}(y,X) = \int_0^X \tilde{h}^{(n)}(y,\xi)\, \exp\left[\int_\xi^X \{\tilde{g}^{(n)}(y,\zeta)/g_o - \alpha'\}\, d\zeta \right] d\xi \qquad (C.7)$$

After some number of iterations, $\tilde{I}^{(n)}(y,X)$ converges uniformly. This method is good even when $I(\nu,z)$ has a narrow spectrum width in comparison to $\Delta\nu_N$, but it is not suitable for large s and large X_o because the iteration $\tilde{I}^{(n)}(y,X)$ begins to oscillate.

APPENDIX D

Equation (2.1.5) is

$$d\rho/dt = -\frac{i}{\hbar}[H,\rho] + \frac{1}{2}(F\rho + \rho F) + G \tag{D.1}$$

From Eq. (2.1.13) the left hand side of the above relation is rewritten as

$$d\rho/dt = \frac{1}{2}\{ d\rho_0/dt + (d\vec{r}/dt)\cdot\vec{\sigma}\} \tag{D.2}$$

With the help of Eqs. (2.1.13) and (2.1.14) the first term on the right hand side of Eq. (D.1) is simplified to

$$\begin{aligned} -\frac{i}{\hbar}[H,\rho] &= -\frac{i}{4}[H_0 + \vec{\omega}\cdot\vec{\sigma}, \rho_0 + \vec{r}\cdot\vec{\sigma}] \\ &= -\frac{i}{4}[\vec{\omega}\cdot\vec{\sigma}, \vec{r}\cdot\vec{\sigma}] \\ &= -\frac{i}{4}\sum_{\alpha,\beta=1,2,3} \omega_\alpha r_\beta [\sigma_\alpha, \sigma_\beta] \\ &= \frac{1}{2}\sum_{\alpha,\beta,\gamma} \omega_\alpha r_\beta \varepsilon_{\alpha\beta\gamma}\sigma_\gamma \end{aligned} \tag{D.3}$$

where we assume the commutation of H_0 and ρ_0 with other terms. $\varepsilon_{\alpha\beta\gamma}$ is the antisymmetric tensor satisfying

$$\varepsilon_{\alpha\beta\gamma} = \begin{cases} 1 & \text{even permutation of } (1,2,3) \\ -1 & \text{odd permutation of } (1,2,3) \end{cases}$$

Then we find

$$-\frac{i}{\hbar}[H,\rho] = \frac{1}{2}(\vec{\omega}\times\vec{r})\cdot\vec{\sigma} \tag{D.4}$$

The second term is given by Eq. (2.1.15) as

$$\frac{1}{2}(F\rho + \rho F) =$$

$$\frac{1}{4}\{2F_0\rho_0 + 2\rho_0\vec{F}\cdot\vec{\sigma} + 2F_0\vec{r}\cdot\vec{\sigma}$$

$$+ (\vec{F}\cdot\vec{\sigma})(\vec{r}\cdot\vec{\sigma}) + (\vec{r}\cdot\vec{\sigma})(\vec{F}\cdot\vec{\sigma})\}$$

The last two terms in the above equation are simplified in the following way:

$$(\vec{F}\cdot\vec{\sigma})(\vec{r}\cdot\vec{\sigma}) + (\vec{r}\cdot\vec{\sigma})(\vec{F}\cdot\vec{\sigma})$$

$$= \sum (F_\alpha r_\beta \sigma_\alpha\sigma_\beta + r_\beta F_\alpha \sigma_\beta\sigma_\alpha)$$

$$= \sum F_\alpha r_\beta(\sigma_\alpha\sigma_\beta + \sigma_\beta\sigma_\alpha)$$

$$= 2\sum F_\alpha r_\beta \delta_{\alpha\beta} = 2\vec{F}\cdot\vec{r} \tag{D.5}$$

Thus, from Eqs. (D.2) through (D.5) we have

$$d\rho_0/dt + (d\vec{r}/dt)\vec{\sigma} = (\vec{\omega}\times\vec{r})\cdot\vec{\sigma} + F_0\rho_0$$

$$+ (\rho_0\vec{F} + F_0\vec{r})\cdot\vec{\sigma} + \vec{F}\cdot\vec{r} + G_0 + \vec{G}\cdot\vec{\sigma} \tag{D.6}$$

We can separate Eq. (D.6) into two parts--into identity matrix term and Pauli spin matrices.

$$d\rho_0/dt = F_0\rho_0 + \vec{F}\cdot\vec{r} + G_0 \tag{D.7}$$

$$d\vec{r}/dt = \vec{\omega}\times\vec{r} + \rho_0 F + \vec{F}_0\vec{r} + \vec{G} \tag{D.8}$$

APPENDIX E

We have four equations

$$\dot{f}^{(1)} = -\gamma S_3^{(1)} \tag{E.1}$$

$$\dot{S}_1^{(1)} = -\omega_o S_2^{(1)} \tag{E.2}$$

$$\dot{S}_2^{(1)} = -\omega_{p1} S_3^{(0)} + \omega_o S_1^{(1)} \tag{E.3}$$

$$\dot{S}_3^{(1)} = \omega_{p1} S_2^{(0)} - \gamma f^{(1)} \tag{E.4}$$

Taking the time derivative of both sides of Eq. (E.2) we have the second order differential equation for $S_1^{(1)}$

$$\begin{aligned} \ddot{S}_1^{(1)} &= -\omega_o \dot{S}_2^{(1)} \\ &= -\omega_o^2 S_1^{(1)} + \omega_o \omega_{p1} S_3^{(0)} \end{aligned} \tag{E.5}$$

Using the relations (2.2.20) and (2.2.22), we get

$$\ddot{S}_1^{(1)} + \omega_o^2 S_1^{(1)} = -\frac{\omega_o \bar{N} \mu_{ab} e^{\Gamma_o t}}{\hbar} \sum E_n \, \mathrm{Im}[e^{ik_n z} \{e^{i(\omega_n + k_n v)t} + e^{-i(\omega_n - k_n v)t}\}] \tag{E.6}$$

We may neglect the solution of the homogeneous part in the above equation which does not evolve as $e^{\Gamma_o t}$. The solution for inhomogeneous parts are

$$S_1^{(1)} = -\frac{\omega_o \bar{N} \mu_{ab} e^{\Gamma_o t}}{\hbar} \sum E_n \, \mathrm{Im}[D(\omega_n + k_n v) e^{ik_n z + i(\omega_n + k_n v)t} + D(-\omega_n + k_n v) e^{ik_n z - i(\omega_n - k_n v)t}] \tag{E.7}$$

Putting this into Eq. (E.2) we get

$$S_2^{(1)} = -\frac{\bar{N}\,\mu_{ab}\,e^{\Gamma_o t}}{\hbar}\sum E_n\,\mathrm{Im}[g(\omega_n + k_n v)\,e^{ik_n z + i(\omega_n + k_n v)t} + g(-\omega_n + k_n v)\,e^{ik_n z - i(\omega_n - k_n v)t}] \tag{E.8}$$

$$S_3^{(1)} = f^{(1)} = 0 \tag{E.9}$$

where

$$D(\omega) = \frac{1}{(\Gamma_o + i\omega)^2 + \omega_o^2} \tag{E.10}$$

$$g(\omega) = \frac{\Gamma_o + i\omega}{(\Gamma_o + i\omega)^2 + \omega_o^2} \tag{E.11}$$

APPENDIX F

To evaluate the integration in Eq. (2.2.45), the following integration has to be carried out:

$$J_n = \frac{1}{u\sqrt{\pi}} \int_{-\infty}^{\infty} [D(\omega_n + k_n v)\, e^{i\omega_n t} + D(-\omega_n + k_n v)\, e^{-i\omega_n t}]\, e^{-v^2/u^2}\, dv \qquad (F.1)$$

Changing the sign of v in the second term in the integration, and using the relation $D(-\omega) = D^*(\omega)$, we get

$$J_n = \frac{1}{u\sqrt{\pi}} \int_{-\infty}^{\infty} [D(\omega_n + k_n v)\, e^{i\omega_n t} + \text{c.c.}]\, e^{-v^2/u^2} dv$$

$$= \frac{2}{u\sqrt{\pi}} \text{Re}[e^{i\omega_n t} \int_{-\infty}^{\infty} D(\omega_n + k_n v)\, e^{-v^2/u^2}\, dv] \qquad (F.2)$$

We have the above integration in a simple form by changing the variable

$$s = v/u$$

$$\zeta_n^{\pm} = (\pm\omega_o - \omega_n + i\Gamma_o)/(k_n u) \qquad (F.3)$$

$$J_n = -\frac{1}{2\omega_o k_n u\sqrt{\pi}}\, 2\, \text{Re}\{[\int_{-\infty}^{\infty} \frac{e^{-s^2}}{s-\zeta_+} ds - \int_{-\infty}^{\infty} \frac{e^{-s^2}}{s-\zeta_-} ds]\, e^{i\omega_n t}\} \qquad (F.4)$$

We are given in the table of mathematics,[1]

$$\underset{\sim}{W}(\zeta) = \frac{i}{\pi} \int_{-\infty}^{\infty} \frac{e^{-s^2}}{\zeta - s} ds$$

$$= e^{-\zeta^2} \text{erfc}(-i\zeta) \qquad (F.5)$$

where erfc is the complementary error function. Using this relation we get more explicit form of Eq. (F.4) as

$$J_n = - \frac{\pi}{\omega_o k_n u\sqrt{\pi}} \mathrm{Re}[e^{i\omega_n t} \{i\underset{\sim}{W}(\zeta_n^+) - i\underset{\sim}{W}(\zeta_n^-)\}] \qquad (F.6)$$

Generally,

$$|\omega_n - \omega_o| << |\omega_n + \omega_o|$$

then we can neglect the second term in Eq. (F.6) in comparison with the first term, so we have

$$J_n = + \frac{\pi}{\omega_o k_n u\sqrt{\pi}} \mathrm{Im}[\underset{\sim}{W}(\zeta_n^+)\, e^{i\omega_n t}] \qquad (F.7)$$

$$= \frac{\pi}{\omega_o k_n u\sqrt{\pi}} \left\{\mathrm{Im}[\underset{\sim}{W}(\zeta_n^+)]\cos \omega_n t + \mathrm{Re}[\underset{\sim}{W}(\zeta_n^+)]\sin \omega_n t\right\} \qquad (F.8)$$

When J_n is substituted into Eq. (2.2.45) the following equation is obtained:

$$P^{(1)} = - \frac{\overline{N}\, \mu_{ab}^2 \sqrt{\pi}}{\pi\, k_n u} \sum E_n \sin k_n z \{\mathrm{Im}[\underset{\sim}{W}(\zeta_n^+)] \cos \omega_n t + \mathrm{Re}[\underset{\sim}{W}(\zeta_n^+)] \sin \omega_n t \} \qquad (F.9)$$

APPENDIX G

More rigorously, one has to use Laplace transformation. But as shown in this appendix, the results are the same if one is interested in the steady state. Equations (2.3.3) are as follows:

$$[\frac{d^2}{dt^2} - \gamma^2]\, f^{(n)} = -\gamma\, \omega_{p1} S_2^{(n-1)} \tag{G.1}$$

$$[\frac{d^2}{dt^2} + \omega_o^2]\, S_1^{(n)} = \omega_o \omega_{p1} S_3^{(n-1)} \tag{G.2}$$

$$[\frac{d^2}{dt^2} + \omega_o^2]\, S_2^{(n)} = -\frac{d}{dt}[\omega_{p1} S_3^{(n-1)}] \tag{G.3}$$

$$[\frac{d^2}{dt^2} - \gamma^2]\, S_3^{(n)} = \frac{d}{dt}[\omega_{p1} S_2^{(n-1)}] \tag{G.4}$$

The Laplace transform[2] of $f(x)$ is defined by

$$\tilde{f}(p) = \int_0^\infty f(x)\, e^{-px}\, dx \tag{G.5}$$

Taking the Laplace transform of both sides of Eqs. (G.1) to (G.4) and assuming ω_{p1} has a simple form as

$$\omega_{p1} = \omega_{po}(e^{i\omega t} + e^{-i\omega t}) \quad , \tag{G.6}$$

one finds

$$-\dot{f}^{(n)}(0) - pf^{(n)}(0) + (p^2 - \gamma^2)\tilde{f}^{(n)}(p)$$

$$= -\gamma\, \omega_{po}\, \{\tilde{S}_2^{(n-1)}(p + i\omega) + \tilde{S}_2^{(n-1)}(p - i\omega)\} \tag{G.7}$$

$$-\dot{S}_1^{(n)}(0) - pS_1^{(n)}(0) + (p^2+\omega_o^2)\tilde{S}_1^{(n)}(p)$$

$$= \omega_o\omega_{po}\{\tilde{S}_3^{(n-1)}(p+i\omega) + \tilde{S}_3^{(n-1)}(p-i\omega)\} \qquad (G.8)$$

$$-\dot{S}_2^{(n)}(0) - pS_2^{(n)}(0) + (p^2+\omega_o^2)\,\tilde{S}_2^{(n)}(p)$$

$$= 2\omega_{po}S_3^{(n-1)}(0) - p\omega_{po}\{\tilde{S}_3^{(n-1)}(p+i\omega) + \tilde{S}_3^{(n-1)}(p-i\omega)\} \qquad (G.9)$$

$$-\dot{S}_3^{(n)}(0) - pS_3^{(n)}(0) + (p^2-\gamma^2)\,\tilde{S}_3^{(n)}(p)$$

$$= -2\omega_{po}S_2^{(n-1)}(0) + p\omega_{po}\{\tilde{S}_2^{(n-1)}(p+i\omega) + \tilde{S}_2^{(n-1)}(p-i\omega)\} \qquad (G.10)$$

From Eqs. (G.9) and (G.10) one finds

$$\tilde{S}_3^{(n)}(p) = \frac{1}{p^2-\gamma^2}\{\dot{S}_3^{(n)}(0) + pS_3^{(n)}(0) - 2\omega_{po}S_2^{(n-1)}(0)\} +$$

$$+ \frac{1}{p^2-\gamma^2}\,\frac{p\omega_{po}}{(p+i\omega)^2+\omega_o^2}\{\dot{S}_2^{(n)}(0) + (p+i\omega)S_2^{(n)}(0)$$

$$+ 2\omega_{po}S_3^{(n-1)}(0)\} + \frac{1}{p^2-\gamma^2}\,\frac{p\omega_{po}}{(p-i\omega)^2+\omega_o^2}\{\dot{S}_2^{(n)}(0)$$

$$+ (p-i\omega)S_2^{(n)}(0) + 2\omega_{po}S_3^{(n-1)}(0)\} \; - \frac{p\omega_{po}^2}{p^2-\gamma^2}$$

$$\times \left[\frac{p+i\omega}{(p+i\omega)^2+\omega_o^2}\{\tilde{S}_3^{(n-2)}(p+2i\omega) + \tilde{S}_3^{(n-2)}(p)\}\right.$$

$$\left. + \frac{p-i\omega}{(p-i\omega)^2+\omega_o^2}\{\tilde{S}_3^{(n-2)}(p-2i\omega) + \tilde{S}_3^{(n-2)}(p)\}\right] \qquad (G.11)$$

The inverse Laplace transform of the first three terms has the time dependence of $e^{\pm\gamma t}$. When we go back to the real physical quantities we have to multiply with $e^{-\Gamma_o t}$ as in Eq. (2.2.33). Therefore we may neglect the first three terms in Eq. (G.11), and the recursion relation for $\tilde{S}_3^{(n)}(p)$ is rewritten as

$$\tilde{S}_3^{(n)}(p) = -\omega_{po}^2 \frac{p}{p^2-\gamma^2}\left[\frac{p+i\omega}{(p+i\omega)^2+\omega_o^2}\{\tilde{S}_3^{(n-2)}(p+2i\omega)+\tilde{S}_3^{(n-2)}(p)\}\right.$$

$$\left.+\frac{p-i\omega}{(p-i\omega)^2+\omega_o^2}\{\tilde{S}_3^{(n-2)}(p)+\tilde{S}_3^{(n-2)}(p-2i\omega)\}\right] \qquad (G.12)$$

For $n = 0$ the initial recursion relation is given by Eq. (2.2.33) as

$$\tilde{S}_3^{(0)}(p) = \frac{\bar{N}}{p-\Gamma_o} \qquad (G.13)$$

and

$$S_3^{(2)}(p) = -\omega_{po}^2 \frac{p\bar{N}}{p^2-\gamma^2}\left[\frac{p+i\omega}{(p+i\omega)^2+\omega_o^2}\left\{\frac{1}{p+2i\omega-\Gamma_o}+\frac{1}{p-\Gamma_o}\right\}\right.$$

$$\left.+\frac{p-i\omega}{(p-i\omega)^2+\omega_o^2}\left\{\frac{1}{p-\Gamma_o}+\frac{1}{p-2i\omega-\Gamma_o}\right\}\right] \qquad (G.14)$$

If we carry the Laplace inverse transformation and neglect all the terms that do not have the time dependence $e^{\Gamma_o t}$, we will get

$$S_3^{(2)}(t) = -\omega_{po}^2 \frac{\Gamma_o\bar{N}}{\Gamma_o^2-\gamma^2}\left\{\frac{\Gamma_o+i\omega}{(\Gamma_o+i\omega)^2+\omega_o^2}+\frac{\Gamma_o-i\omega}{(\Gamma_o-i\omega)^2+\omega_o^2}\right\}e^{\Gamma_o t}$$

$$-\omega_{po}^2\bar{N}\left\{\frac{\Gamma_o-2i\omega}{(\Gamma_o-2i\omega)^2-\gamma^2}\frac{\Gamma_o-i\omega}{(\Gamma_o-i\omega)^2+\omega_o^2}e^{-2i\omega t}\right. \quad +$$

$$+ \frac{\Gamma_o + 2i\omega}{(\Gamma_o + 2i\omega)^2 - \gamma^2} \frac{\Gamma_o + i\omega}{(\Gamma_o + i\omega)^2 + \omega_o^2} e^{2i\omega t} \} e^{\Gamma_o t} \qquad \text{(G.15)}$$

since

$$\left| \frac{\Gamma_o \pm 2i\omega}{(\Gamma_o \pm 2i\omega)^2 - \gamma^2} \right| \ll \frac{\Gamma_o}{\Gamma_o^2 - \gamma^2} \qquad \text{(G.16)}$$

we may neglect the last two terms in Eq. (G.15). As mentioned above, we may neglect $S_3^{(n-2)}(p+2i\omega)$ and $S_3^{(n-2)}(p-2i\omega)$ in Eq. (G.12), and finally we get the recursion relation

$$\tilde{S}_3^{(n)}(p) = -\omega_{po}^2 \frac{p}{p^2 - \gamma^2} \{ \frac{p + i\omega}{(p+i\omega)^2 + \omega_o^2} \frac{p - i\omega}{(p-i\omega)^2 + \omega_o^2} \} \tilde{S}_3^{(n-2)}(p) \qquad \text{(G.17)}$$

and we can obtain the same results as mentioned in Section 2.3.

APPENDIX H

We have Eq. (2.4.14) as

$$S_3 = \bar{N} e^{\Gamma_o t} - \frac{D}{D^2 - \gamma^2} \omega_{pl} \frac{D}{D^2 + \omega_o^2} \omega_{pl} S_3 \tag{H.1}$$

With the substitution

$$S_3 = \bar{N} e^{\Gamma_o t} T \tag{H.2}$$

Eq. (H.1) is simplified to

$$T = 1 - \mathcal{D}(D)\, \omega_{pl}\, L^{+}(D)\, \omega_{pl} T \tag{H.3}$$

Since ω_{pl} is a linear combination of $e^{\pm i\omega t}$ and $e^{\pm i(kz+kvt)}$, T has only the even harmonics of these. Thus we may assume the solution of T can be expanded as

$$T = \sum_{m,n=-\infty}^{\infty} T_{m,n}\, e^{2im\omega t}\, e^{2in(kz + kvt)} \tag{H.4}$$

The factor $T_{m,n}$ $(m \neq 0)$ is coupled to other terms by the following relation:

$$T_{m,n} = - \mathcal{D}(2im)[\text{The terms with time dependence } e^{2im\omega t} \text{ of } \omega_{pl} L^{+}(D)\, \omega_{pl} T] \tag{H.5}$$

However $|\mathcal{D}(2im)|$ is $1/\omega_o$ times smaller than $|\mathcal{D}(0)|$. Thus we may neglect the terms which have higher harmonics of $e^{2i\omega t}$. We may re-write Eq. (H.4) as

$$T = \sum_{n=-\infty}^{\infty} A_n \, e^{2in(kz + vt)} \qquad (H.6)$$

APPENDIX I

We can rewrite expression (2.4.16) as follows:

$$b_n A_{n+1} + a_n A_n + c_n A_{n-1} = \delta_{n,0} \tag{I.1}$$

where

$$a_n = 1 + \frac{\mu_{ab}^2 E_o^2}{16\hbar^2} \mathcal{D}(2iknv)[L^+(\omega + (2n+1)kv) + L^+(\omega - (2n+1)kv)$$

$$+ L^+(\omega + (2n-1)kv) + L^+(\omega - (2n-1)kv)] \tag{I.2}$$

$$b_n = - \frac{\mu_{ab}^2 E_o^2}{16\hbar^2} \mathcal{D}(2iknv)[L^+(\omega + (2n+1)kv) + L^+(\omega - (2n+1)kv)] \tag{I.3}$$

and

$$c_n = - \frac{\mu_{ab}^2 E_o^2}{16\hbar^2} \mathcal{D}(2iknv)[L^+(\omega + (2n-1)kv) + L^+(\omega - (2n-1)kv)] \tag{I.4}$$

Assuming that

$$A_{\pm j} = 0 \qquad \text{for} \qquad j \geq N+1 \tag{I.5}$$

we have $2N+1$ linear equations for $2N+1$ unknowns. Thus we obtain

$$\begin{pmatrix} a_N & c_N & & & \\ b_{N-1} & a_{N-1} & \ddots & & \\ & \ddots & \ddots & \ddots & \\ & & a_{-N+1} & c_{-N+1} & \\ & & b_{-N} & a_{-N} \end{pmatrix} \begin{pmatrix} A_N \\ \\ \\ \\ A_{-N} \end{pmatrix} = \begin{pmatrix} 0 \\ \vdots \\ 1 \\ 0 \\ \vdots \\ 0 \end{pmatrix} \tag{I.6}$$

We can solve this numerically[3]. We took $N = 5$, where the relative convergence to $N = 6$ is a part of 10^{15}.

APPENDIX J

Assume the amplitude has the following relation

$$\tilde{E}_n^2(t) = \overline{\tilde{E}^2(t)} + \tilde{e}_n(t) \tag{J.1}$$

where $\tilde{e}_n(t)$ is a fluctuation of the squared field from its temporary average $\overline{\tilde{E}_n^2(t)}$. Then the ensemble average of the Nth power of the squared field is approximately,

$$\overline{\{\tilde{E}_n^2(t)\}^N} \cong \{\tilde{E}_n^2(t)\}^N + \frac{N(N-1)}{2} \overline{\tilde{e}_n^2(t)} \ \overline{\{\tilde{E}_n^2(t)\}^{N-2}} + \cdots \tag{J.2}$$

We assume $\overline{\tilde{e}(t)} = 0$. When we sum up the following power series from zero to infinity:

$$\{- \mathcal{D}(D)\ \omega_{pl}\ L^+(D)\ \omega_{pl}\}^N \tag{J.3}$$

the contribution from the second term on the right hand side of Eq. (J.2) is approximately the same order of magnitude as $\mu_{ab}^4\ \overline{\tilde{e}^2(t)}/\hbar^4 \gamma_a^2\ \gamma_b^2$. Thus we have Eq. (2.5.21).

APPENDIX K

From Eqs. (2.2.33) and (2.2.38), zero and first order solutions for S_3 are written as

$$S_3^{(0)} = \bar{N}\, e^{\Gamma_o t}$$

$$S_3^{(1)} = 0 \tag{K.1}$$

S_3 is formally given by Eq. (2.3.12) as

$$S_3 = \bar{N}\, e^{\Gamma_o t} \sum_0^{\infty} \left[- \frac{D+\Gamma_o}{(D+\Gamma_o)^2 - \gamma^2}\, \omega_{pl}\, \frac{D+\Gamma_o}{(D+\Gamma_o)^2 + \gamma_o^2}\, \omega_{pl} \right]^m \tag{K.2}$$

In the moving frame ω_{pl} is given by Eq. (2.2.23) as

$$\omega_{pl} = \frac{\mu_{ab} E_o}{\hbar} \mathrm{Im}\left[e^{ikz} \left\{ e^{i(\omega+kv)t} + e^{-i(\omega-kv)t} \right\} \right] \tag{K.3}$$

Neglecting the higher harmonic terms (RWA) we have

$$- \frac{D+\Gamma_o}{(D+\Gamma_o)^2 - \gamma^2}\, \omega_{pl}\, \frac{D+\Gamma_o}{(D+\Gamma_o)^2 + \omega_o^2}\, \omega_{pl}$$

$$= I_o\, L(\omega, v) \tag{K.4}$$

where

$$I_o = \frac{\mu_{ab}^2 E_o^2}{4\hbar^2 \gamma_a \gamma_b}$$

$$L(\omega, v) = \frac{\Gamma_o^2}{\Gamma_o^2 + (\omega - \omega_o - kv)^2} + \frac{\Gamma_o^2}{\Gamma_o^2 + (\omega - \omega_o + kv)^2}$$

Then the summation in Eq. (K.2) becomes

$$S_3 = \frac{\bar{N}\, e^{\Gamma_0 t}}{1 + I_0\, L(\omega,v)} \tag{K.5}$$

S_1 is given by Eq. (2.3.13) as

$$S_1 = \frac{\omega_0}{D^2 + \omega_0^2}\, \omega_{p1} S_3$$

After an algebraic manipulation, we have

$$S_1 = \frac{\bar{N}\, \mu_{ab} E_0 e^{\Gamma_0 t}}{2\hbar} \left\{ \frac{\Gamma_0 \cos(kz+\omega t) + (\omega-\omega_0+kv)\, \sin(kz+\omega t)}{\Gamma_0^2 + (\omega-\omega_0+kv)^2} \right.$$

$$\left. - \frac{\Gamma_0 \cos(kz-\omega t) - (\omega-\omega_0-kv)\, \sin(kz-\omega t)}{\Gamma_0^2 + (\omega-\omega_0-kv)^2} \right\} \frac{1}{1 + I_0\, L(\omega,v)} \tag{K.6}$$

To get the macroscopic polarization P, we have to sum up the above for all possible v, multiplying with the weighting function

$$w(v) = \frac{1}{u\sqrt{\pi}}\, e^{-v^2/u^2} \tag{K.7}$$

Thus we get

$$P = \mu_{ab}\, e^{-\Gamma_0 t} \int_{-\infty}^{\infty} S_1\, w(v)\, dv \tag{K.8}$$

Since $w(v)$ and $L(\omega,v)$ are symmetric about $v = 0$ the above integral simplifies to

$$P = \frac{\bar{N}\, \mu_{ab}^2 E_0}{\hbar u\sqrt{\pi}} \sin kz \int \frac{-\Gamma_0 \sin\omega t + (\omega-\omega_0+kv) \cos\omega t}{\Gamma_0^2 + (\omega-\omega_0+kv)^2}$$

$$\times \frac{e^{-v^2/u^2}}{1 + I_0 L(\omega,v)}\, dv \tag{K.9}$$

APPENDIX L

It may be justified to neglect the term $kr^2/2R$ in $C(z,r,t)$ and $S(z,r,t)$ and compare term by term on both sides of the wave equation, if the following is true:

$$s(r)\sin(\omega t - \frac{k}{2R}r^2) + c(r)\cos(\omega t - \frac{k}{2R}r^2) \equiv 0 \qquad (L.1)$$

for all t and r, then

$$s(r) \equiv c(r) \equiv 0$$

Proof:

Equation (L.1) is rewritten

$$\{s(r)\cos\frac{kr^2}{2R} + c(r)\sin\frac{kr^2}{2R}\}\sin\omega t + \{-s(r)\sin\frac{kr^2}{2R} + c(r)\cos\frac{kr^2}{2R}\}\cos\omega t \equiv 0 \qquad (L.2)$$

for all t, then each factor of sine and cosine should be equal to zero,

$$s(r)\cos\frac{kr^2}{2R} + c(r)\sin\frac{kr^2}{2R} = 0 \qquad (L.3)$$

$$-s(r)\sin\frac{kr^2}{2R} + c(r)\cos\frac{kr^2}{2R} = 0 \qquad (L.4)$$

One finds from Eq. (L.3) the following, if $\sin\frac{kr^2}{2R} \neq 0$

$$c(r) = -s(r)\cot\frac{kr^2}{2R}$$

Plugging this into Eq. (L.4), one finds

$$s(r)\left[\sin\frac{kr^2}{2R}+\frac{\cos^2\frac{kr^2}{2R}}{\sin kr^2/2R}\right]=\frac{s(r)}{\sin\frac{kr^2}{2R}}=0 \qquad (L.5)$$

Then

$$s(r)=0 \qquad (L.6)$$

and when $\sin\frac{kr^2}{2R}=0$, we have $s(r)=0$ from Eq. (L.3). Thus

$$s(r)=0$$

$$c(r)=0$$

APPENDIX M

P_{phase} is given by

$$P_{phase} = \frac{k^2}{2R^2} \frac{\bar{N}_o \mu_{ab}^2 u}{\hbar\pi^{1/2}} \int_{-\infty}^{\infty} \{P_s\, S(z,0,t) + P_c\, C(z,0,t)\}\, e^{-v^2/u^2}\, dv \tag{M.1}$$

For simplification of notation, we introduce

$$I_o = \frac{\mu_{ab}^2 E^2(0)}{4\hbar^2 \gamma_a \gamma_b} \tag{M.2}$$

$$\Gamma = \frac{1}{\Gamma_o^2 + (\omega-\omega_o+ kv)^2} \tag{M.3}$$

$$L = \frac{\Gamma_o^2}{\Gamma_o^2 + (\omega-\omega_o+ kv)^2} + \frac{\Gamma_o^2}{\Gamma_o^2 + (\omega-\omega_o- kv)^2} \tag{M.4}$$

$$A = \Gamma_o^2 \left\{ \frac{\omega-\omega_o+ kv}{\{\Gamma_o^2 + (\omega-\omega_o+ kv)^2\}^2} + \frac{\omega-\omega_o- kv}{\{\Gamma_o^2 + (\omega-\omega_o- kv)^2\}} \right\} \tag{M.5}$$

$$C = \frac{1}{1 + I_o \cdot L} \tag{M.6}$$

and

$$F = \{3(\omega-\omega_o+ kv)^2 - \Gamma_o^2\}\, \Gamma^3 \tag{M.7}$$

With the help of the above substitutions, we have

$$P_s = -\Gamma_o[FC + \Gamma(4A^2 I_o^2\, C^2 - FI_o C^2) - 4(\omega-\omega_o+kv)\, AI_o \Gamma^2 C^2] \tag{M.8}$$

$$P_c = (\omega-\omega_o+kv)[FC+\Gamma(4A^2 I_o^2 C^3 - FI_o C^2) - 4(\omega-\omega_o+kv)\, AI_o \Gamma^2 C^2]$$
$$- FC + \Gamma(4A^2 I_o^2 C^3 - I_o F C^2) \tag{M.9}$$

References for Appendices

1. M. Abramowitz and I. A. Segun, Handbook of Mathematical Functions, Dover (1965), p. 297.

2. P. M. Morse and H. Feshbach, Method of Theoretical Physics, McGraw-Hill (1953), p. 467.

3. E. Isaacson and H. B. Keller, Analysis of Numerical Method, John Wiley & Sons, Inc. (1966), p. 58.